REPORT DOCUMENTATION PAGE

Form Approved OMB No. 0704-0188

1. REPORT DATE *(DD-MM-YYYY)*	2. REPORT TYPE	3. DATES COVERED *(From – To)*
17-11-2006	Final Report	01-Nov-03 - 14-Mar-07

4. TITLE AND SUBTITLE

Study Of Properties Of The Microwave Streamer Discharge In A High-Speed Flow Of Gas And In Two-Phase Medium

5a. CONTRACT NUMBER
ISTC Registration No: 2820

5b. GRANT NUMBER

5c. PROGRAM ELEMENT NUMBER

6. AUTHOR(S)

Dr. Kirill Victorovich Khodataev

5d. PROJECT NUMBER

5d. TASK NUMBER

5e. WORK UNIT NUMBER

7. PERFORMING ORGANIZATION NAME(S) AND ADDRESS(ES)

Federal State Unitary Firm 'MRTI' of RAS
Warshavskoe shosse 132
Moscow 117519
Russia

8. PERFORMING ORGANIZATION REPORT NUMBER

N/A

9. SPONSORING/MONITORING AGENCY NAME(S) AND ADDRESS(ES)

EOARD
PSC 821 BOX 14
FPO AE 09421-0014

10. SPONSOR/MONITOR'S ACRONYM(S)

11. SPONSOR/MONITOR'S REPORT NUMBER(S)
ISTC 02-7007

12. DISTRIBUTION/AVAILABILITY STATEMENT

Approved for public release; distribution is unlimited.

13. SUPPLEMENTARY NOTES

14. ABSTRACT

This report results from a contract tasking Federal State Unitary Firm 'MRTI' of RAS as follows: The contractor will investigate the use of undercritical streamer microwave discharges for ignition of fuel-air mixtures. The system of microwave radiation initiated spark filaments can uniformly fill a volume with streamers of several thousand degrees Kelvin. Thus, quick ignition of fuel-air mixtures over the whole cross-section of the discharge is anticipated. Experimental and theoretical investigations will be carried out. Effects of variation in radiation field wavelength (2.5 cm to 12.5 cm), relative humidity (up to 100%), in a motionless gas and in a gas flow will be investigated. Spatial and temporal characteristics of the discharges will be documented.

15. SUBJECT TERMS
EOARD, Physics, Plasma Physics and Magnetohydrodynamics

16. SECURITY CLASSIFICATION OF:			17. LIMITATION OF ABSTRACT	18, NUMBER OF PAGES	19a. NAME OF RESPONSIBLE PERSON
a. REPORT	b. ABSTRACT	c. THIS PAGE			SURYA SURAMPUDI
UNCLAS	UNCLAS	UNCLAS	UL	102	19b. TELEPHONE NUMBER *(Include area code)* +44 (0)20 7514 4299

ISTC #2820p

Approved

Director
FSUE «MRTI RAS»

V.V. Vetrov

«___» _____2006.

Final technical report on ISTC Project № 2820p (027007)

Investigations of microwave streamer discharge properties in a high-speed flow and in two-phase medium

(01 November 2003 – 31 October 2006)

Project Manager 

Kirill Viktorovich Khodataev
Federal State Unitary enterprise «Moscow radiotechnical institute RAS »

2006

This work is financed by European Office of Aerospace Research and Development and is executed by agreement with International Scientific – Technical Center (ISTC)

ISTC 2820p

Investigations of microwave streamer discharge properties in a high-speed flow and in two-phase medium (01 November 2003 – 31 October 2006)

Kirill Viktorovich Khodataev (Project Manager)
Federal State Unitary enterprise «Moscow radiotechnical institute RAS »*

The Project goal consists in electrical discharge investigations in air in a microwave (MW) wavelength λ range of electromagnetic (EM) radiation. We studied the discharge in quasi-optical beam of linearly polarized EM radiation. It was far from experimental installation construction elements surrounding the discharge area.

We studied this MW discharge type features experimentally and theoretically in different conditions and in a wide range of gas and radiation parameters.

Experiments have shown that this discharge energy effectively interacts with EM field exciting it at comparably high air pressure $\boldsymbol{p}$. This allows to analyze different ways of its practical application, and stimulates fundamental investigations of its features.

Keywords: microwave, diffuse, streamer, electric discharge, surface discharge, high-speed flow, aerosol, humidity, two-phase medium, propane-air mixture.

* 117519, Warschavskoe shosse 132, Moscow, Russia Phone +7-(495) 312-3111, Fax +7-(495) 314-10-53
E-mail:mrti_d@ors.ru

ISTC 2820p

The work has been performed by the following institutes and collaborators.

1. Participated institutes:

1.1 Leading institute:

Federal State Unitary enterprise «Moscow radiotechnical institute RAS »
117519, Warschavskoe shosse 132, Moscow, Russia Phone +7-(495) 312-3111,
Fax +7-(495) 314-10-53
E-mail:mrti_d@orc.ru

1.2 Subcontracted institutes:

None

2. Partner

The European Office of Aerospace Research and Development (EOARD)
223-231 Old Marylebone Road, London, United Kingdom,
Phone +44 207 514 4354, Fax +44 207 514 4960
Email: Surya.surampudi@london.af.mil

Contents

1. Introduction

Present report sums results of scientific investigations executed in MRTI RAS in frames of ISTC Project №2820p **«Investigations of microwave streamer discharge properties in a high-speed flow and in two-phase medium»**. Investigations were carried out during three years from November 1, 2003 to October 31, 2006.

Electrical discharge in microwave (MW) range of electromagnetic (EM) radiation wavelengths, λ, in air was investigated**.** A typical feature of the investigated discharge consists in the fact that it is created in a quasi-optical beam of linearly polarized EM radiation far from experimental setup construction elements surrounding a discharge area. Electric field in the discharge area in this case represents a superposition of EM beam initial field and an induced field of a discharge plasma. A field reflected from objects surrounding the discharge area practically does not influence on a discharge development, so the initial field can be considered as unchangeable. Undertaken experiments showed that this discharge energy effectively interacts with EM field exciting it at comparably high air pressure, ***p.*** This allows to analyze different variants of its practical application and stimulates undertaking of fundamental investigations of its features.

A simplified realization scheme of this discharge is represented in Fig.**1.1.** It includes a MW generator of magnetron of klystron types and a device forming linearly polarized EM beam with TEM field structure. A discharge is usually realized in a focal area of this beam. EM beam is a quasi-optical one in a sense that transversal sizes of elements forming it are only of several (up to ten) wavelengths, λ. Typical transversal sizes of these beams focal areas as usual have a scale of λ, and the longitudinal ones are smaller than λ or insignificantly exceed it.

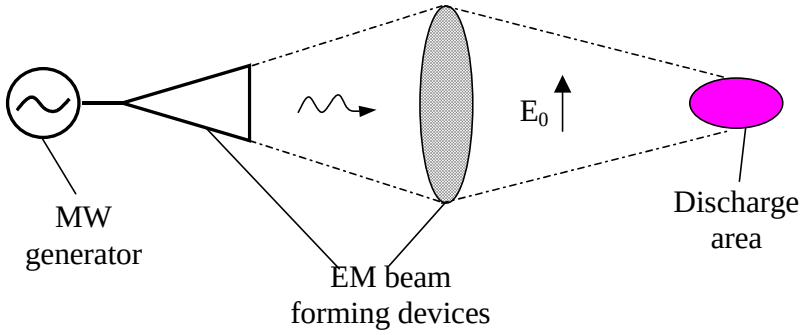

Fig.1.1. Realization scheme of electrodeless MW discharge in a quasi-optical wave beam of EM waves.

Experiments showed that typical features of this discharge remain the same in a range of λ approximately from two to ten centimeters. At that investigated range of air pressure ***p*** – was from several Torr to the atmospheric pressure. These λ and ***p*** values at discharge realization correspond to a range of collisional and essentially collisional plasma: $\nu_c \sim \omega$ and $\nu_c >> \omega$. Here $\boldsymbol{\nu_c}$ is a collisional frequency of plasma electrons with molecules of air and ω is a circular field frequency.

For creation of investigated discharge type at pressure p ~100 Torr and initial levels of electric component of EM field $\boldsymbol{E_0}$ (close to the critical breakdown level $\boldsymbol{E_{cr}}$) one requires EM beam power $P_{MW} \sim 10^5$ W . In realty such values of $\boldsymbol{P_{MW}}$ can be realized only in a pulse mode at EM pulse duration $\boldsymbol{\tau_{pul}}$ up to several tens of microseconds both in conditions of a unique pulse and in chain of pulses at a mean power up to hundred of watts. At realization of investigated discharge type in a field with $E_0 << E_{cr}$ in this pressure ***p*** range one can use EM beams with the power $\boldsymbol{P_{MW}}$ close to 10^3 W. In this case one can investigate discharges in the continuous mode of realization.

Study of this discharge features encounters great difficulties especially at its pulse realization. Pulsed MW discharge is especially dynamic object. Its spatial structure is exceedingly complicated

and non-uniform at comparably high gaseous pressure. At that in principle it conserves its appearance in consecutive MW pulses but it does not repeat its form in different realization. Placing of local sensors into the discharge region substantially change its properties. This fact leads only to contact less means of this discharge investigation. Spectral methods have also difficulties at investigation of this discharge plasma. At their application it is not clear from which discharge area an information was obtained and to which time moment of the discharge development it corresponded.

One method of these difficulties overcoming consists in controlled variation of experimental conditions and corresponding development of physical process models describing this discharge development. Namely this method was used in the present investigations. So in a simplest version of studies we change air pressure, EM pulse duration τ_{pul} and a level of initial field E_0 in the discharge area. Experiments in described investigations were carried out at different wavelengths λ of EM field: λ=2.5 cm, λ=8.9 cm and λ=12.5 cm. We used different configurations of EM beam- a mode of "meeting" waves and a mode of "running" wave. The discharge was realized in dead air and in its high-speed flow; it was realized in humid air and in air with water aerosol. We also made investigations in the high-speed flow of air-propane flammable mixture.

Our investigations in absolutely different conditions have allowed to define more exactly MW air electric breakdown conditions at a field level $E_0 \approx E_{cr}$ and to determine breakdown ignition possibility at $E_0 < E_{cr}$ and $E_0 << E_{cr}$. During these experiments we have determined $p - E_0$ boundaries of MW discharge different forms existence with respect to λ. We have defined more precisely spatial and temporary discharge development characteristics; we hade determined maximum gas temperatures of the discharge plasma formations, etc.

Our work included twelve definite Tasks:

Task 1. Investigations aimed at determination of a boundary separating undercritical and deeply undercritical discharges with respect to the field level in wide pressure range at the wavelength λ = 2.5 cm;

Task 2. Investigations at the wavelength λ = 2.5 cm of the undercritical discharge with propagating volumetric structure using a method of propane-air mixture ignition in the high-speed flow;

Task 3. Investigations aimed at determination of breakdown field threshold in the dead gas in the radiation beam with the wavelength λ = 9 cm with respect to air humidity and water aerosol concentration;

Task 4. Investigations of spatial and temporary characteristics of the undercritical and deeply undercritical discharges at the wavelength λ = 9 cm in the dead air with respect to air humidity and water aerosol concentration;

Task 5. Theoretical assistance of the experimental program and further development of the undercritical and deeply undercritical discharge models in the dead gas and in the high-speed flow:

Task 6. Investigations of spatial and temporary characteristics of the undercritical and deeply undercritical discharges at the wavelength λ = 2.5 cm in the dead air;

Task 7. Investigations of deeply undercritical discharge features at the wavelength λ = 12.5 cm in two-phase medium and in high-speed flow;

Task 8. Investigations of pulsed microwave discharge features on a surface of the dielectric plate at the wavelength λ = 9 cm;

Task 9. Theoretical assistance of the experimental program and undercritical discharge on a surface of a dielectric plate in a dead gas theoretical model development;

Task 10. Investigations aimed at additional experimental data obtaining about undercritical and deeply undercritical discharges with volumetric streamer structure at the wavelength λ = 2.5 cm with an application of the discharge realization method in the two-phase medium in the high-speed flow;

Task 11. Investigations of surface undercritical discharge features in the high-speed flow at the wavelength $\lambda = 2.5$ cm;

Task 12. Theoretical assistance of the experimental program and development of theoretical models of: undercritical volumetric discharge in two-phase medium; surface discharge in the high-speed flow.

Results of first nine Tasks of Stage 1 and Stage 2 are in details reflected in intermediate Reports [1] and [2]. Their main results are summarized in this Final Report. Works on three last Tasks were carried out during Stage 3, their results are represented in this Final Report in sufficient details.

In the present report have grouped obtained data for each wavelength λ of EM radiation. Surface MW discharges are singled out in a special section in it.

2. Preliminary information about MW discharge in quasi-optical EM beam

Main preliminary information about pulsed MW discharge in quasi-optical EM beam was obtained with a help of a setup with the wavelength $\lambda = 8.9$ cm at $\tau_{pul} \le 40$ μs , $E_0 \le 6.5$ kV/cm and in pressure range $p = 3 \div 760$ Torr.

In investigations [3] we have developed of local field $\boldsymbol{E_0}$ level measuring with a help of metallic ball location in investigated point. At that we measured maximum threshold air pressure $\boldsymbol{p_b}$, , at which MW breakdown was realized. After this we calculated the field amplitude $\boldsymbol{E_0}$ with a help of specially developed method.

We have developed a method of discharge initiation at initial field level $\boldsymbol{E_0}$ in EM beam that was smaller and much smaller than the minimum breakdown critical field value $\boldsymbol{E_{cr}}$ necessary for self-maintained electrodeless air breakdown at the given pressure $\boldsymbol{p}$. At that we used either a metallic ball or a thin metallic cylindrical EM vibrator with axis parallel to the vector $\boldsymbol{E_0}$.

In this chapter below we describe types of MW discharges in quasi-optical MW beam known from preliminary investigations and some main properties of them.

2.1. MW discharge types in different $E_0 - p$ regions

In Fig.**2.1.1** in coordinates $\mathbf{E_0 - p}$ one can see existence regions of different MW discharge types revealed experimentally. Typical "integral" discharge photo is placed in each region, this photo was obtained at exposure time greater than $\boldsymbol{\tau_{pul}}$. These photos illustrate principle differences of the discharge appearance in different regions.

Line **I** in **Fig.2.1.1** shows $\boldsymbol{E_{cr}(p)}$ dependence and is an analog to Paschen curve in MW range of EM field. Self-maintained electrical MW air breakdown is possible above it in spatially uniform and continuous field. Such a breakdown is impossible below it, but it can be initiated.

Line **II** separates diffuse types of MW discharge and discharges that can be conditionally called streamer MW discharges.

Diffuse discharges are realized at comparably low air pressure $\boldsymbol{p}$. They can be divided into separate diffuse plasma formations. This reveals ionization-field processes of plasma EM field interaction. These discharges interact energy-ineffectively with the field exciting them. EM radiation either is reflected from the discharge area boundary or propagates though it with weak attenuation.

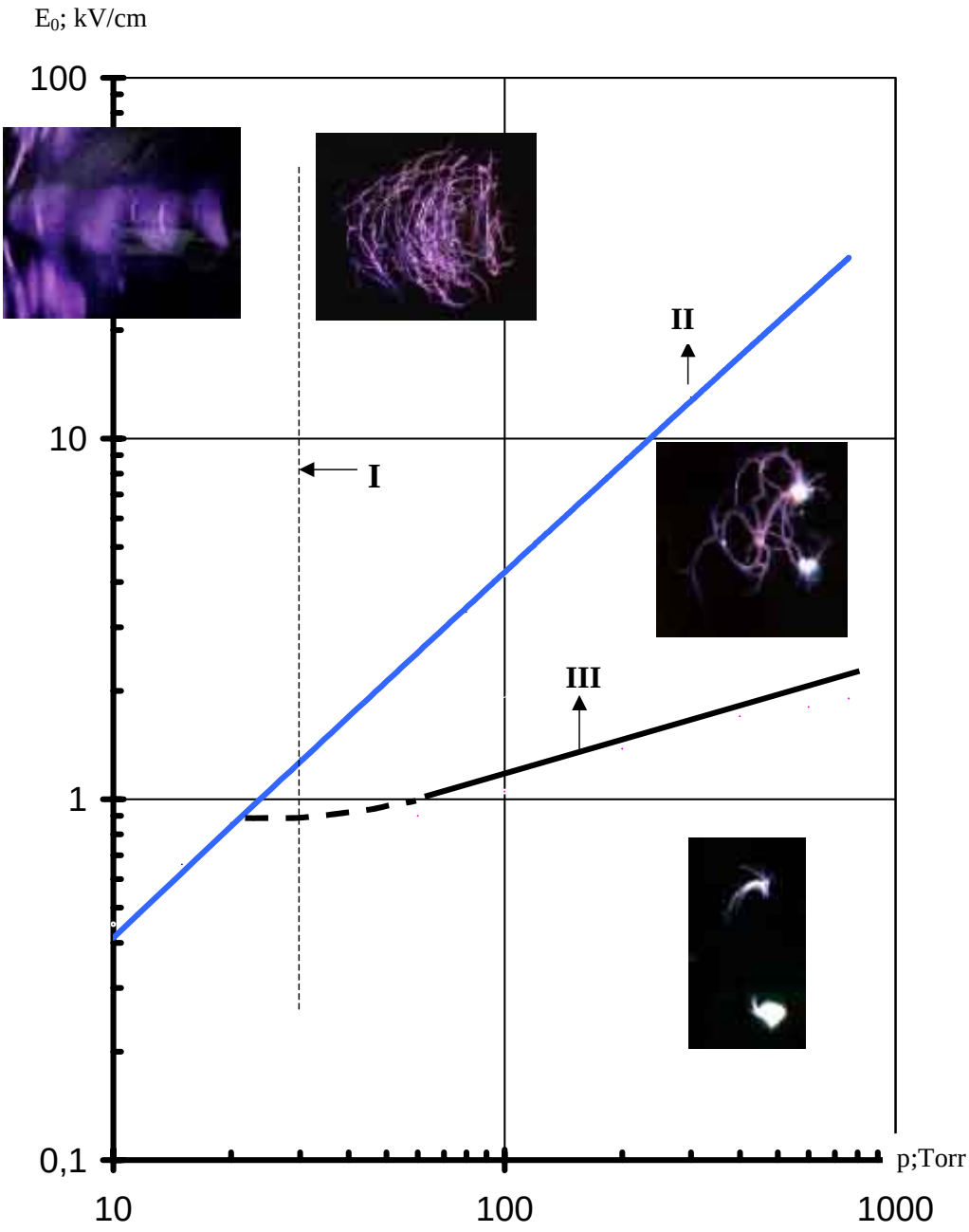

Fig.2.1.1. Existence regions of different MW discharge types in air with respect to MW field level and air pressure at λ = 8.9 cm

In Fig**. 2.1.1** one can see that MW discharge in the streamer type is realized at high pressure ***p*** . It represents a system of thin plasma channels in integral photos. First of all ionization-overheating processes in plasma and Ionization-field processes essentially impact its formation Investigations have shown that MW discharge in this form interacts with EM field exciting it energy-effectively.

Free localized streamer discharge in the overcritical field can be technically realized at comparably high pressure ***p*** only at p<100 Torr. This is connected with technical limitations of comparably high power $\boldsymbol{P_{MW}}$ generation even with a help of pulsed MW generators. However, experience has shown, see **Fig. 2.1.1**, that MW discharge in the streamer form with spatially developed structure can be realized also in the undercritical field at $E_0 < E_{cr}$. In this figure one can see its photo at breakdown initiation with a help of linear EM vibrator. In the photo it is vertical and to the right. This discharge is originated near vibrator's poles where $E_0 > E_{cr}$. Then discharge channels begin to grow and branch. They propagate mainly towards EM radiation to EM beam area

with $E_0 < E_{cr}$. A mechanism of their growth is analogous to a mechanism of streamer discharges propagation in a constant field of low level. They grow due to local field reinforcement up to a level of $E_0 > E_{cr}$ at ends, heads of plasma channels. Namely because of this analogy such MW discharges were called the streamer ones.

Plasma streamer channels loose their capability to separate from the initiator's poles and create volumetrically developed structure in the deeply undercritical field with $E_0 << E_{cr}$. They stay attached to the poles - initiator ends during the whole time of EM field existence. These discharge we call deeply undercritical streamer MW discharges. Line III in Fig.**2.1.1** separates existence regions of initiated undercritical MW discharges with $E_0 < E_{cr}$ and deeply undercritical ones with $E_0 << E_{cr}$.

Namely the undercritical and deeply undercritical MW discharges can be realized in practice at high pressure values starting from p ~100 Torr up to the atmospheric pressure. At that the undercritical ones can be realized in the pulse mode with τ_{pul} of tens microseconds and the deeply undercritical ones – both in the pulsed and in continuous modes. This works is devoted to investigations namely of these discharges.

2.2. MW streamer discharge features in quasi-optical EM beam

Volumetrically developed spatial structure of the undercritical MW discharge is created due to growing and branching streamer channels, as it was indicated above. Estimates show that the growth velocity of these channels $\mathbf{v_{str}}$ lies in the range $10^5 \div 10^6$ cm/s. At that the discharge front propagation velocity $\mathbf{v_{fr}}$ in EM beam towards the radiation exceeds 10^5 cm/s. Both these values exceed sound velocity $\mathbf{v_s}$ in air. We conducted a special experiment for testing of this estimate. The discharge region in it was blown by a high-speed flow with a velocity of $v_{fl} = 5 \cdot 10^4$ cm/s. It is substantially lower than $\mathbf{v_{str}}$ and $\mathbf{v_{fr}}$, so it does not have to essentially influence the discharge structure. Experiments confirmed this supposition, this is illustrated by Fig.**2.2.1**.

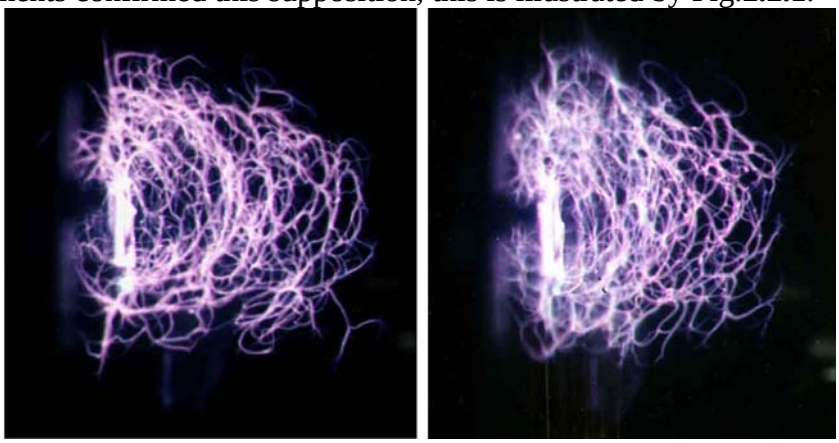

Fig.2.2.1. MW streamer initiated undercritical discharge structure appearance in dead air (to the left) and in air flow with $v_{fl} = 5 \cdot 10^4$ cm/s (to the right).

Energy efficiency of MW streamer discharge interaction with EM field exciting it is conditioned by EM resonance phenomenon.

Plasma channels of the undercritical discharge with volumetrically developed structure are stretched mainly along the vector $\boldsymbol{E_0}$. A length of the plasma channel separate section $\boldsymbol{2L}$ is comparable with $\boldsymbol{\lambda/2}$. Such channels posses resonance properties. Area of their interaction with EM field is approximately equal to $\boldsymbol{(\lambda/2)^2}$. At that the energy intercepted by the plasma EM vibrator is localized in the plasma channel only. So the local density of energy putted into a gas is very high in it. Estimates sow that the air temperature in these plasma sections can reach several thousands of Kelvin degrees. The vibrator itself and plasma channels localized near its poles form a resonance system in the case of the deeply undercritical discharges initiated by EM vibrator. Their temperature

can also reach several thousands of Kelvin degrees. In order to confirm this supposition we undertook a special experiment. A stoichiometric air-propane flammable mixture was injected to the discharge areas in this experiment, as it is shown in **Fig.2.2.2** and **Fig.2.2.3**. Its ignition temperature exceeds 10^3 °K. MW discharges in the undercritical and deeply undercritical forms have ignited this mixture.

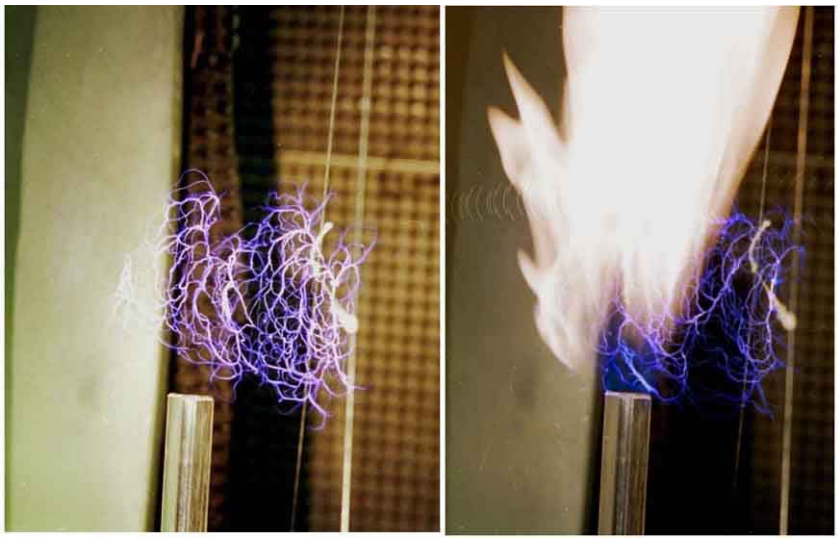

Fig.2.2.2 Undercritical streamer MW discharge in dead air at p=760Topp (to the left) and at presence of flammable mixture stream (to the right)

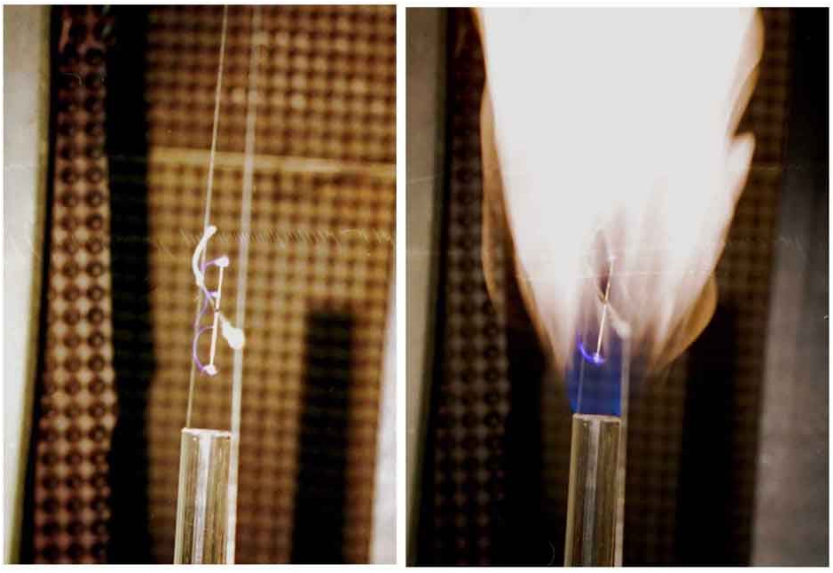

Fig.2.2.3 Deeply undercritical streamer MW discharge in dead air at p=760Topp (to the left) and at presence of flammable mixture stream (to the right).

3. Experimental set ups

Three experimental set ups were used during the present investigations. Quasi-optical EM beams with $\lambda = 8.9$ cm, $\lambda = 2.5$ cm and $\lambda = 12.5$ cm were formed by them. In this section will describe in details their main elements. Equipment applied in each definite experiment will be described in a corresponding section.

All the applied set ups in principle include the following main elements : MW generator and a power source; elements forming quasi-optical EM beam and insuring its inlet to a hermetic

chamber; a hermetic chamber; MW discharge is realized in its central area; auxiliary and measuring equipment; a source of pulsed ultra violet (UV) radiation located in the chamber outside EM beam; devices synchronizing functioning of different elements of the set up.

3.1. Setup with λ = 8.9 cm

In Fig.**3.1.1** one can see a scheme of the set up, in which working area we form quasi-optical EM beam with λ = 8.9 cm [3]. A photo of its appearance is represented in Fig. **3.1.2**.

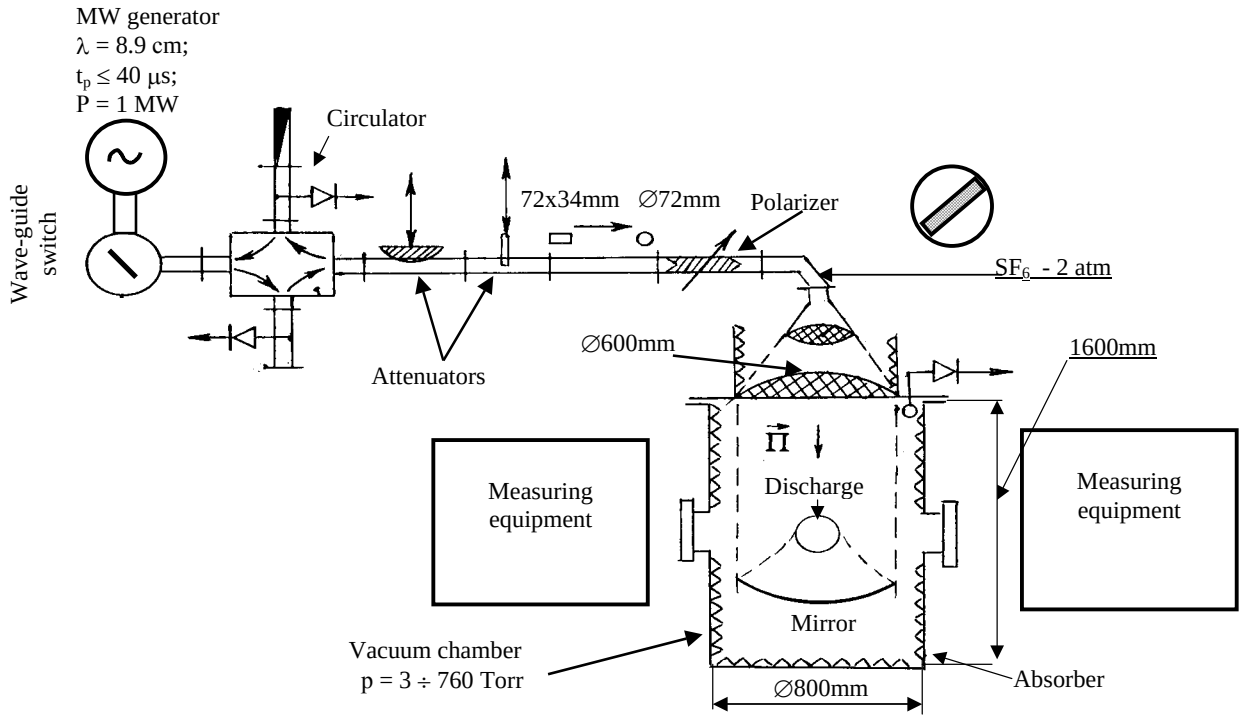

Fig.3.1.1. A scheme of the setup with λ = 8.9 cm

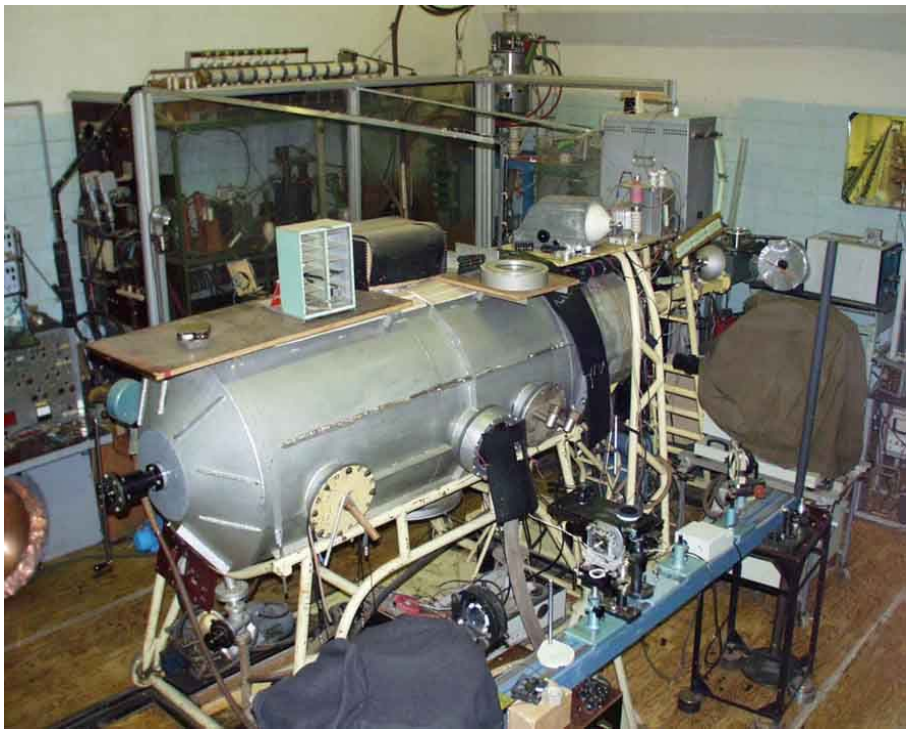

Fig.3.1.2 Setup with λ = 8.9 cm appearance

It consists of MW generator, which generates a single pulse with $\tau_{pul} \leq 40$ μs and power $P_{gen} = 1$ MW. EM propagates over a waveguide from the outlet of the generator; controlled calibrated attenuators are included into the waveguide. Linearly polarized TEM wave with a plain phase front and a transversal cross section size of 60 cm comes to the hermetic "EM echoless" working chamber through the corresponding lens system. A wave falls on a concave surface of a metallic mirror and it is focused in a central area of the chamber. Typical transversal sizes of the focal area are 10 cm along the vector $\boldsymbol{E_0}$ and 5 cm transversally to the vector $\boldsymbol{E_0}$ at the focus depth of 8 cm. The field amplitude in the focal area of EM beam can be set in the range $E_0 = 50 \div 6.5 \cdot 10^3$ V/cm.

A diameter of the working chamber of the set is approximately 80 cm, and its length is about 1 m. It can be opened as it is shown in Fig. **3.1.3** allowing access to a working volume. The working chamber can be pumped out down to $p \approx 3$ Torr.

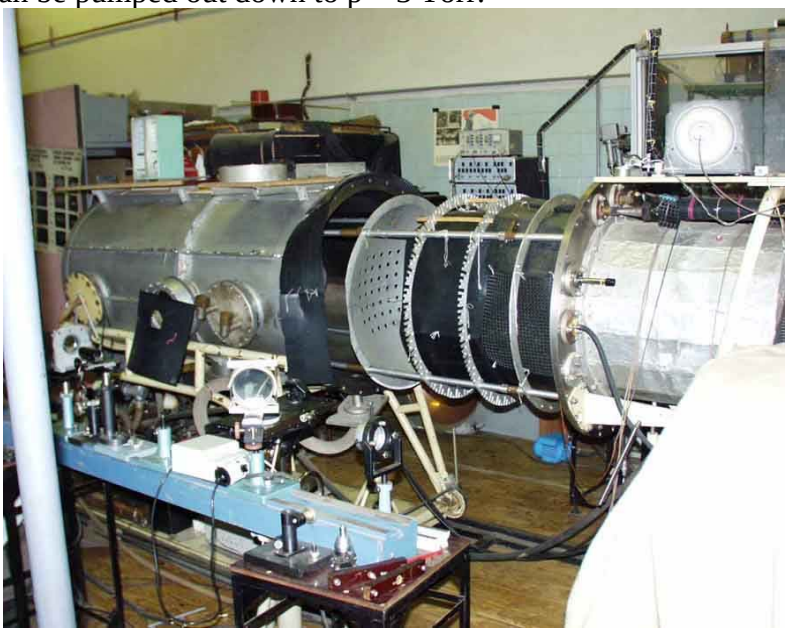

Fig.3.1.3.The appearance of the setup with λ = 8.9 cm and open working chamber

3.2. Setup with λ = 2.5 cm

In Fig.**3.2.1** one can see a scheme of the setup where we form linearly polarized quasi-optical TEM beam with λ = 2.5 cm [1]. A photo of its appearance is represented in Fig. **3.2.2**.

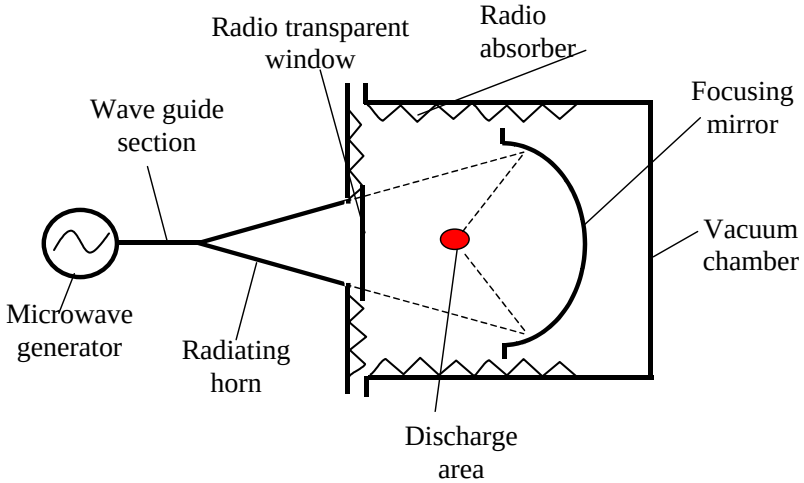

Fig.3.2.1. A scheme of the experimental setup with λ = 2.5 cm

Fig.3.2.2. Setup with λ = 2.5 cm appearance

MW generator is included in a composition of the set up. It generates pulses with a pulse time τ_{pul} in a range 1÷36 μs at pulsed power $P_{gen} \approx 100$ kW. P_{gen} is not controlled in this set up. Pulses can be either single or they can have a regular repetition frequency $f_{rep} \leq 100$ Hz. EM wave from an outlet of the generator propagates along a waveguide. With a help of a horn with an outlet diameter of 82 mm it is irradiated in a hermetic «EM echoless» working chamber. EM wave in the chamber irradiates a concave surface of the focusing mirror with a diameter of 250 mm. Its photo is represented in Fig.**3.2.3**.

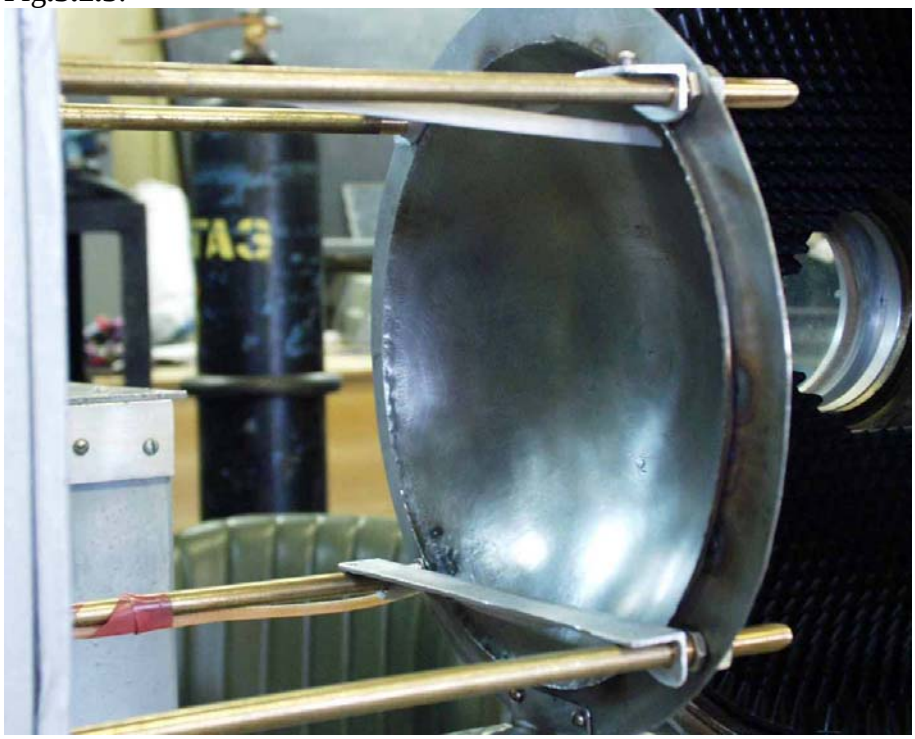

Fig.3.2.3. Focusing mirror appearance

It is concentrated in a central area of the chamber after reflection from the mirror. A scale of EM beam focal area transversal sizes typical sizes is 15 mm. The beam is modulated in the

longitudinal direction over an amplitude with typical period also approximately equal to 15 mm. The field amplitude in the focus reaches $E_0 \approx 3.7$ kV/cm.

A diameter of the working chamber of the setup is approximately 34 cm, and its length is about cm. It can be opened allowing access to a working volume. The working chamber can be pumped out down to $p \approx 3$ Torr.

3.3. Setup with $\lambda = 12.5$ cm

In Fig.**3.3.1** one can see a scheme of an experimental setup where we form linear polarized quasi-optical TEM beam with $\lambda = 12.5$ cm [4]. A photo of its appearance is represented in Fig.**3.3.2**.

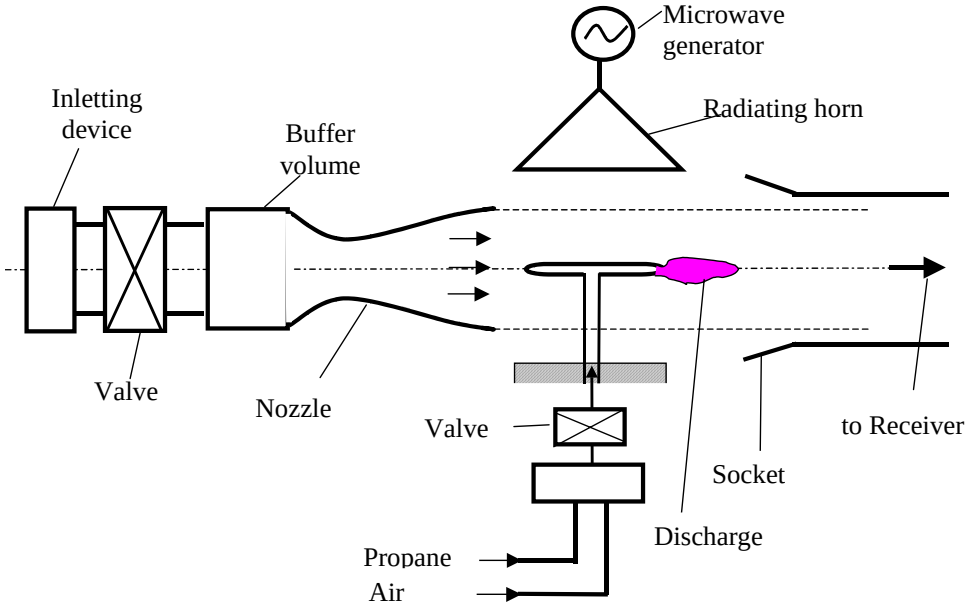

Fig.3.3.1. A scheme of an experimental setup $\lambda = 12.5$ cm

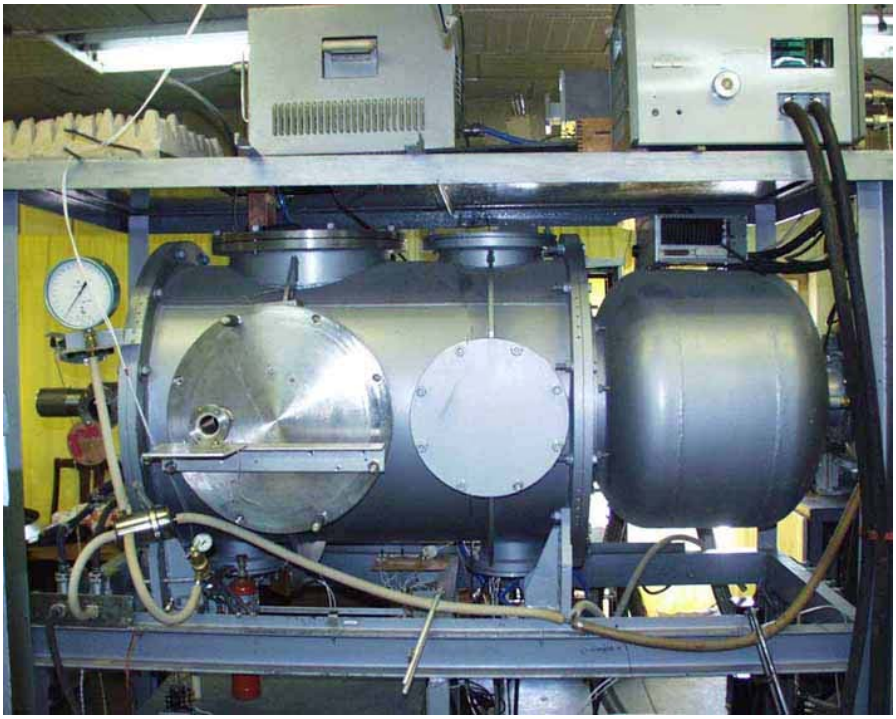

Fig.3.3.2. Appearance of the setup with $\lambda = 12.5$ cm

MW generator with outlet power of $P_{gen} \leq 2$ kW is included in a composition of this set up. It allows to work in a continuous mode. EM wave from an outlet of the generator propagates along a waveguide. With a help of a horn it is irradiated in a hermetic «EM echoless» working chamber. The horn has rectangular radiating opening with a size 9x9 cm. Experiments are carried out in a near radiation zone of the horn at a distance of approximately 8 cm from its opening. Linearly polarized field amplitude in this cross section is $E_0 \sim 100$ V/cm. A special commutator sets EM radiation duration in a range of units of a second.

The working chamber represents a horizontal cylinder, its diameter is 70 cm and a length is 1 m. It can be pumped out down to $p \approx 3$ Torr.

A Laval nozzle is located in one of the cylinder flanges. Air leaking from the atmosphere to the preliminary pumped out chamber can be realized through it. The chamber in this case is connected with a hermetic receiver, which volume is about 4 m^3. The nozzle can form a cylindrical submerged high-speed air stream (along the chamber axis at the preliminary pumped out chamber) down to $p \approx 100$ Torr. The process duration is approximately 1 s, at stream velocity $v_{fl} \approx 500$ m/s, and at static temperature T = 150 °K, i.e. at Mach number M = 2. The stream axis crosses EM beam axis at right angle.

4. MW discharge features in quasi-optical EM beam with $\lambda = 8.9$ cm

In frames of this work we additionally to already made investigations studied an influence of air humidity and water aerosol presence in air on a breakdown threshold, spatial and temporary characteristics of MW discharge in quasi-optical EM beam with $\lambda = 8.9$ cm (Tasks 3 and 4). The results of these investigations reflected in detail in the annual Report for the 1-st Stage [1] were reported at the Conference [5].

4.1. Experimental conditions in dead air at its different humidity

A scheme of the setup in a configuration allowing to investigate MW discharge in EM field in dead air at different values of its humidity is represented in Fig.**4.1.1**. It includes: a device of the working chamber filling by dry air; a device insuring air humidity variation in the working chamber; humidity sensor and a device controlling a temperature in the chamber.

The chamber was initially is pumped out down to p = 3 Torr during experiments, then it is filled by the atmospheric air up to required pressure ***p*** through a special drier. The drier represents a ceolite filled capacity.

For insuring of atmospheric composition air required humidity a special device was located in the working chamber outside EM beam under its focal area. It represents a vessel partially filled with water. There is a small hole in its upper cover. An electric heater is located inside the vessel. A voltage comes to it from a regulator placed outside the chamber. One With a help of this regulator one selects such a temperature of the heater that the water in the vessel is boiling at the set pressure ***p*** . Vapor generation in the air volume of this vessel is incurred at boiling. The vapor going from the hole in the cover gradually changes humidity in the working chamber. Relative humidity value ***RH*** growth rate is some % units per minute.

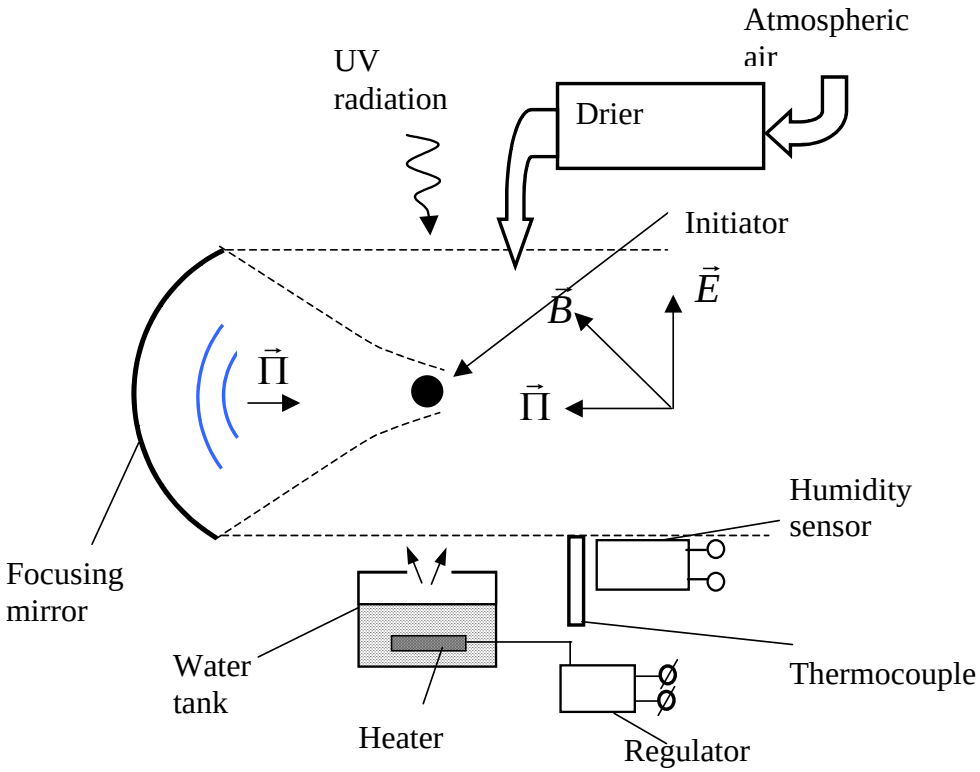

Fig.4.1.1. A scheme of humidity variation and control in the working chamber

Air humidity percent %*RH* in the chamber was measured by an electrical scheme made on a basis of "Honeywell" company sensor IH-3602L. Measuring unit %*RH* is a miscellaneous unit. During physical investigations it is more convenient to use a ratio of volumetric weight humidity content in air and air density - $\eta = \rho_{H_2O} / \rho_{aer}$. At that $\eta = 1.4 \cdot 10^{-2}$ corresponds to 100 %RH, or to the dew point at the atmospheric pressure and 20 °C. A special calibration has shown that measuring system readings are linearly proportional to η value in the whole experimental range of ***p***.

Since ***%RH*** depends on air temperature then for temperature control in the working chamber we placed a chromel - alumel thermocouple in the chamber at a distance of 5 mm from the IH-3602L sensor's body. Our experiments have shown that at humidity variation readings of ***T*** measurer practically did not change at a comparably large chamber's surface area being at room temperature ***T*** .

4.2. Air humidity influence on MW field minimum value ensuring electrodeless air breakdown

The electrodeless breakdown of "normal" atmospheric air was realized at maximum pressure $p \approx 100$ Torr in our experiments at realized EM beam configuration and at maximum field level in its focus $E_0 = 6.5$ kV/cm. In this connection in order to have a range for E_0 variation we undertook experiments in the humid air at $p = 50$ Torr. The experiments were carried out at constant MW pulse duration $\tau_{pul} = 40$ μs. An interval between separate pulses was not smaller than 0.5 min.

Experimental results are represented in Fig.**4.2.1** in coordinates. Here E_{br} – is a minimum value of EM field electric component in the EM beam focus, which insures air breakdown at a fixed η value. One can see that the humid air E_{br} is substantially higher than those of the dry air critical breakdown field $E_{cr} \approx 42 \cdot p$; V/cm = 2.1 kV/cm (air pressure ***p*** is in Torr in this and analogous formulas in the following text). At that E_{br} rises with η growth at fixed ***p***.

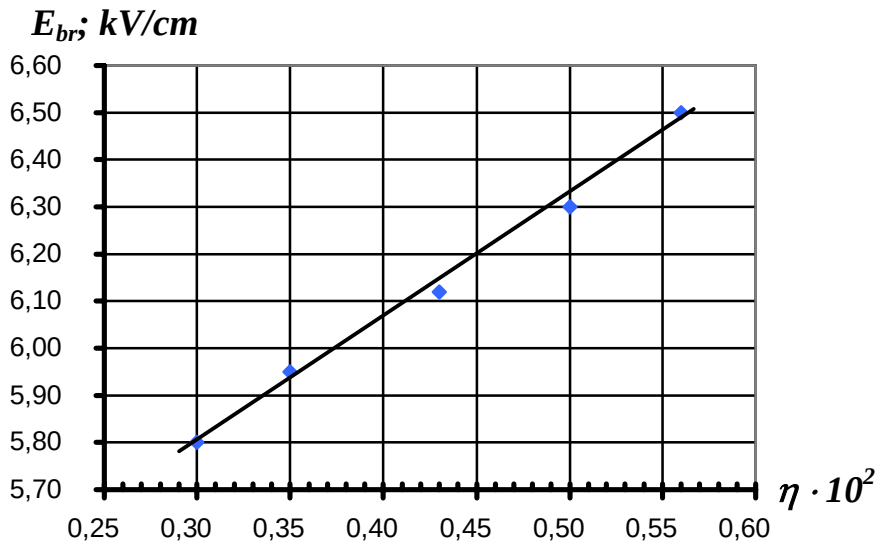

Fig.4.2.1. Breakdown electric field strength E_{br} experimental dependence via mass moisture content η in air

This result can be explained by, for example by, decrease of free electrons number in initial electron breakdown avalanche in the focal area of the setup with $E_0 \approx E_{cr}$ at increase of water molecules relative number in it. "Background" electrons in the dry air disappear only in the result of three-body attachment to oxygen molecules. They additionally are attached to water molecules in the humid air.

4.3. Air humidity influence on MW breakdown in an undercritical field at presence of EM initiator in EM beam

Electrodeless air breakdown could be realized during experiments at pressure $p \lesssim 100$ Torr, as it was indicated above. The breakdown has to be initiated at higher pressure ***p***. EM vibrator was used as an initiator in our experiments; it was located in the EM beam focus parallel to the field vector $\boldsymbol{E_0}$.

A cylindrical EM vibrator with rounded ends, a diameter of $2a = 5$ mm and a length of $2L = 20$ mm was applied in the given experiments. At $\tau_{pul} = 40$ μs it insured dry air breakdown pressures up to the atmospheric one at $E_0 = E_{br} = 4.5$ kV/cm. At that the breakdown was realized very irregularly at the given $\boldsymbol{E_0}$ in different pulses at the absence of UV illumination of one of the ionizing vibrator's poles. The breakdown is fixed in each pulse at presence of UV illumination. At that the minimum breakdown field $E_{br} = 4.5$ kV/cm did not change with air humidity growth up to its 100 % value.

Obtained result is natural in some sense. Field amplification at ionizing vibrator poles is determined only by its geometry and it does not depend on air humidity. A number of photoelectrons originated near vibrator's pole surface in the are of amplified field also does not depend on it. A humidity influence on a rate of avalanche type electron concentration rise in this area has to be understood.

4.4. Air humidity influence on spatial characteristics of streamer undercritical and deeply undercritical MW discharges

MW discharge in quasi-optical EM beam is realized in a streamer form at a comparably high air pressure ***p*** as it was indicated earlier. MW discharge namely in this form energy effectively interacts with EM field exciting it. The streamer discharge form is conserved both in the

undercritical field at $E_0 < E_{cr}$ and in the deeply undercritical field at $E_0 << E_{cr}$ in some definite E_0 – p ranges.

In the present investigations we studied air humidity influence on an appearance of high pressure initiated MW discharges in a field with $E_0 < E_{cr}$ and $E_0 << E_{cr}$ and spatial characteristics of these discharges.

Our experiments have shown that air humidity practically does not influence characteristics of investigated discharges up to its 100 % level. They stay to be the streamer ones.

Front propagation velocity $\mathbf{v_{fr}}$ of the undercritical discharges with spatially developed streamer structure towards EM radiation exciting it is insignificantly decreased. For example, in Fig. **4.4.1** one can see integral photos of the undercritical discharge in atmospheric pressure air at τ_{pul} = 40 μs, E_0= 6.5 kV/cm, η= $0.6 \cdot 10^{-2}$, $0.95 \cdot 10^{-2}$ and $1.3 \cdot 10^{-2}$. A scale of an image in them can be estimated by sizes of a vibrator initiating a discharge, they are 2a = 0.5 mm and 2L = 40 mm.

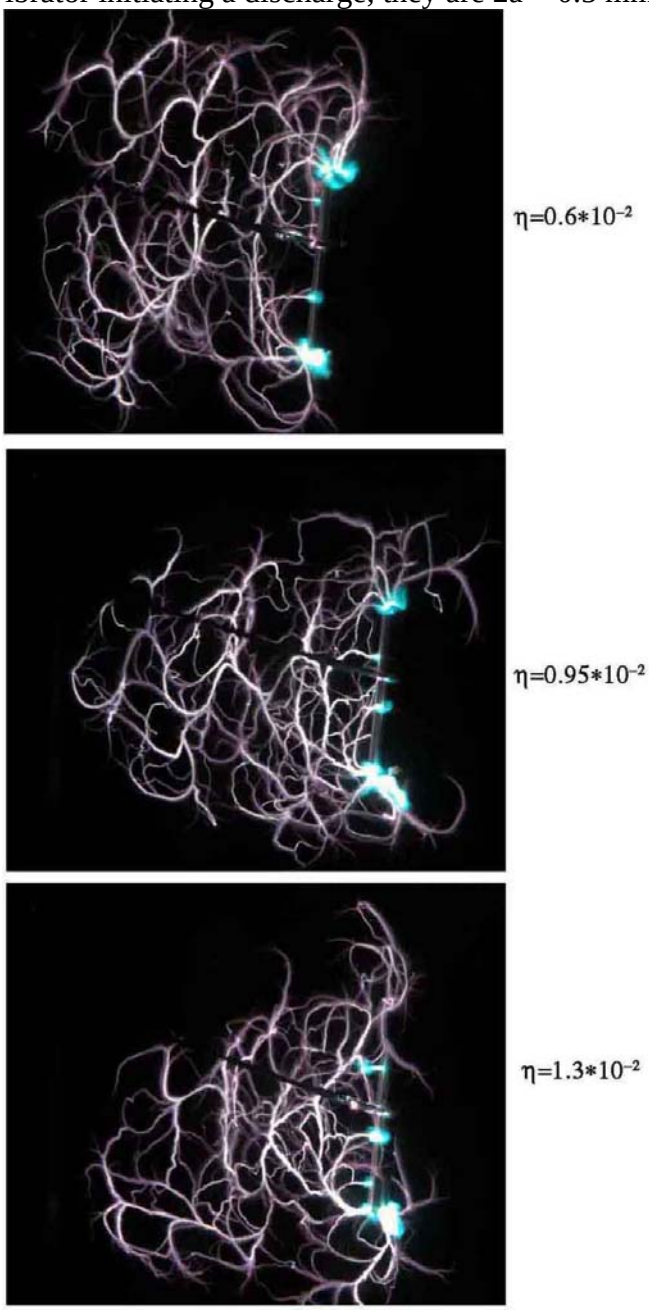

Fig.4.4.1. Typical realizations of the undercritical microwave discharge at E_0 = 6.5 kV/cm and its different humidity

Radiation in photos comes from the left to the right. Differences observed in discharge photos at different humidity are not out of the frames typical for different discharge realizations in consecutive pulses. The discharge stays to be the streamer one at the atmospheric pressure, and its qualitative and quantitative characteristics do not change noticeably.

In Fig. **4.4.2** one can see, also for example, integral photos of the deeply undercritical discharge in atmospheric pressure air, which was initiated by the same vibrator at the same humidity values but at smaller field E_0= 2.8 kV/cm. Note that pulsed streamer discharge definite spatial realizations of plasma channels forming them are different in different pulses in the dry air.

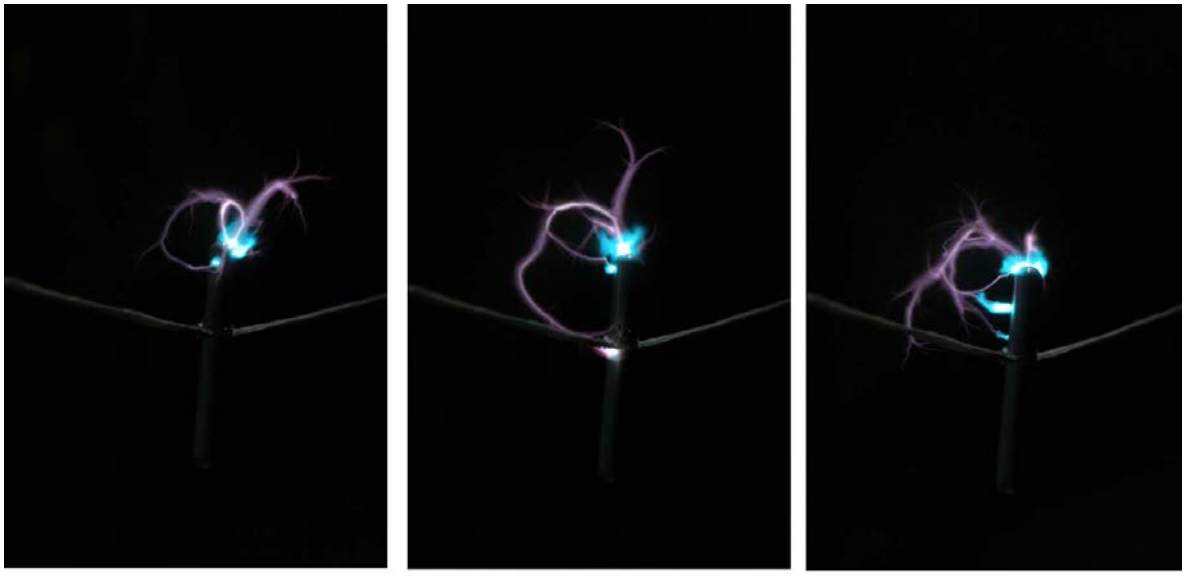

Fig.4.4.2. Typical manifistations of the deeply undercritical microwave discharge at E_0 = 2.8 kV/cm: a)-η= 0.6·10^{-2}; b)-η= 0.95·10^{-2}; c)-η= 1.3·10^{-2};

They are different also in the humid air. So there is no a possibility to analyze small variations of the deeply undercritical discharge connected with air humidity variation with a help of data in photos.

4.5. Experimental conditions in dead air at water aerosol presence in it

In Fig**.4.5.1** one can see a scheme of a device for creation of an aerosol cloud in EM beam focal area. It consists of high pressure hermetic vessel partially filled with water. A tube immersed into water is in the vessel. A hydraulic line is connected with it. An electromechanical controlled valve is included into the line. This line is put into the working chamber of the set up; one of two aerosol spraying atomizers is set on its end. High pressure p_0 up to 6 atm is created in the high pressure vessel volume. The atomizer creates an aerosol cloud in the working chamber at the valve opening for a time period of τ_{aer} = 1 s.

We conditionally call the atomizers applied in experiments as the atomizer **1** and the atomizer **2**. They are placed over the focal area of EM beam. For example in Fig. **4.5.2** one can see photos of the atomizer **2**. The atomizer location in the working chamber with respect to the EM vibrator (with 2a = 5 mm and 2L = 40 mm) initiating MW discharge is clear from the photos. The aerosol cloud is distinguishable in the photos.

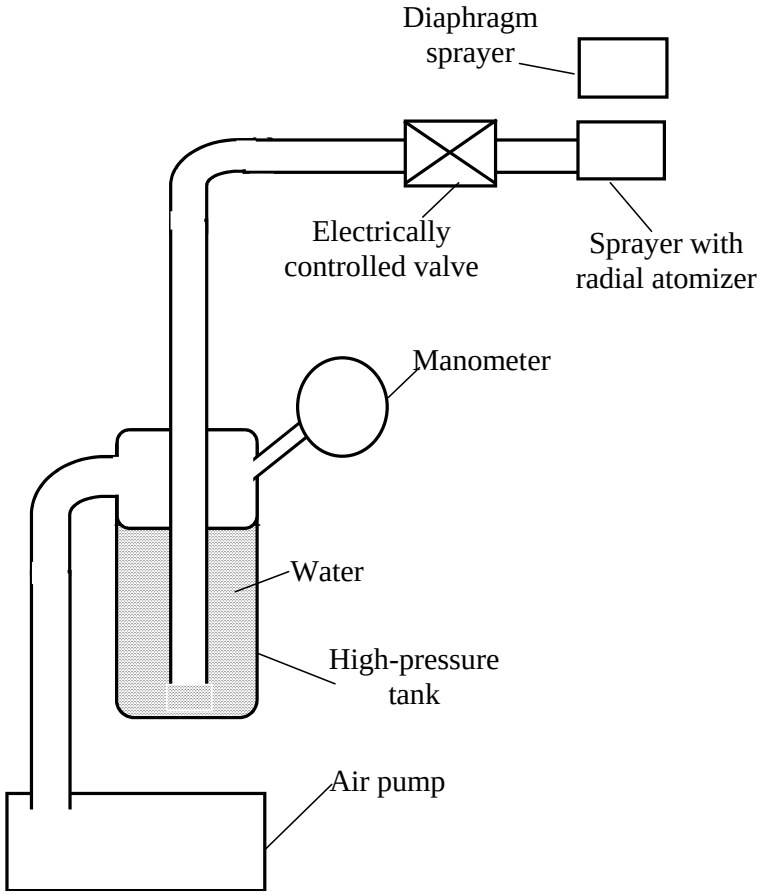

Fig.4.5.1. A scheme of a device for an aerosol cloud creation in the EM beam focal area

.

Fig.4.5.2. The atomizer 2: left photo –the appearance, right photo the displacement in the working chamber

By a special experiment we estimated maximum aerosol particle concentrations $\boldsymbol{n_{aer}}$ and the corresponding average diameters of water particles $\boldsymbol{d_{aer}}$ for both the atomizers. The experiment has

shown that the concentration n_{aer} rises with rise of p_0 , but d_{aer} – decreases. Main experiments were carried out at the absolute value p_0 = 4 atm. Control experiment scheme is represented in Fig. **4.5.3**. An aerosol beam in was collimated by a slot, and it had a thickness of about 8 mm in an area of EM vibrator.

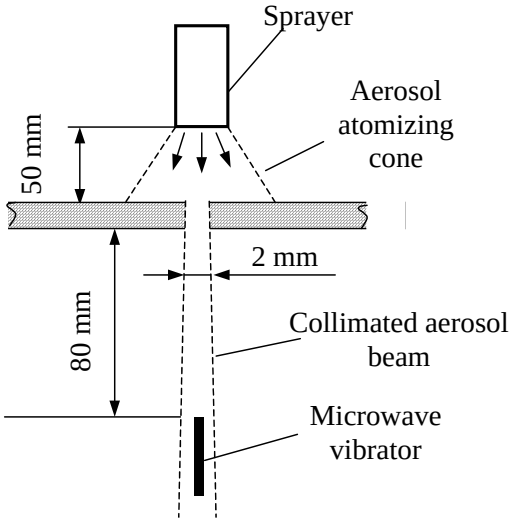

Fig.4.5.3. Control experiment scheme on measurements of n_{aer} and d_{aer} in aerosol.

The beam was photographed with exposure time about of 250 μs, this practically allowed to "freeze" positions of particles in the photo. In Fig.**4.5.4** one can see the corresponding photos obtained with a help of two atomizers.

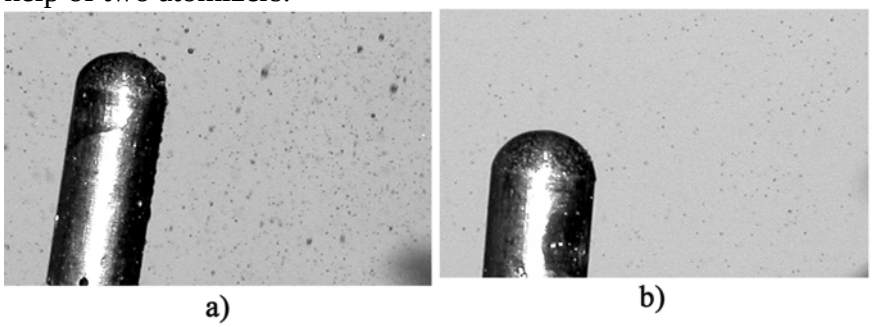

Fig.4.5.4. Fragments of aerosol clouds created by the atomizer 1 (a) and by the atomizer 2 (b)

The experiment has given $n_{aer} \approx 10^3$ 1/cm^3 at $d_{aer} = 60 \div 120$ μm for the atomizer **1**; and $n_{aer} \approx 2 \cdot 10^2$ 1/cm^3 at $d_{aer} = 50 \div 80$ μm for the atomizer **2**.

4.6. Influence of aerosol presence in air on MW breakdown

Aerosol particles were created during experiments only at air atmospheric pressure. The maximum possible field in the focus of EM beam, E_0 = 6.5 kV/cm, does not insure electrodeless breakdown at this pressure ***p***. Because of it experiments on MW breakdown at aerosol presence in air have been carried out only with initiated discharge both with the undercritical at $E_0 < E_{cr}$ and with deeply undercritical ones at $E_0 << E_{cr}$.

Experiments were carried out with a help of EM vibrator made of aluminum, with 2a = 5 mm (this size at photos represented below can be a scale of an image) and 2L = 40 mm at τ_{pul} = 40 μs. Experimental results did not repeat in consecutive EM pulses as usual in the absence of the vibrator surface UV radiation, so experiments were carried out only at presence of UV illumination. Air without aerosol particles in it was broken at minimum value $E_0 = E_{br}$ = 1.5 kV/cm with this Em vibrator initiating a discharge.

Air drops constituting the aerosol at its generation were deposited on the surface of the vibrator as it is shown in Fig.**4.6.1**. Because of it initial experiments were carried out in a single mode. The surface of EM vibrator initiating a discharge was dried in this mode between the consecutive MW pulses. Experiments that were carried out in this formulation have shown that aerosol presence in air (realized by both atomizers) did not lead to variation of $\boldsymbol{E_{br}}$. MW breakdown was initiated still at the minimum amplitude E_{br} = 1.5 kV/cm of EM field electrical component in the focal area of EM beam.

Fig.4.6.1. Appearance of the initiating vibrator surface covered by separate water aerosol particles deposed on it

Drops deposited on the surface of the vibrator begin to coalesce at several switching on of the aerosol source with intervals equal to several seconds between pulses. They created water film on it as it is shown, for example, in Fig.**4.6.2**. The experiments have shown that this film presence did not change $\boldsymbol{E_{br}}$. A stability of a breakdown process in consecutive MW pulses also remained. There arose some interpretation definite difficulty of initial electrons generation photoelectric effect from the water surface, cause by UV irradiation of it. Remember that the “red boundary” of photoelectrons from water work function lies near 200 nm.

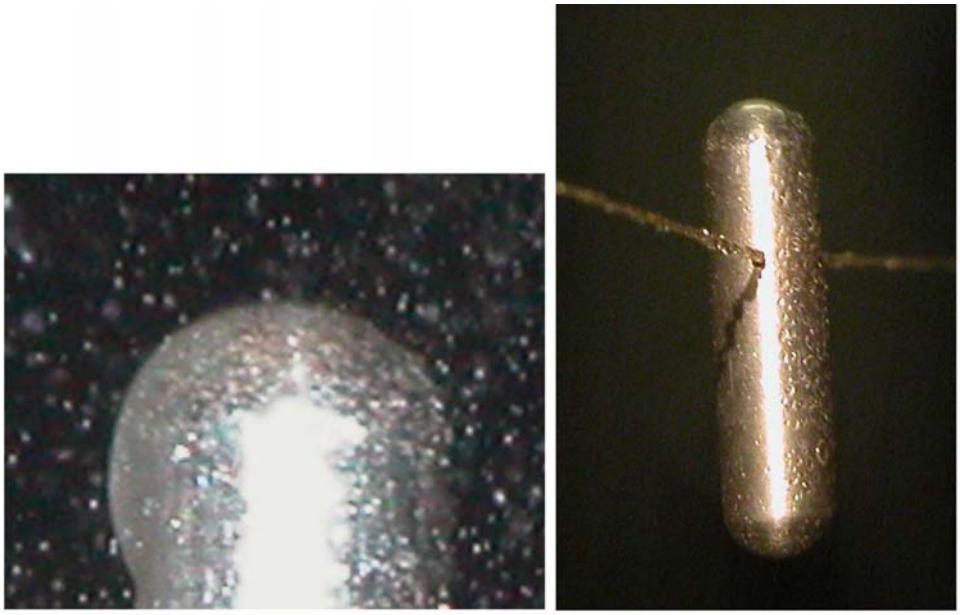

Fig.4.6.2. Appearance of the initiating vibrator covered by deposited water aerosol separated particles coalesced into a continuous film

Water drops appear on the vibrator poles at following increase of consecutive switching on of the aerosol source as it is, for example, shown in Fig.**4.6.3**. $\boldsymbol{E_{br}}$ value in this case decreases at the drop presence in the range of experimental data reliability level, i.e. in the range of 10 %. This result can be sufficiently explained. Water is characterized by a very high dielectric permittivity

Fig.4.6.3. Appearance of the initiating vibrator surface with a drop on a pole.

coefficient $\varepsilon \approx 80$, and it behaves practically as metallic material in EM field. So a small surface deformation of initiating EM vibrator pole surface made by a water drop leads to insignificant change of $\boldsymbol{E_{br}}$ value.

4.7. Influence of aerosol presence in air on spatial and temporary characteristics of streamer undercritical and deeply undercritical MW discharges

Initiating EM vibrator with 2a = 5 mm and 2L = 20mm was applied in the present investigations. $\boldsymbol{E_0}$ variation at these sizes of the initiating EM vibrator allows to realize both the undercritical with $E_0 < E_{cr}$, and the deeply undercritical with c $E_0 << E_{cr}$ initiated MW discharges.

The experiments have shown that MW discharge at air atmospheric pressure and at presence of water aerosol in it continues to keep its streamer form. Since the discharge appearance in experiments at aerosol presence qualitatively did not varied at change of the atomizer type and its work mode then we executed main experiments with the atomizer **2** at $p_0 = 4.5$ atm.

Spatial and temporary characteristics of the streamer undercritical discharge in air at water aerosol presence in it were investigated by a variation of $\boldsymbol{\tau_{pul}}$. For example in Fig. **4.7.1** one can see integral photos of this discharge with exposure time $\tau_{exp} >> \tau_{pul}$ at $E_0 = 4.5$ kV/cm $< E_{cr} = 30$ kV/cm and at $\tau_{pul} = 40$, 30, 20 and 10 μs. The photos are represented in pairs: the left ones are without aerosol, the right ones are at aerosol presence in air. EM radiation in them comes to the discharge area from the left, and the $\boldsymbol{E_0}$ vector in EM beam is parallel to EM vibrator axis, i.e. it is vertical, as it was indicated above.

It follows from the photos that spatially developed discharge structure is formed by growing and branching streamer channels also at aerosol presence in air. Channels mainly grow towards EM radiation exciting the discharge. Streamer channels spatial configuration does not remain in consecutive pulses. Undercritical discharge with volumetrically developed streamer structure front propagation velocity keeps a scale of $v_{fr} \approx 10^5$ cm/s. At the same time it is for about of 25 % smaller than this discharge type velocity in air without aerosol. Separate section of the streamer plasma channels comparable with $\boldsymbol{\lambda/2}$ have brighter glow. At that in clean air their color is pink-violet and blue tint appears in air with aerosol. Plasma channel transversal size, i.e. a diameter, is somewhat larger in air with aerosol. For example in Fig..**4.7.2** we represent undercritical discharge structure comparable fragments in the same scale in pure air and in air with aerosol.

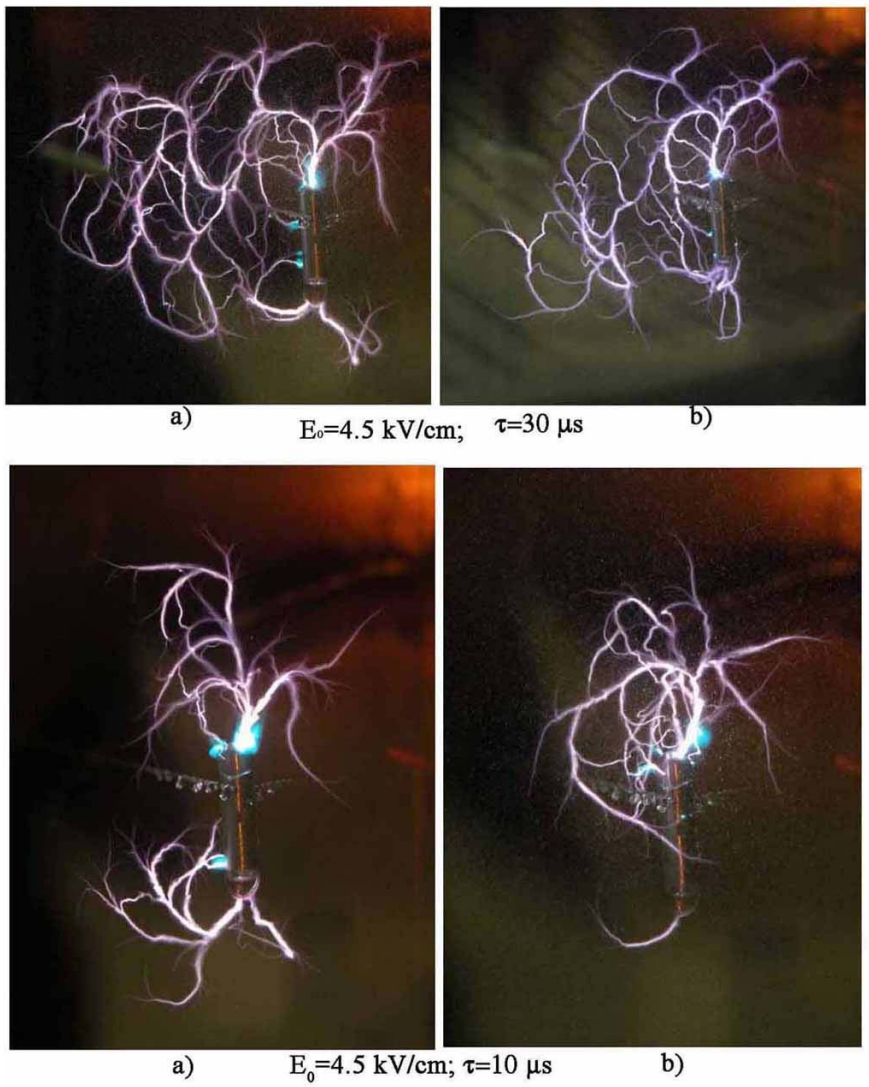

Fig.4.7.1. The undercritical discharge in a field with E_0 = 4.5 kV/cm: a)- a discharge in air; b)- a discharge in water aerosol

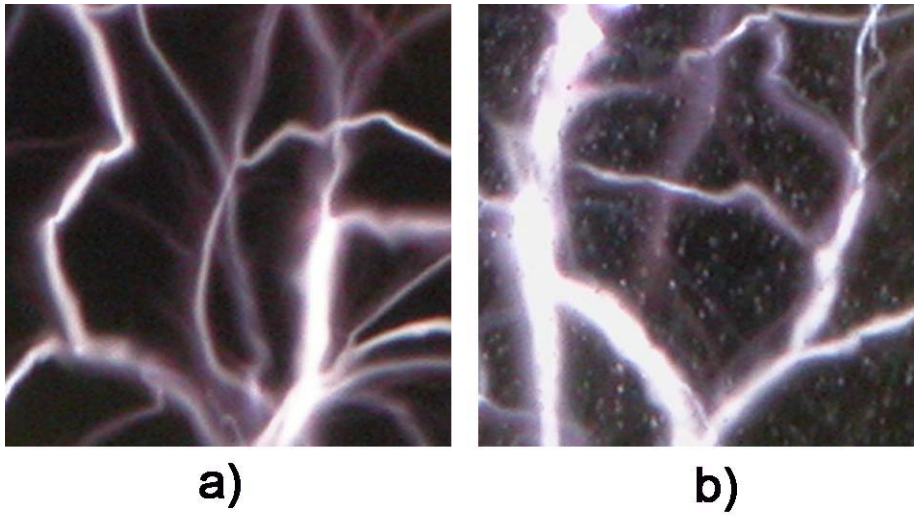

Fig..4.7.2. Undercritical discharge structure fragments in the field E_0= 4.5·10^4 V/cm at τ = 40 μs: a)- a discharge in air; b)-a discharge in water aerosol

Streamer plasma channels start namely from a surface of a water drop in the case when a water drop is on a pole of EM vibrator initiating a discharge, as it is represented in Fig..**4.7.3**. This meets expressed above supposition that water acts analogous to metal material in MW field.

Fig.4.7.3. Undercritical discharge fragment near vibrator's surface at water drop in developed state on it

In Fig.**4.7.4** one can see integral photos of EM vibrator initiated deeply undercritical MW discharge at E_0 = 1.5 kV/cm << E_{cr} = 30 kV/cm and τ_{pul} = 40 μs. The left photo still corresponds to air without aerosol and the right one – to air with aerosol. It follows from them that the discharge remains to be the streamer one at aerosol presence. Its plasma channels loose a capability to separate from the initiator poles in a small field.

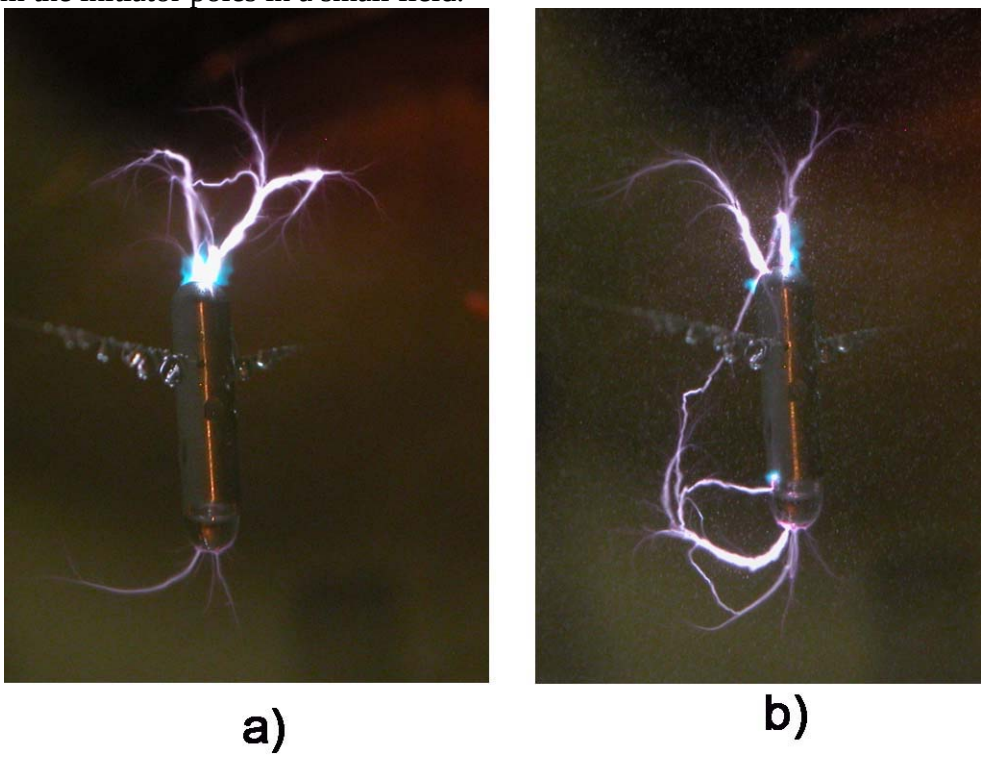

Fig.4.7.4. The deeply undercritical discharge: a) –at aerosol absence in the discharge area; b)-at aerosol presence

Channels of the deeply undercritical discharge grow from a surface of a drop at its presence near a pole of the initiator, it is analogous to the case of the undercritical discharge. For example in Fig.**4.7.5** this situation is illustrated by a photo.

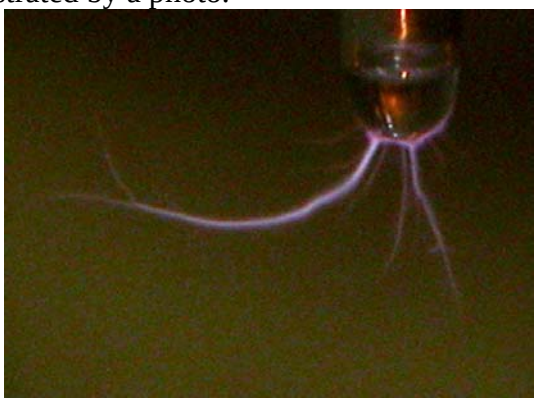

Fig.4.7.5. Undercritical discharge fragment near the vibrator's pole at water dro on it, initial state of the discharge τ_{pul} ***= 2*** μ***s***

5. MW discharge features in quasi-optical EM beam with λ = 2.5 cm

MW discharge investigations main experimental method used in the present work is essential variation of this discharge realization conditions, as it was indicated above. So if earlier we investigated this discharge in EM beam with λ = 8.9 cm, then in this part we describe results of its investigations in EM beam with substantially shorter wavelength то λ = 2.5 cm.

In the work we analyze air breakdown conditions in quasi-optical EM beam, at that we consider electrodeless discharge, its breakdown and air breakdown initiation possibility in small level fields. A possibility of this discharge realization on the streamer for has been demonstrated in experiments. We have determined a boundary over ***p***, which separates a diffuse type of MW discharge from its streamer form. $E_0 - p$ existence range of initiated streamer undercritical MW discharge with volumetrically developed structure has been determined; also we have determined $E_0 - p$ existence range of deeply undercritical streamer MW discharge, which plasma channels are "attached" to EM initiator. This discharge was realized in model propane-air mixture for air temperature estimation in streamer channel discharge plasma. We have investigated spatial and temporary characteristics of the undercritical discharge in order to determine a velocity $\mathbf{v_{str}}$ of the streamer channels composing it and its front propagation velocity towards EM field exciting the discharge. We have estimated temporary scales of processes determining MW discharge features by the discharge realization in a high-speed air flow and in a flow of model flammable mixture and in a mixture of air with water aerosol.

These investigations have been carried out on frames of Task **1**, **Task 2**, **Task 6**, **Task 10** and **Task 11**. Works on two last Tasks were carried out at Stage 3 so they are described in details in this Report. Investigation results on other Tasks are in details reflected in intermediate year Reports on the subject in Reports on Stage 1 and Stage 2 [1], [2]. They were also reported at Conferences [5], [6], [7].

5.1. Electrodeless air breakdown in quasi-optical EM beam

One method of a field visualizing in quasi-optical EM beam consists in realization of electrodeless MW discharge in it at comparably low air pressure. We used this method in described below investigations.

In Fig.**5.1.1** one can see a photo of MW discharge in the focal area of our setup at p = 10 Torr and τ_{pul}= 10 μs. A mirror focusing EM radiation in it is to the left, and a vector $\boldsymbol{E_0}$ of electric field component is vertical. One can in the photo that a field of EM beam used in the investigations is focused, and a discharge is divided separated into separate plasmoids along the axis of EM beam.

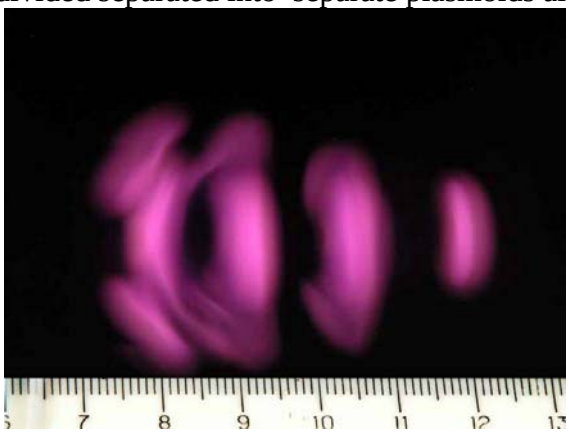

Fig.5.1.1. EM field spatial distribution picture in the focal area, which was visualized by a microwave diffuse discharge

Remember that EM beam power in the pulse can not be regulated in the applied set up. It was determined in the experiment that the maximum air pressure $\boldsymbol{p}$ lies in the range $p_{max} \approx 100$Torr, at which its electrodeless breakdown was realized. The scale of $\boldsymbol{p_{max}}$ is natural at expected $\boldsymbol{E_0}$ in the focus of EM beam, which is close to this field in the setup with $\lambda = 8.9$ cm. Indeed breakdown phenomena and discharge development in greater extent correspond to the collisional plasma with decrease of λ in experimental range of pressure $\boldsymbol{p}$. $E_{cr} \approx 42 \cdot p$; V/cm for this mode and it does not depend on λ, as it was indicated above.

5.2. MW breakdown initiation in an undercritical field

Experiments have shown that MW breakdown in the undercritical field can be initiated at this λ as well by location of a metallic ball or a metallic EM vibrator in EM beam parallel to the vector $\boldsymbol{E_0}$.

A method of breakdown initiation with a help of a metallic ball was used for determination of quantitative spatial field distribution along EM beam axis. Results of experiments are represented in Fig. **5.2.1** in a form of a graph $\boldsymbol{p_{br}(x)}$. Axis $\boldsymbol{x}$ in the graph goes along the EM beam axis and is count out from the axial point of the focusing mirror internal surface, and $\boldsymbol{p_{br}}$ was obtained at location of a metallic ball with a diameter 2a = 1.35 mm in different points $\boldsymbol{x}$.

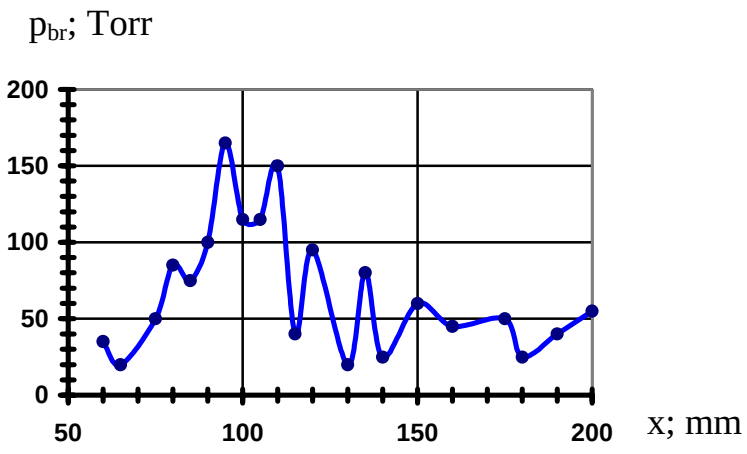

Fig.5.2.1. A dependence of Breakdown pressure p_{br} on the initiatin ball placed along EM beam axis near the focus

A method developed bus allows to recount p_{br} into the field amplitude E_0 . The corresponding graph is represented in Fig.**5.2.2**.

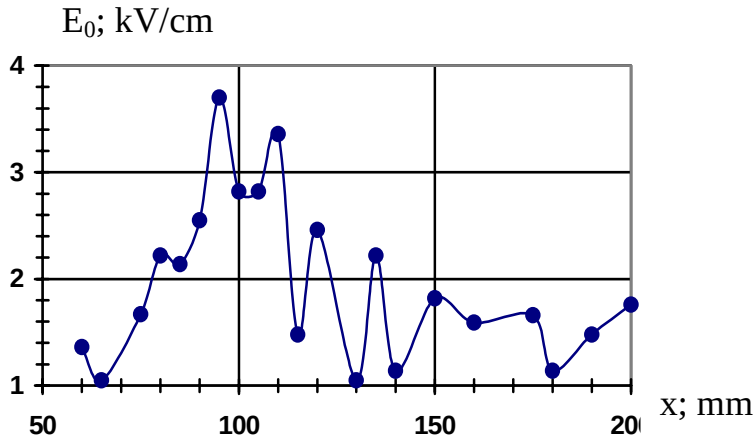

Fig.5.2.2. $E_0(x)$ dependence along EM beam axix near the focus

Air breakdown in experiments can be realized with a help of a metallic cylyndrical EM vibrator of corresponding diameter ***2a*** and length ***2L*** at p > 160 Torr up to the atmospheric pressure ***p***. At that 2a has to be naturally much less than 1/k, where a wave vector is $k=\lambda/(2\cdot\pi)$ and the maximum length is $2L\approx\lambda/2$. In Fig.**5.2.3** one can see photos of discharge initiating ball and EM vibrator located in EM beam. They are located in a given point of EM beam on a dielectric radio transparent thread.

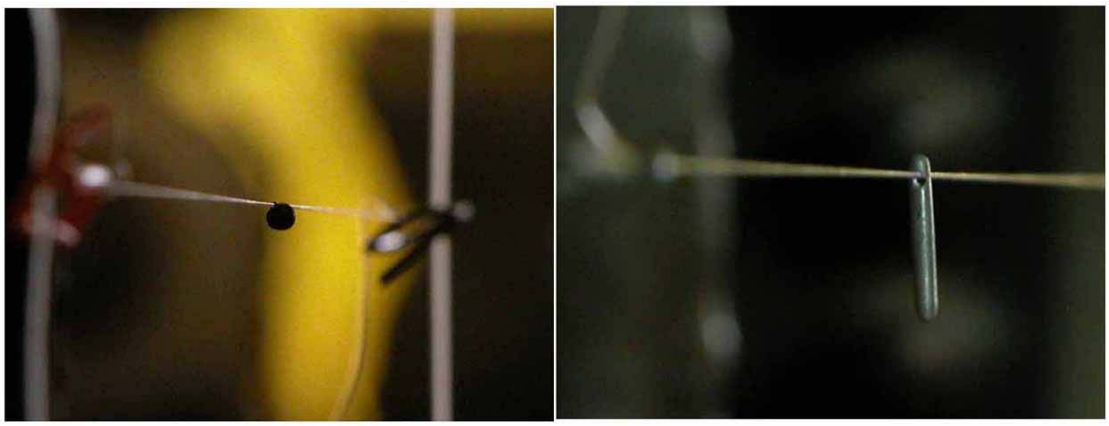

Fig.5.2.3. Fixing means of initiating ball (left photo) and initiating vibrator (right photo) in the focal area

Since it is impossible to change the pulsed power of EM beam in this setup then the discharge initiator was placed in different axial points of EM beam at discharge investigations at different values of $E_0 < E_{cr}$ or $E_0 << E_{cr}$.

5.3. A boundary dependence over pressure separating diffuse and streamer types of MW discharges

Our experiments have shown that MW discharge in the field with $\lambda = 2.5$ cm can also be realized either in diffuse or streamer form with respect to air pressure ***p***. Typical photos of free localized non-initiated discharges in a field $E_0 > E_{cr}$ in diffuse and streamer forms are represented in Fig.**5.3.1**, and of initiated by a ball at $E_0 < E_{cr}$ – in Fig.**5.3.2**. The discharge were realized at $\tau_{pul} = 36$ μs. Diffuse electrodeless discharge was realized at p = 20 Torr, and the streamer one was realized at p = 80 Torr. The initiating ball with 2a = 1 mm was located in the maximum field of the

EM beam. At that the diffuse discharge in the photo was realized at p = 50 Torr, and the streamer one - at p = 90 Torr.

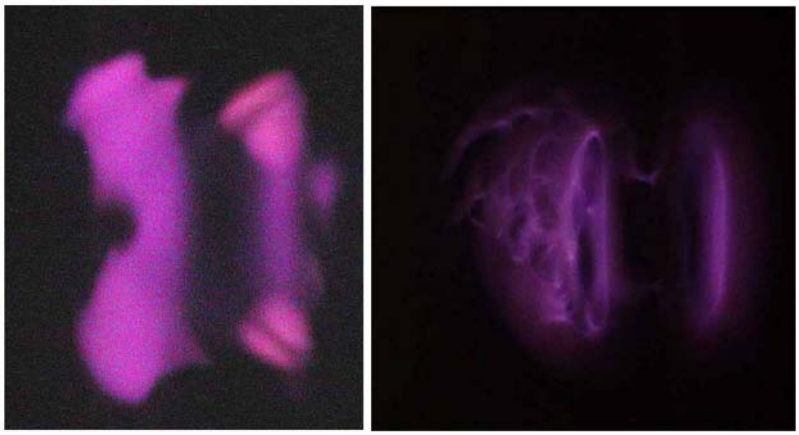

Fig.5.3.1. Typical appearance of non-initiated discharge in a diffuse form at p = 20 Torr (left photo)and in a streamer form at p = 80 Torr (right photo)

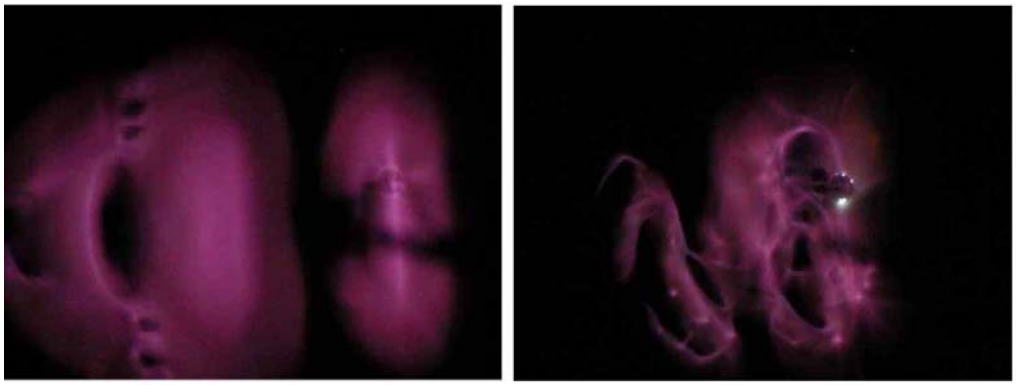

Fig.5.3.2. Photos of microwave discharge initiated by the ball with 2a = 1.35 mm: a)-the diffuse form at p = 50Torr and b)-the streamer form at 90Torr

The whole experimental series allowed to determine that the boundary pressure ***p*** separating diffuse and streamer discharge types at a given λ is in the range of $p_{th} \approx 90$ Torr. Here a sign ≈ reflects an experimental fact that this boundary is as if smoothed in the range ±10 Torr. p_{th} value at a level of experimental accuracy does not depend on discharge initiation method, i.e. it is determined by air properties only.

5.4. Streamer undercritical and deeply undercritical MW discharge types realization ranges

Experiments have shown that initiated streamer discharge in the undercritical field can be realized in undercritical and deeply undercritical forms at comparably high air pressure ***p*** both in the field with $\lambda = 8.9$ cm and in the field with $\lambda = 2.5$ cm. Their typical photos are represented in Fig. **5.4.1.** There were initiated by a vibrator with $2a = 1$ mm and $2L = 7$ mm at $\tau_{pul} = 36$ μs. The streamer channels are capable to separate from vibrator's poles still in the undercritical field with $E_0 < E_{cr}$. Growing and branching they create a volumetrically developed plasma structure. The streamer channel loose their capability to separate from vibrator's poles in the deeply undercritical field with $E_0 << E_{cr}$.

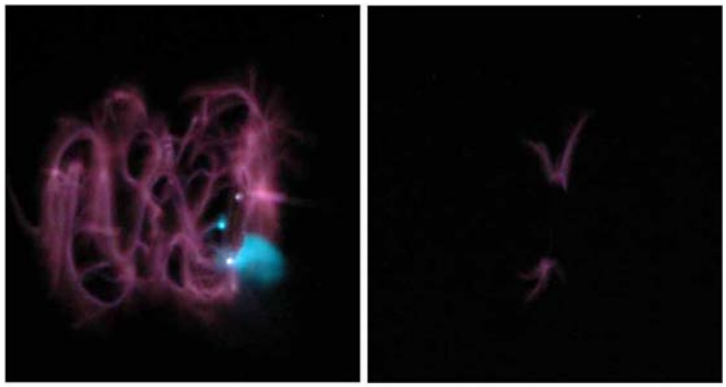

Fig.5.4.1. Photos of typical microwave discharges initiated by a vibrator with 2a = 1 mm 2L = 7 mm; a left photo corresponds to the undercritical discharge; the right photo- to the deeply undercritical discharge

E_0 - p boundary separating these discharge types was obtained at photographing of the discharge area at variation of air pressure ***p*** in experiments and at location of the vibrator in different points on the axis of EM beam.

In Fig. **5.4.2** one can see corresponding graphs showing existence areas of MW discharge different types in quasi-optical EM beams at λ = 8.9 cm and λ = 2.5 cm. Their comparison shows

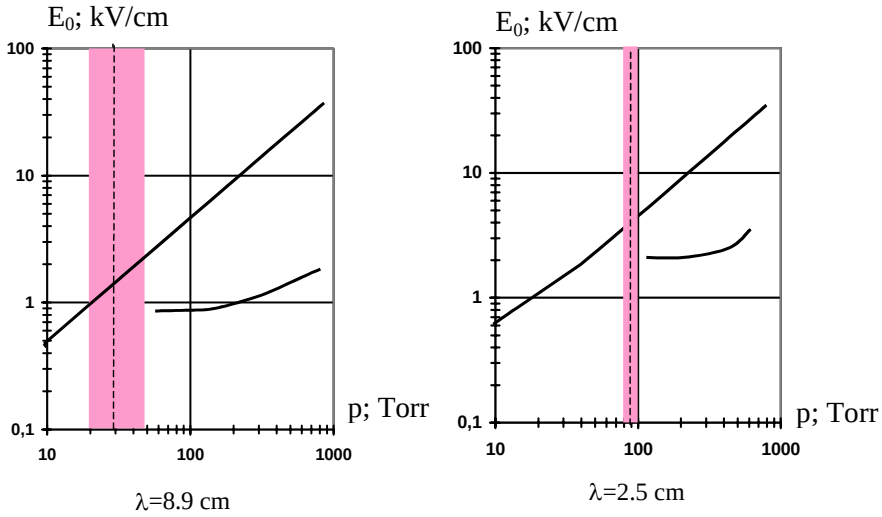

Fig.5.4.2. Existence areas of MW discharge different types in quasi-optical EM beams at λ = 8.9 cm (to the left) and λ = 2.5 cm (to the right)

that a realization area of the undercritical MW discharge with volumetrically developed structure is substantially shifted to the side of larger ***p*** and ***E_0*** at λ = 2.5 cm. One can suppose that this discharge type at p < 1 atm already will not be realized at decrease of ***λ***.

5.5. Spatial and temporary characteristics of undercritical MW discharge

It follows from Fig. **5.2.2** that EM beam realized in the experimental setup is essentially modulated over a field amplitude in a longitudinal direction. This circumstance limits possibilities of discharge area propagation velocity $\mathbf{v_{fr}}$ towards EM radiation exciting it experimental determination. The discharge area is occupied by growing and branching streamer channels of the undercritical MW discharge in the field $E_0<E_{cr}$. The discharge can not "overcome" next field minimum. And nevertheless $\mathbf{v_{fr}}$ can be estimated by the value of $4.5\cdot10^4$ cm/s with a help of the photo represented in Fig.**5.4.1**

Spatial position of the undercritical discharge streamer channels is not repeated in consecutive EM pulses, as it was indicated earlier. Photo detection of discharge series in different EM pulses allows to determine a “regularity” of separate streamer growth process. A typical photo illustrating this process is represented in Fig**.5.5.1**. Initiator’s length 2L = 12 mm can be a scale in it. In the photo one can see a typical snake-sinusoid with vertical branches. Namely, inclined sections of this snake having a small inclination angle with respect to vector $\boldsymbol{E_0}$ of the initial field insure a high energy efficiency of MW discharge interaction with EM field. A set of such snakes forms a volumetric structure of the undercritical streamer discharge in EM fields also with other investigated λ values.

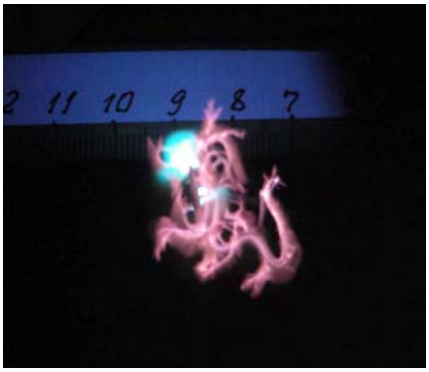

Fig.5.5.1. A photo of streamer MW discharge with typical streamer “snake-sinusoid”

A local growth velocity of definite streamer was determined in a specially formulated experiment. A duration of $\boldsymbol{\tau_{pul}}$ was varied in it at constant $\boldsymbol{E_0}$ and $\boldsymbol{p}$. In Fig**.5.5.2** one can see corresponding photos at p = 240 Torr, E_0 = 3.7 kV/cm and 2L = 12 mm. They were obtained at $\boldsymbol{\tau_{pul}}$

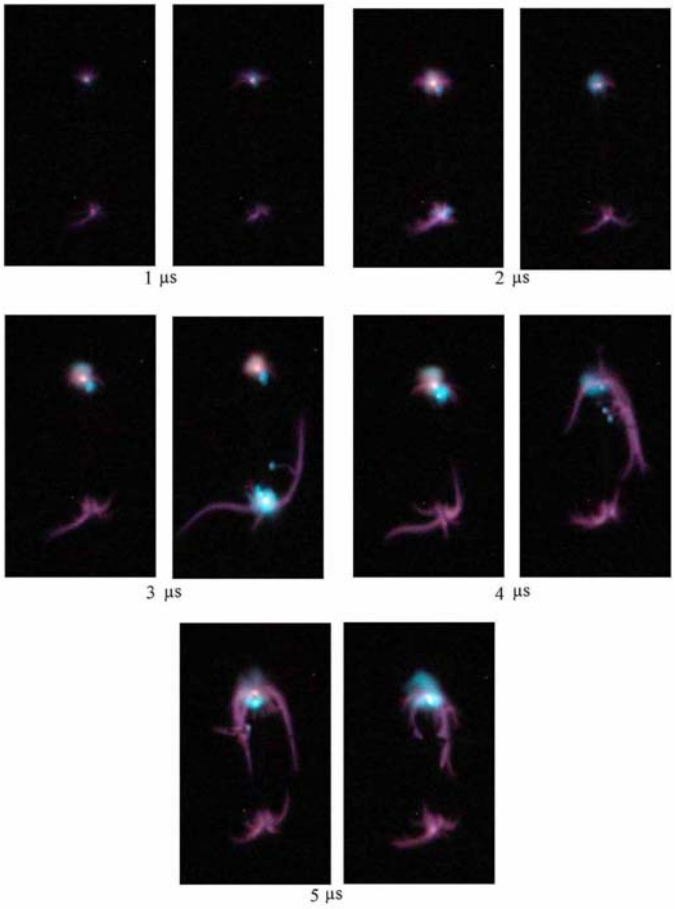

Fig.5.5.2. Appearances of the undercritical vibrator initiated MW discharge at E_0 = 3.7 kV/cm with respect to τ_{pul} value

in the range from 1 μs to 5 μs, one has to take into account that growing streamers are in a field of approximately constant value during this time. Treatment of experimental results gave the following estimate $v_{str} \approx 4.7 \cdot 10^5$ cm/s. This value is close to the analogous value $\mathbf{v_{str}}$ estimated in the case of the undercritical discharge in the field with λ = 8.9 cm.

5.6. Spatial and temporary characteristics of deeply undercritical MW discharge

Spatial and temporary characteristics of deeply undercritical MW discharge in a field with $E_0 << E_{cr}$ were investigated by its photo detection at constant E_0 and p at variation of τ_{pul}.

For example in Fig.**5.6.1** one can see photos of deeply undercritical discharge at E_0 = 3.7 kV/cm, p = 760 Torr and $\boldsymbol{\tau_{pul}}$ in the range from 1 μs to 5 μs. There are represented three discharge realizations for each $\boldsymbol{\tau_{pul}}$. Discharges represented in the picture were initiated by a vibrator with 2L = 12 mm.

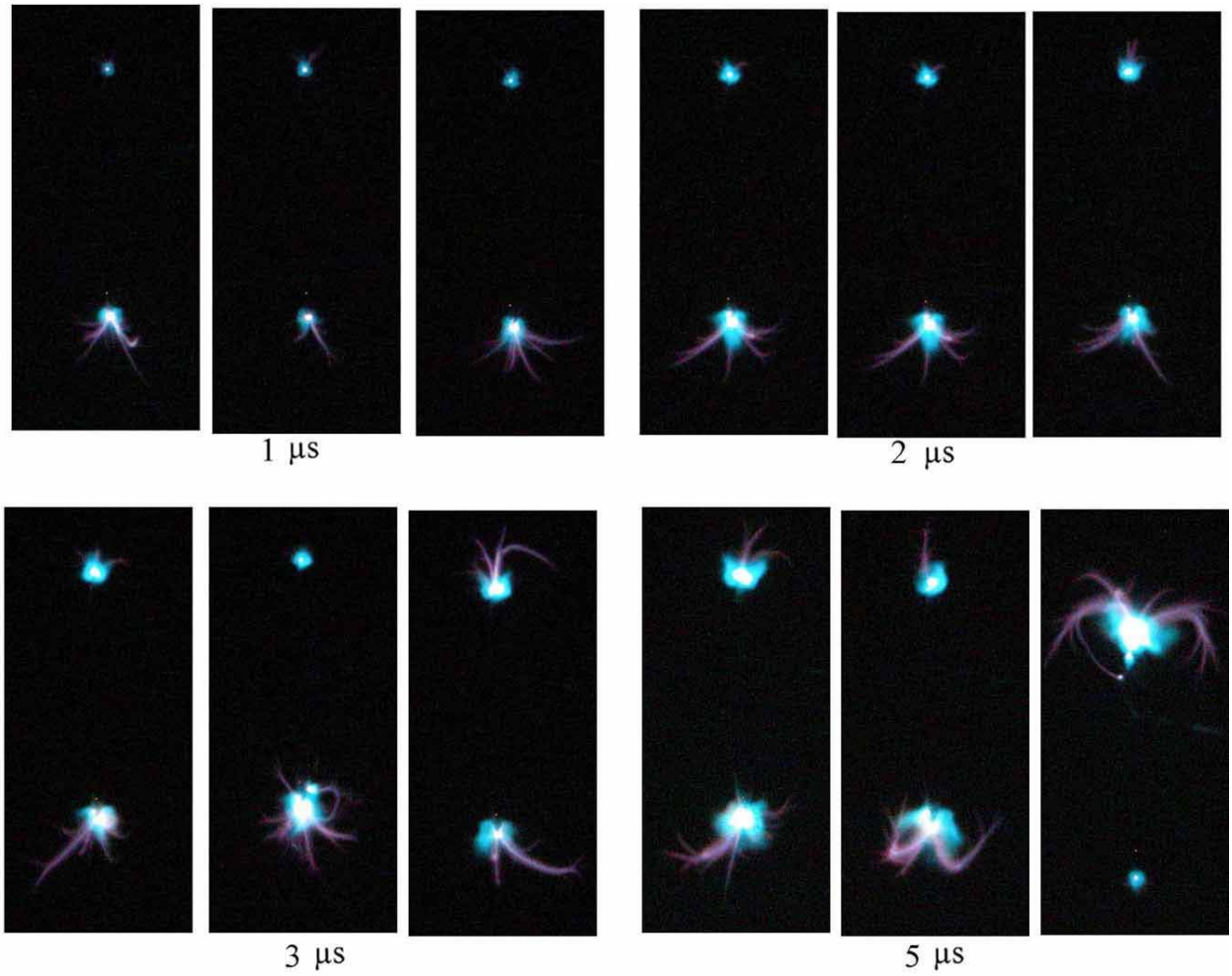

Fig.5.6.1. Appearances of deeply undercritical MW discharge at E_0 = 3.7 kV/cm with respect to τ_{pul} value

Analysis of experimental data gives a following picture of deeply undercritical MW discharge development. Streamer channels start from the initiator poles with some periodicity, grow with average velocity $v_{str} \approx 2.5$ cm/s, reach a length of several centimeters and become dim. This method of detection does not give an answer to a question about a number of discharge channels that exist simultaneously. Plasma of these discharges still energy effectively interacts with EM field since EM

vibrator and plasma channels create a resonance system. Air in the streamer plasma channel is substantially heated in the result of this. It leads to evaporation of initiator poles surface.

5.7. Streamer undercritical MW discharge in a high-speed flow

Streamer channels forming undercritical MW discharge have average growth velocity $\mathbf{v_{str}}$ of a scale 10^5 cm/s as it was shown in the part 5.5. One can suppose that air movement in the discharge area with a velocity $v_{fl} < v_{str}$ will not impact this discharge type formation. This supposition was checked in the experiment, in which the undercritical MW discharge was ignited in a high-speed air flow with $v_{fl} = 5 \cdot 10^4$ cm/s.

A scheme of the experimental setup with EM beam with $\lambda = 2.5$ cm in this configuration is represented in Fig.**5.7.1**. A Laval nozzle formed a submerged stream with M = 2 at gas temperature of T = 150 °K in the set up, in preliminary pumped out working chamber down to p = 100 Torr. A photo of the setup appearance in this configuration is represented in Fig.**5.7.2** .

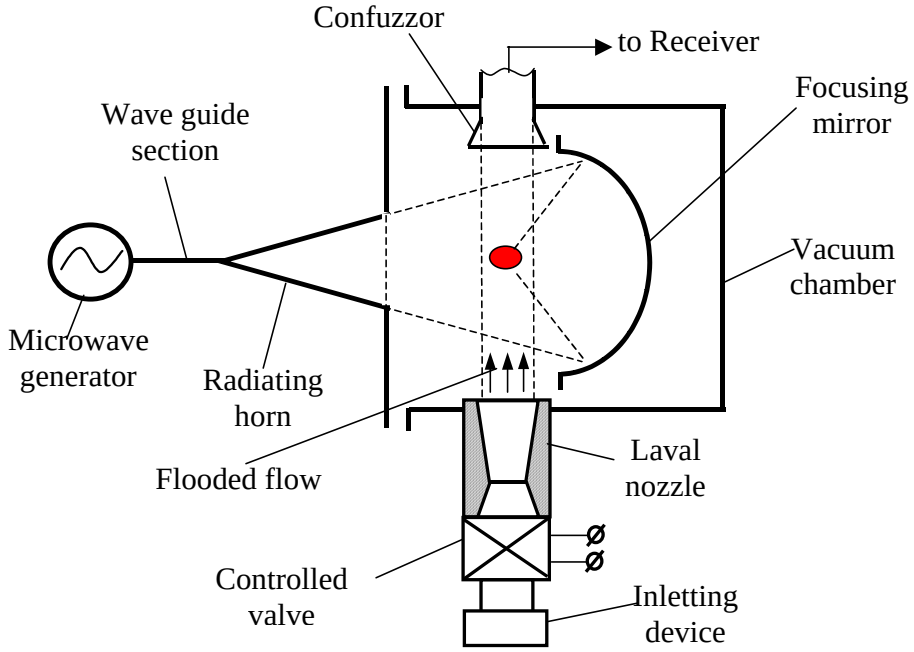

Fig.5.7.1. A scheme of the setup with $\lambda = 2.5$ cm completed for creation of supersonic submerged stream and propane injection

Linear EM vibrator initiating a discharge was placed in EM focus during these experiments; it was parallel to its vector $\boldsymbol{E_0}$. The vibrator was fixed to a streamlined dielectric radiotransparent batten, as it is shown in Fig.**5.7.3**.

In Fig.**5.7.4** one can see integral photos of MW discharges in a single pulse with $\tau_{pul} = 34$ μs, in dead air and in its high-speed flow. One can see that discharges are essentially different in appearance. One practically can not see streamer channels in the flow. They are as if pained over by a diffuse background blown off along the flow.

Fig.5.7.2. Appearance of air line connecting a working chamber and a receiver

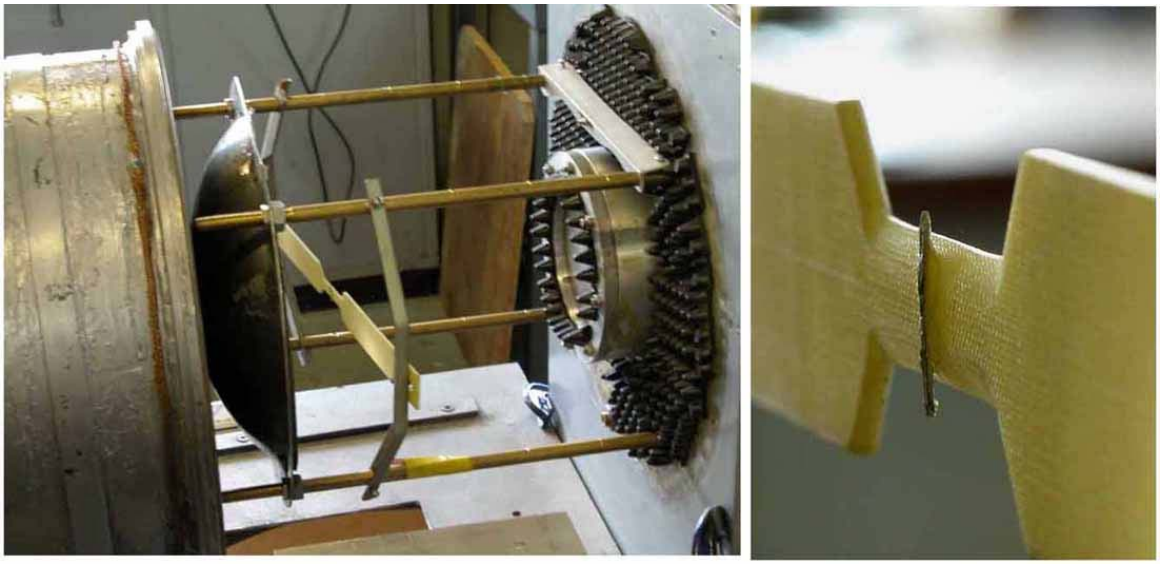

Fig.5.7.3. Position of a batten for initiating vibrator fixing inside the working chamber (left photo) and appearance of the batten with initiating vibrator fixed to it in the area of crossing with the submerged stream (right photo)

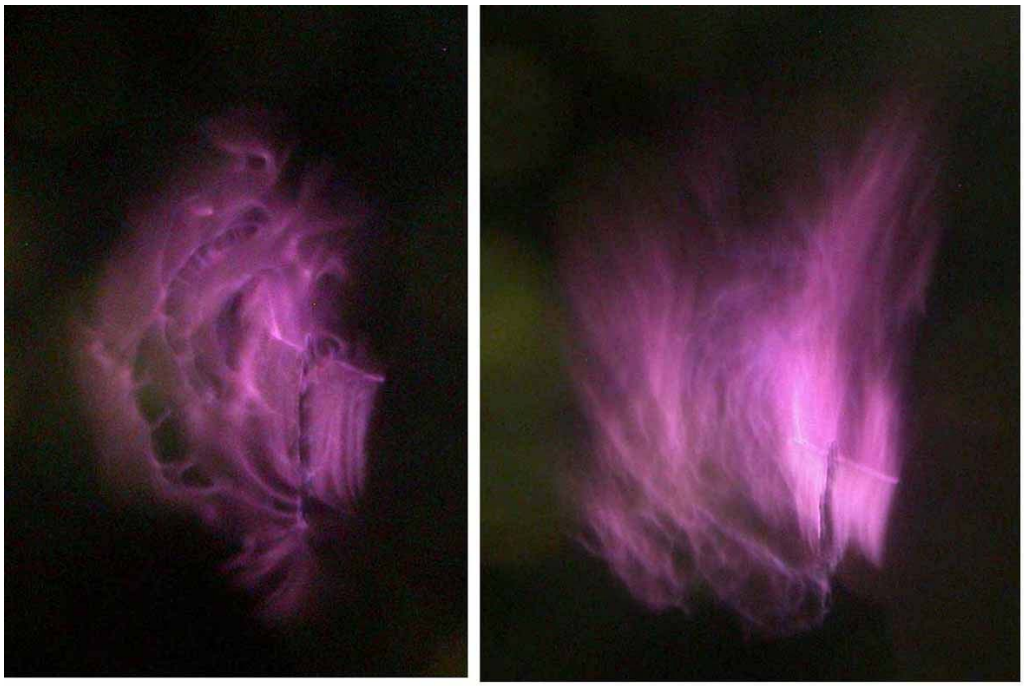

Fig.5.7.4. Appearance of the undercritical discharge with λ = 2.5 cm in the single pulse at τ_{pul} = 34 μs in dead air (left photo) and in the stream at the velocity v_{fl} = 500 m/s (right photo)

In Fig.**5.7.5** one can see integral photos of MW discharge area in a pulse bunch with τ_{pul} = 34 μs and f_{rep} = 100 Hz, in dead air and in its high-speed flow.

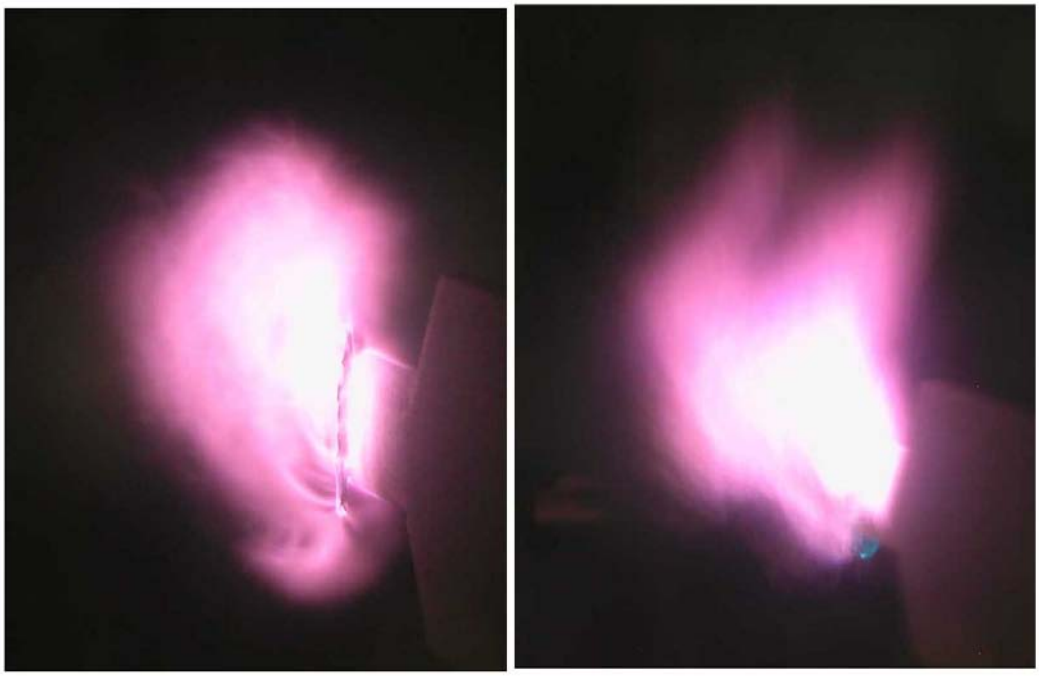

Fig.5.7.5. Appearance of the undercritical discharge with λ = 2.5 cm in periodical mode at τ_{pul} = 34 μs, f_{rep} = 100 Hz indead air (left photo) and in the stream with a velocity v_{fl} = 500 m/s (right photo)

5.8. Streamer undercritical MW discharge in a high-speed flow of propane-air flammable mixture

One of methods, which we used for estimation of a gas temperature ***T*** in the streamer channels of MW discharge in quasi-optical EM beam, consists in its realization in model propane-air flammable mixture. Such an experiment at the setup with the given λ could be undertaken only at low gas pressure and in high-speed mixture flow. Note, that in the previous part we detected that appearance of the undercritical MW discharge in air flow was essentially changed, so it was unknown beforehand if the appearance of the streamer discharge with high temperature ***T*** in its channels is the same.

An answer to this question we obtained experimentally. A device of propane injection to air flow in these experiments was installed in the inlet device represented in Fig. **5.7.1**. This device allowed to set a definite propane injection rate $m_{C_3H_8}$; g/s. In Fig**.5.8.1** one can see a set of MW discharge area photos in a single pulse with τ_{pul} = 34 μs. The discharge was realized in a supersonic (SS) flow of propane-air mixture at $m_{C_3H_8}$ = 2 g/s, 8 g/s and 9.3 g/s, photos are given from the left to the right, respectively.

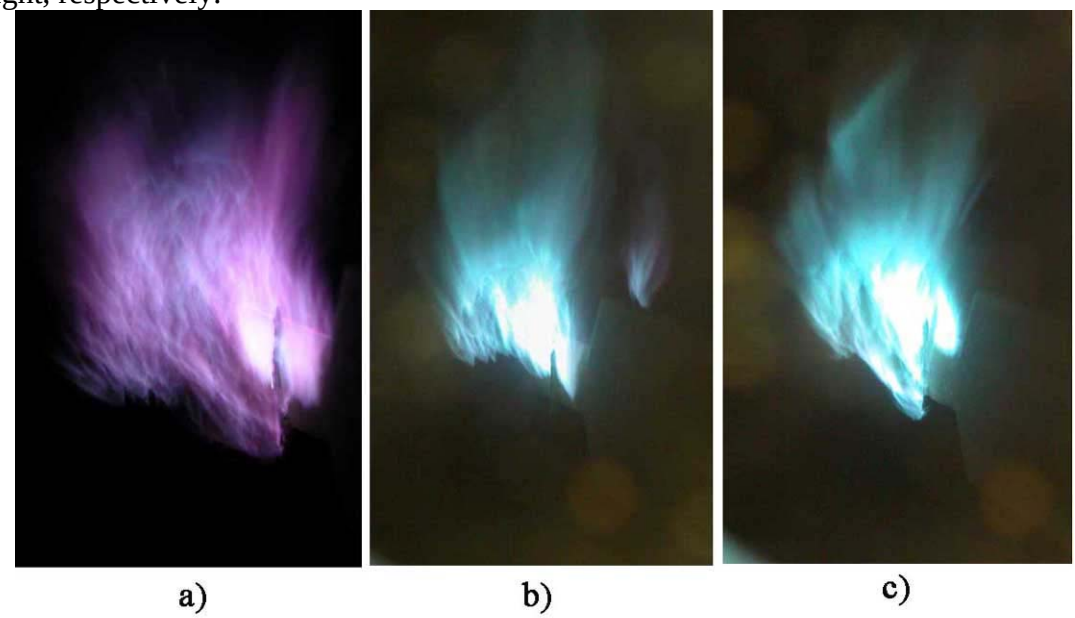

Fig.5.8.1. The undercritical discharge in the single pulse at τ_{pul} = 34 μs in flammable mixture supersonic flow, v_{fl} = 500 m/s, propane mass flow rate is $m_{C_3H_8}$ = a)-2g/s; b)-8 g/s; c)-9.3 g/s

The experiments have shown that the undercritical MW discharge is capable to ignite propane-air mixture, i.e. air temperature ***T*** in its streamer channels is higher than the ignition temperature of this mixture. Besides, the discharge in the near zone of its streamer channels substantially influences on a flame front propagation velocity over the flammable mixture. For example in Fig.**5.8.2** one can see a bottom fragment of the photo from the Fig.**5.8.1** in larger scale, $m_{C_3H_8}$ = 8 g/s. It can be seen that “cones” of combusting mixture go up from the low end of the streamer channels along the flow. These cones half-opening angle is $\alpha \approx 20°$.

Fig.5.8.2. A fragment of the undercritical discharge in the single pulse at τ_{pul} = 34 μs in the supersonic flow of the flammable mixture v_{fl} = 500 m/s at $m_{C_3H_8}$ = 8 g/s

This angle allows to obtain a flame front propagation velocity $v_{fr} \approx 150$ m/s. These experimental data require further investigations first of all experimental ones.

5.9. Streamer undercritical MW discharge in a high-speed flow of two-phase medium

In this part we describe experiments that allow to obtain additional information about features of pulsed undercritical MW discharge. We realized this discharge in a high-speed flow of two-phase medium, which represents air stream with admixture of water aerosol. These experiments were undertaken during the last Stage 3 of the present Projects and were not described earlier, so in this part we describe in full details applied experimental method and experimental results.

5.9.1. Experimental conditions

In experiments we used a setup in its version illustrated in Fig.**5.7.1**. MW generator with $\lambda = 2.5$ cm and electrodynamic system of EM quasi-optical beam forming are included into it. Electric component of linear polarized initial MW field was $E_0 = 3.3$ kV/cm in its focus. At that a typical transversal size of the focal area along the vector $\boldsymbol{E_0}$ and along EM beam axis approximately was equal to 1÷2 cm. We used EM pulses of $\tau_{pul} = 30$ μs duration during the experiments.

The focal area of EM beam could be blown through by the supersonic air flow during the experiments. The stream was formed by axially symmetric Laval nozzle. The nozzle formed the submerged air stream with the following parameters at initial air pressure p = 114 Torr in the working chamber of the setup: a transversal diameter is 28 mm; flow Mach number M = 2 at static temperature T = 150 °K in the stream and at flow velocity v = 500 m/s; a direction of a flow vector **v** is collinear to the vector $\boldsymbol{E_0}$.

Air leak into the working chamber through the Laval nozzle takes place from the atmosphere through electrically controlled air valve. The leaking time is $\tau_{fl} = 1$ s in experiments. A special electric synchronizing device allows to synchronize functioning of different setup elements with an accuracy up to 0.1 s, including the work of the controlled air valve itself.

A device of water aerosol injection to leaking air was included in the system of high-speed stream formation in these experiments. The injection device was constructively located at the inlet of controlled air valve of a stream formation scheme. The whole injection system is schematically represented in Fig. **5.9.1.1**.

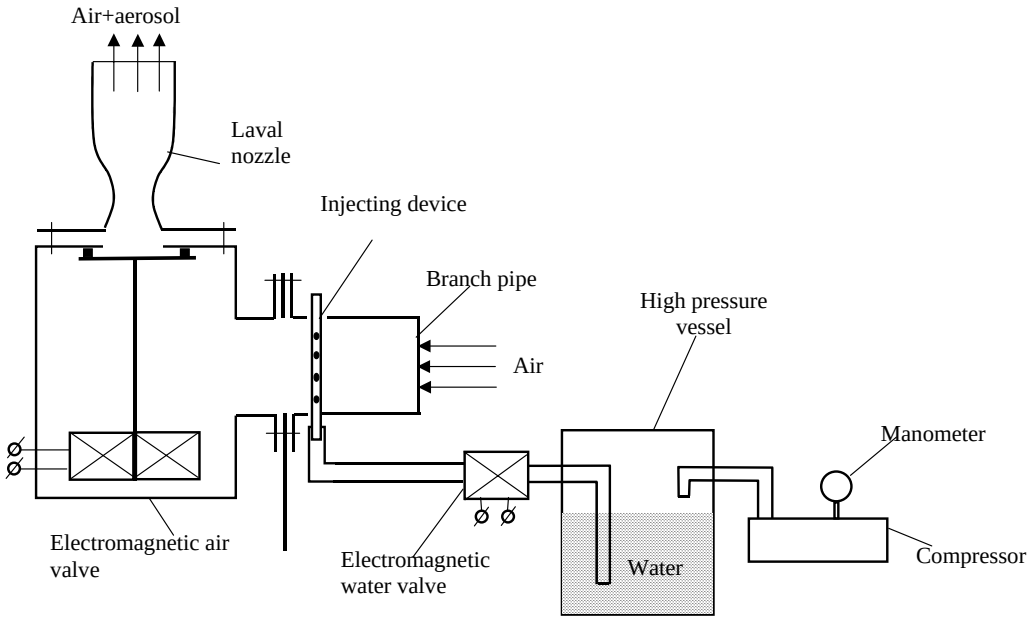

Fig.5.9.1.1. Water aerosol injection scheme to a high-speed air stream

In Fig.**5.9.1.2** one can see a design of air injecting device. Its photo is represented in Fig.**5.9.1.3**. The device consists of a flange with a hole of 65 mm diameter, which is fixed to an inlet flange of the air valve. A pipe with outer diameter of 8 mm and the inner one 4 mm is fastened over the flange hole diameter. There are four holes with a diameter 1.2 mm each in the central part of this pipe wall (over its diameter) as it is shown in Fig.**5.9.1.2**. A side pipe with internal diameter of 65 mm and length of 80 mm is fastened to aerosol injection device flange face, which is opposite to the flange of air valve. Its presence insures comparably laminar air flow over an internal cross section of water aerosol injection device's ring.

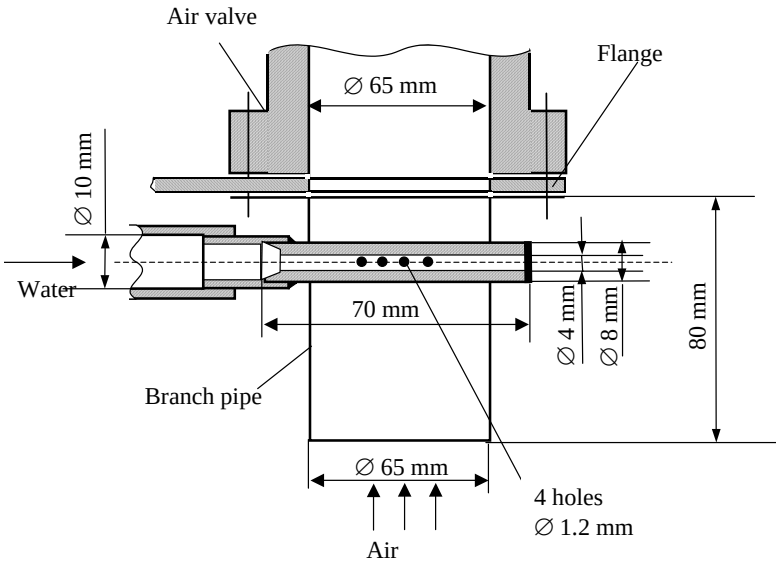

Fig.5.9.1.2. Water aerosol injection device to air flow scheme

In the system one end of the pipe with holes is closed, and water is delivered to another end through a flexible hose. It is shown in the scheme of Fig.**5.9.1.1** that electrically controlled water valve, a high-pressure vessel partially filled with water, high-pressure air line and a compressor insuring this higher pressure p_{in} are connected in series to this hose.

The whole injection system works in the following way. A required pressure of $p_{in} = 4.5$ exceeding atmospheres in initial state is set in the high pressure vessel over a surface of water. The

water valve is opened 0.2 s after opening of the air valve for a time period of τ_{wat} = 0.2 s. Water in the result of this begins to be thrown away through the hole in the injection pipe, and being mixed with air flow it comes to the Laval nozzle inlet in the form of aerosol.

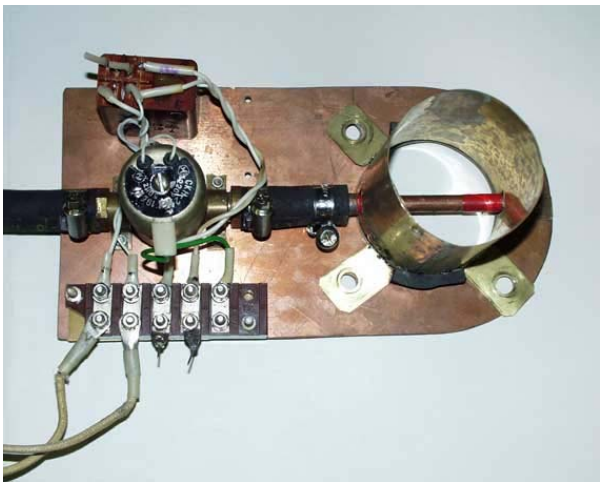

Fig.5.9.1.3. Appearance of water aerosol injection device to air flow

5.9.2. Preliminary experiments on determination of water amount injected to a high-speed airflow

Experiments on MW discharges in air with air aerosol admixture in EM beam with λ = 8.9 cm were carried out at $\eta \approx 1$ % weight percent water content in air volume unit. Our estimates have shown that water delivery to the flow has to be m_{exp} = 80 g/s in order to keep the analogous water content in the present experiments as well. $\boldsymbol{m_{exp}}$ value at the outlet of injecting pipe can be controlled by variation of $\boldsymbol{p_{in}}$ in these experiments. This mass flow rate was achieved in the control experiment at p_{in} = 4.5 excess atmospheres.

Appearance of the flow forming system with water injection device included into this line is represented in Fig.**5.9.2.1**.

Fig.5.9.2.1. Appearance of the flow forming system with water injection device included into this line

5.9.3. Visualization of aerosol high-speed stream

Investigating processes photo detection system was developed in a course of works. In particular we developed visualization of a high-speed aerosol stream.

A scheme of photo detection system elements position relationship is represented in Fig.**5.9.3.1**. Photographing was carried out at closed working chamber. Outside light practically does not get inside the chamber in this case. The experience has shown that illumination of objects being photographed has to be made from the pulsed light source located inside the chamber, as it is shown in Fig.**5.9.3.1.**

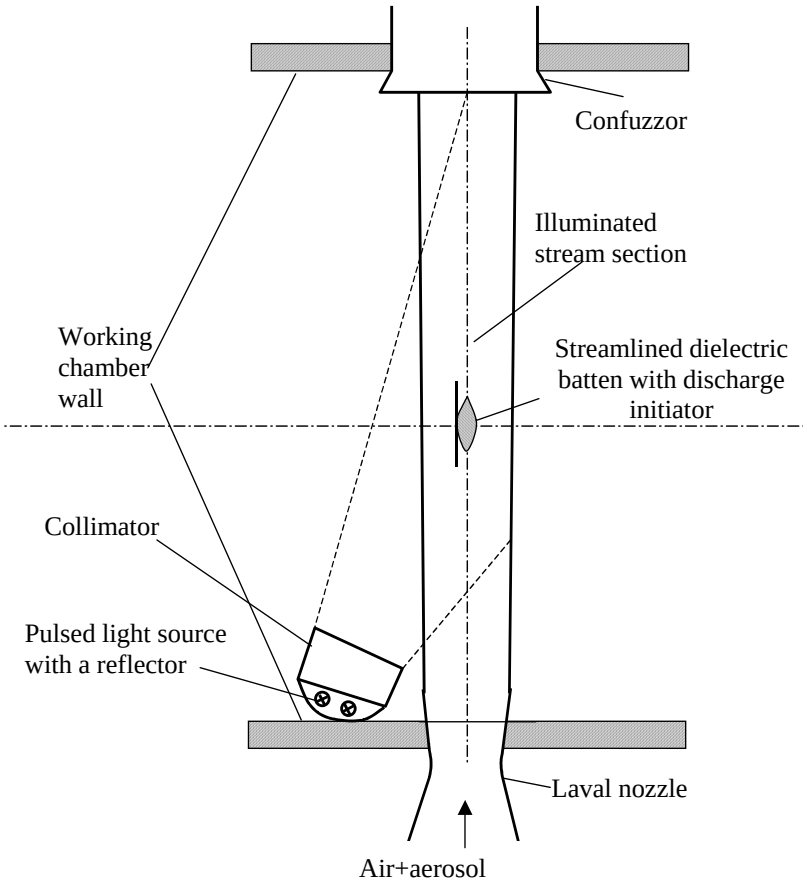

Fig.5.9.3.1. A scheme of photo detection system elements position relationship

A pulsed light source was made on a basis of the pulsed lamp IFK-120 type. Its electrical feeding scheme is represented in Fig. **5.9.3.2**. A key to P_1, shown in the scheme, realized the lamp ignition. It was switched on by signals of logical timer – a synchronization scheme of device elements temporary work. A variable resistance $\boldsymbol{R_{var}}$ and a selection of $\boldsymbol{C_1}$ capacity value allow to regulate a duration of the lamp flash. This duration was in the range (5÷350) ms, it was selected basing on a consideration of investigation processes optimal visualization. Actually the flash durations was controlled from an outlet of a photodiode.

Light flux collimating tube of 35 mm diameter and length of 25 mm was placed at the outlet of the pulsed lamp. The experience has shown that the light scattered from details inside the working chamber did not allow to undertake distinct photo detection of investigated processes in its absence.

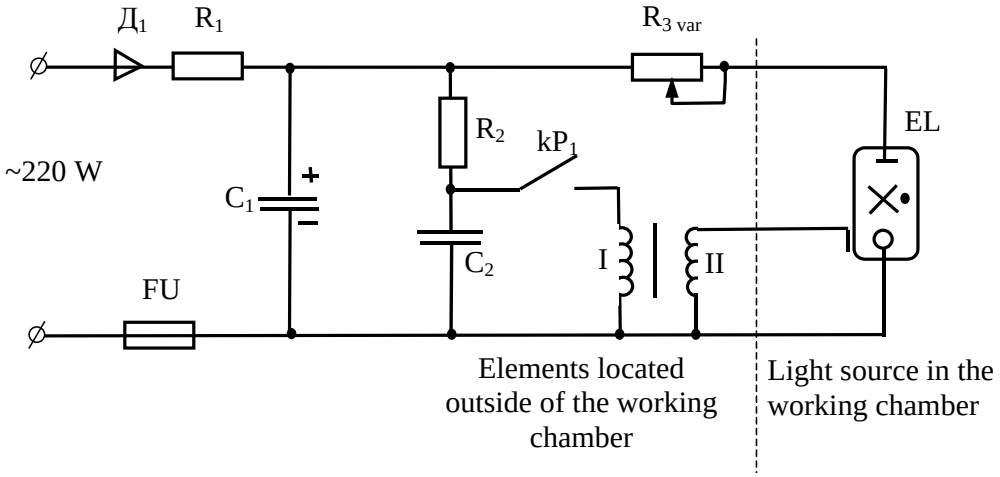

Puc.5.9.3.2. Feeding electrical schemeof the pulsed lamp

5.9.4. Temporary sequence of equipment functioning

A temporary sequence of equipment functioning developed in controlled experiment, a cyclorama, is represented in a form of a corresponding diagram in Fig.**5.9.4.1**. One can see from it that a high-speed air flow existed during τ_{fl} = 1 s in experiments.

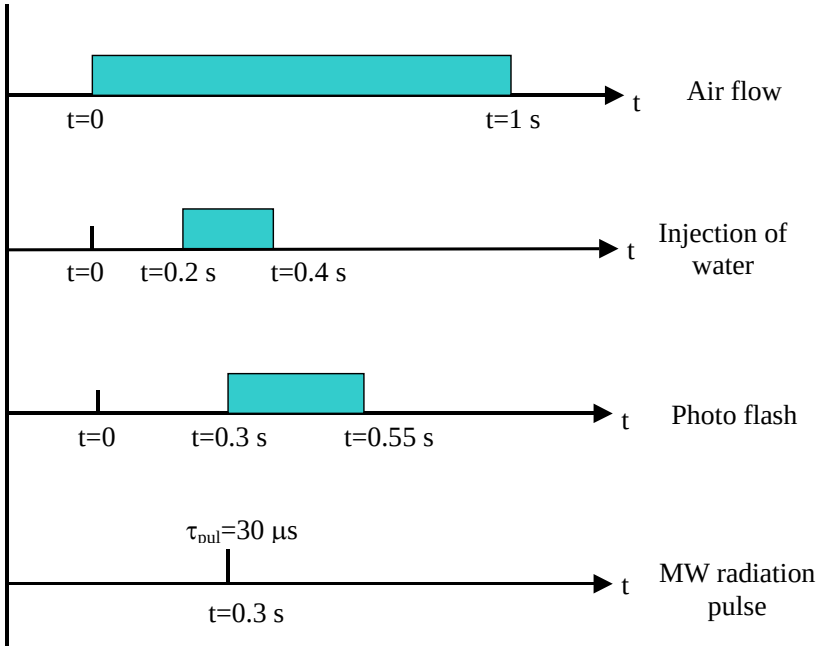

Puc.5.9.4.1. A cyclograma of equipment switching on

Water was injected into this flow during τ_{wat} = 0.2 s and it began to be injected with some delay with respect air valve switching on in the line of flow forming. A duration of a photo flash was 250 ms, and microwave pulse duration was τ_{MW} = 30 μs.

5.9.5. Experimental results

Experimental results are represented in Fig.**5.9.5.1** - **Fig.5.9.5.5** in a form of corresponding photos. The vector $\boldsymbol{E_0}$ is vertical in all the photos. The microwave radiation comes from the left to the right. A flow direction is down – up.

In Fig.**5.9.5.1** one can see a streamlined dielectric batten, EM vibrator initiating a discharge is fixed to it. The batten is made of textolite. Its thickness is 2 mm it has sharpened edges in the stream cross section. Batten maximum width is 5 mm, and in its central part, in a place of the vibrator position at the length ≈40 mm, it has a width of 7 mm. EM vibrated is fixed in the central batten's part, it is made of a copper wire of a diameter 2a = 0.26 mm and length 2L = 12.5 mm.

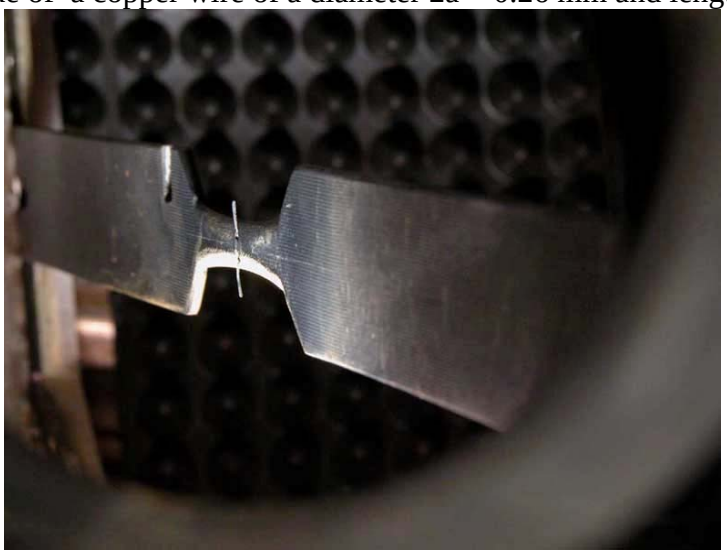

Fig.5.9.5.1. Chamber's working area with the radio transparent batten

In Fig**.5.9.5.2** we again represent a photo of a high-speed stream with water aerosol in it. One can see that the stream is collinear to the vibrator axis.

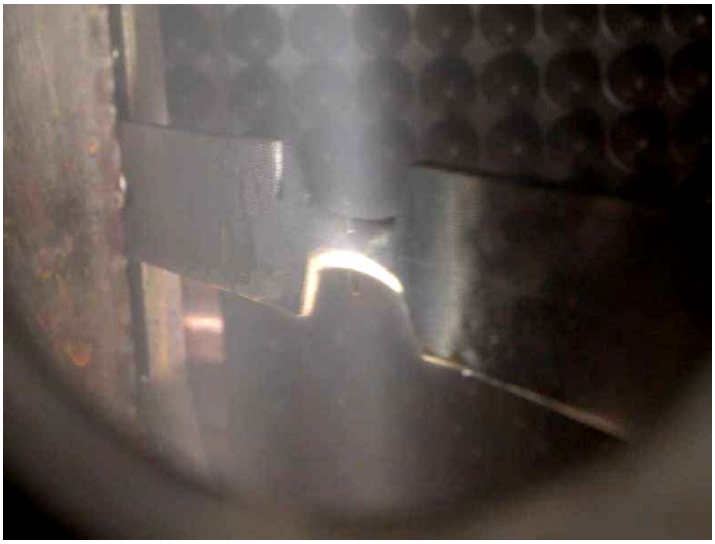

Fig.5.9.5.2. Appearance of a high-speed stream with aerosol

In Fig**.5.9.5.3** one can see a photo of the microwave discharge in dead air at gas pressure of $p \approx 200$ Torr in the working chamber. Air molecules concentration namely at this pressure of the dead air equals to the concentration of air molecules in cold high-speed stream at static pressure in the stream and in the working chamber equal to $p \approx 100$ Torr and air temperature in the stream $T = 150$ °K. It follows from the photo that the initiated discharge is the critical one with volumetrically developed structure at experimental field level $E_0 = 3.3$ kV/cm in the vibrator's area.

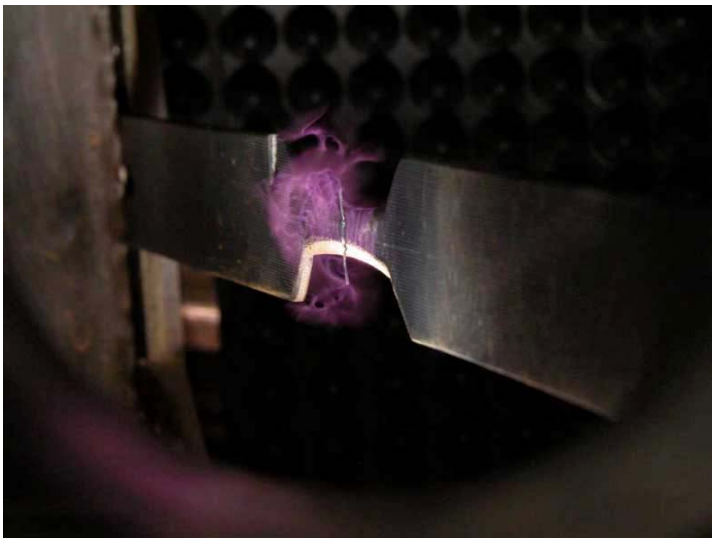

Fig.5.9.5.3. Appearance of the undercritical MW discharge in dead air at p ≈200 Torr

In Fig.**5.9.5.4** one can see a photo of MW discharge in air high-speed stream without aerosol admixture to it. It follows from it that the discharge keeps its streamer volumetrically developed structure also at air flow velocity of v_{fl} ≈500 m/s. At that the discharge plasma is drawn down the flow in a form of glowing diffuse plasma tail. It follows from the photo that discharge streamer channel density is large in the trace of the batten fixing the initiator. It is natural, because there is realized some decrease of air molecule concentration in aerodynamic "shadow" from the batten.

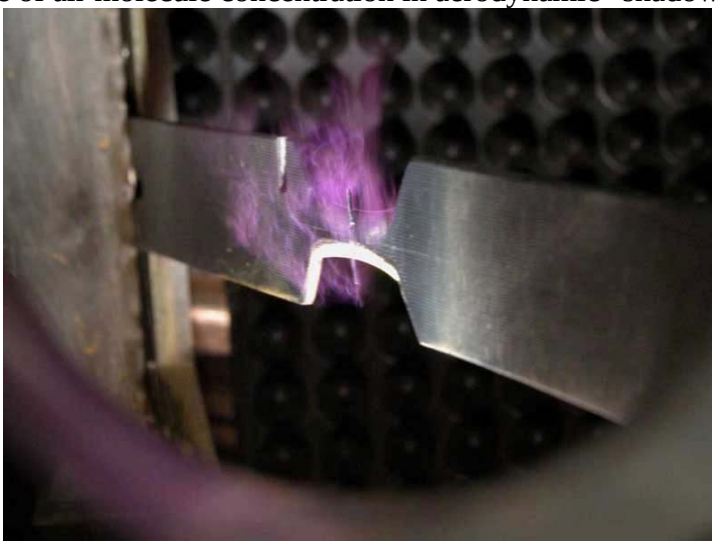

Fig.5.9.5.4. Appearance of the undercritical MW discharge in the high-speed air flow at v_{fl} ≈500 m/s

Finally in Fig.**5.9.5.5** one can see a photo of the microwave discharge in a high-speed air stream at presence of water aerosol in it. One can see that the discharge keeps the streamer volumetrically-developed structure in this case also.

.

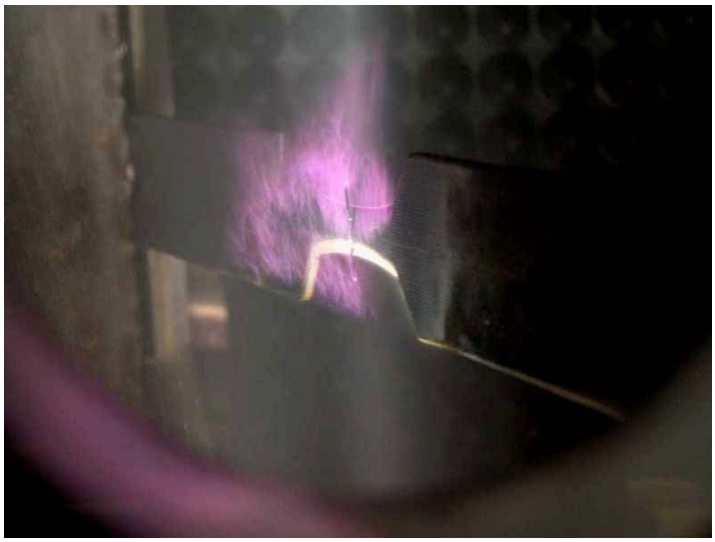

Fig.5.9.5.5. Appearance of the undercritical MW discharge in the high-speed air flow with v_{fl} ≈500 m/s at presence of water aerosol in it

6. Features of MW discharge in quasi-optical EM beam with λ = 12.5 cm

Quasi-optical EM beam with λ = 12.5 cm applied in these experiments has a level of EM field electric component E_0 ≤100 V/cm in areas comparably distant from elements forming this beam. This field level allows to realize only initiated deeply undercritical MW discharges with $E_0 << E_{cr}$ in the studied air pressure ***p*** range. At the same time, this field level in EM beam can be maintained practically continuously. This makes a setup with this ***λ*** to be essentially different from described above pulsed set ups with λ = 2.5 and 8.9 cm. Actually, the experiments were carried out with a discharge working during τ_{dis} = 0.3 s.

6.1. Features of MW discharge in dead air and in its high-speed flow

A typical photo of MW discharge initiated by a cylindrical EM vibrator with 2a = 4 mm and 2L = 50 mm in dead air is represented in Fig.**6.1.1**. A radiation to the vibrator comes from above, and the vector $\boldsymbol{E_0}$ is parallel to the vibrator's axis. The vibrator is fixed to the post perpendicular to it, the post height is 30 mm. In its turn it is fastened to the metallic plate.

The experiment has shown that presence of "discharge hats" does not lead evaporation of vibrator pole's surface at air pressure p ≤20 Torr. The diffuse discharge type is realized in this case, it interacts with EM field exciting it energy weakly effectively. A qualitative jump takes place at p>20 . In this case one observes stormy evaporation of EM vibrator's (initiating the discharge) poles at discharge realization.

One can suppose that this qualitative jump at variation of ***p*** is conditioned by the discharge type transition from the diffuse to the streamer one. EM field wavelength was the largest of investigated ***λ*** in these experiments. The boundary pressure $\boldsymbol{p_{th}}$ separating the diffuse and streamer discharge types had to be shifted in a side of smaller ***p***, as we had to expect (see Fig.**5.4.2).**

Experiments with λ = 8.9 cm shows that pulsed deeply undercritical streamer discharge are formed consequently starting streamer channels from the initiator's pole during MW pulse. These channels with average velocity $v_{str} \approx 10^5$ cm/s grow for a small length of about 1 cm and become

dim. Evidently, if this discharge is realized in air flow with a velocity $v_{fl} < v_{str}$ then the flow presence does not influence of streamer channels formation. One can suppose that a development of MW undercritical discharge at $\lambda = 12.5$ cm also abide this scenario.

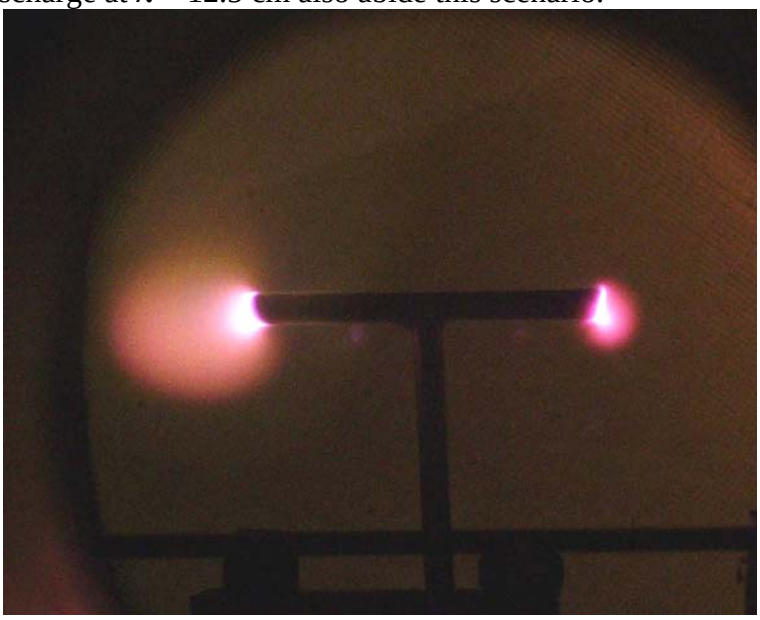

Fig.6.1.1. Appearance of diffuse microwave deeply undercritical discharge at p=20 Torr

This supposition was tested experimentally. One can see the corresponding photos in Fig.**6.1.2**. The left one shows an appearance of the initiator with maximum diameter value $2a = 4$ mm in its central area. The flow in the photos is directed from the left to the right and has a velocity $v_{fl} = 5 \cdot 10^4$ cm/s. A concentration of air in the flow corresponded $p \approx 200$ Torr. The field vector $\boldsymbol{E_0}$ is parallel to the vibrator axis. An analysis of stagnation pressure $\boldsymbol{p_{stag}}$ and stagnation temperature $\boldsymbol{T_{stag}}$ in the discharge trail have shown that the discharge plasma interacts with EM field energy effectively. This feature is inherent namely in streamer MW discharge type.

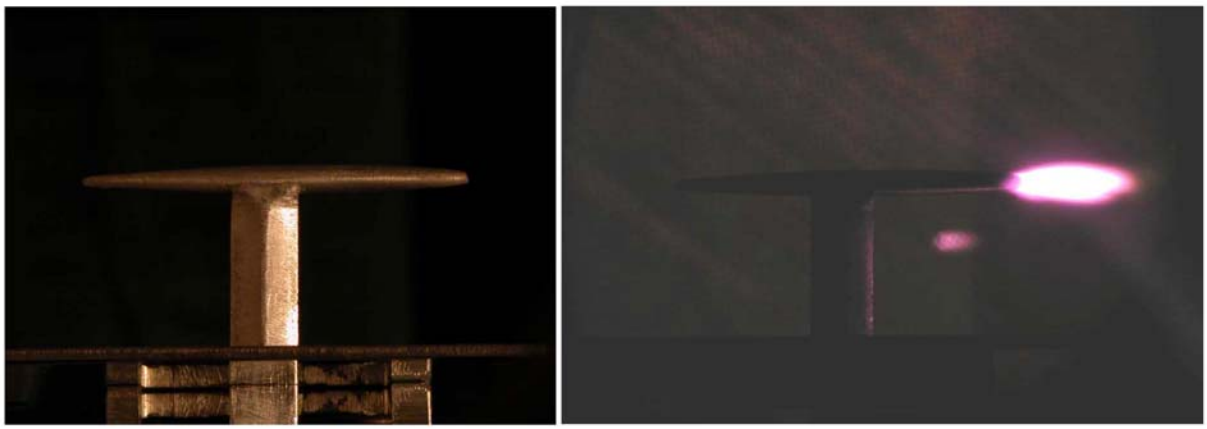

Fig.6.1.2. Appearance of deeply undercritical MW discharge initiated by a thin sharpened vibrator in a high-speed flow.

6.2. Deeply undercritical MW discharge in the high-speed flow of two-phase medium

Initiated deeply undercritical MW discharge was investigated in a high-speed air flow with admixture of water aerosol.

A pipe-type linear EM vibrator was used for a discharge initiation in these experiments. In Fig.**6.2.1** one can see an integral discharge photo. Exposure time was $\tau_{exp} > \tau_{dis}$, here $\tau_{dis} = 0.3$ s is a time of the discharge realization. The discharge was realized in a base part of the pipe-type EM vibrator with 2a = 4 mm and 1 mm width of a wall. The stream in the photo does not have aerosol admixture.

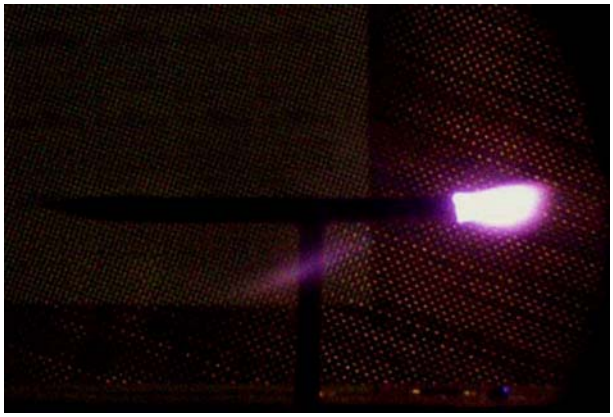

Fig.6.2.1. Deeply undercritical discharge initiated by a pipe-type vibrator (with nose dielectric cowl) in a high-speed flow

Fig.**6.2.2.** illustrates a scheme of water injection to a flow. In Fig.**6.2.3** one can see a photo of vibrator's base area at injection of water aerosol to a high-speed flow. Results of the experiment

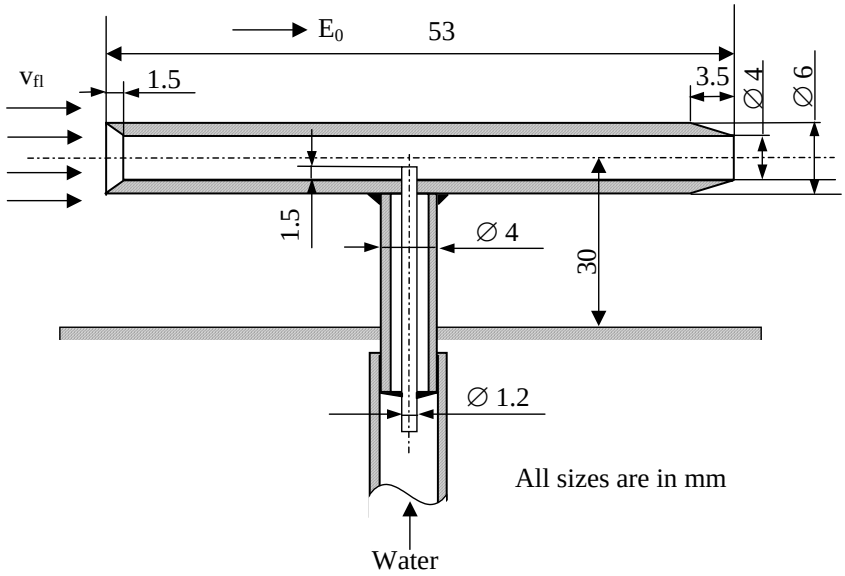

Fig.6.2.2. A schema of a vibrator device initiating deeply undercritical MW discharge in a high-speed flow

become clear from Fig.**6.2.4.** One can see in it photos of deeply undercritical MW discharge in a high-speed air flow and in a high-speed air flow with aerosol. It can be seen that deeply undercritical MW discharge is realized in the last case also. We can emphasize again that this discharge was ignited in the field with the amplitude of about 50 times smaller than those of $\boldsymbol{E_{cr}}$. It

means that it was realized in the beam with power P_{gen} more than by 1000 times smaller that is necessary for electrodeless MW air breakdown at the given concentration of its molecules.

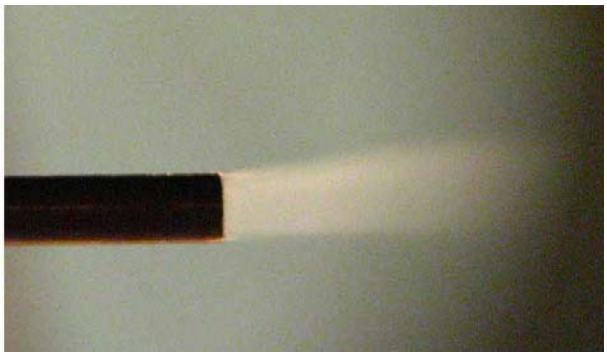

Fig.6.2.3. Appearance of the vibrator's base part at water aerosol injection to the flow

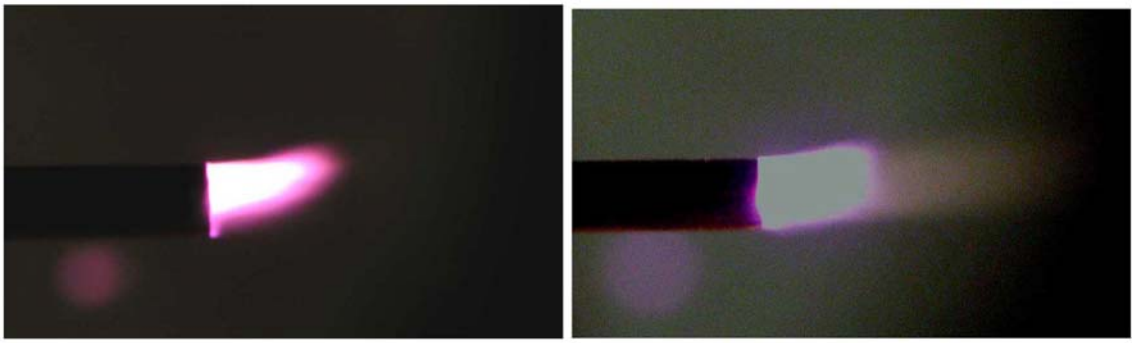

Fig.6.2.4. Appearances of deeply undercritical MW discharge initiated by a pipe in a high-speed flow (left photo) and of deeply undercritical MW discharge initiated by the pipe-type vibrator in a high-speed flow with aerosol admixture (right photo)

7. Undercritical surface streamer MW discharge

The experiment has shown, as it was indicated above, that MW discharge is realized in the streamer form with volumetrically-developed structure at comparably high air pressure ***p*** and in some definite range of undercriticality of EM field. This form is realized by growing and branching streamer plasma channels. The channels mainly grow towards EM field exciting the discharge. If a dielectric radiotransparent obstacle is located on a way of discharge front motion, for example as it is shown in a scheme of Fig.**7.1,** then the discharge propagates over the obstacle surface, and its streamer channels begin to "run about" it.

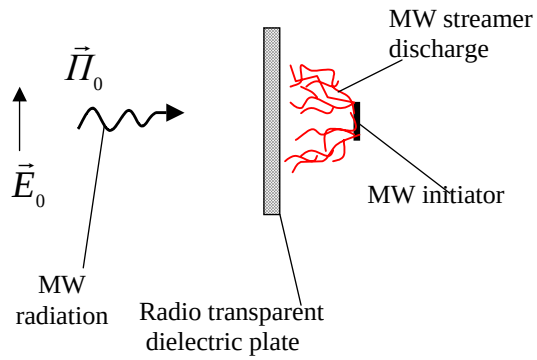

Fig.7.1. Realization scheme of undercritical transversal surface MW discharge

A typical photo of the described situation is represented in Fig.**7.2.** The discharge in it is initiated by a ball located to the right from a quartz plate. The radiation propagates through the plate from the left.

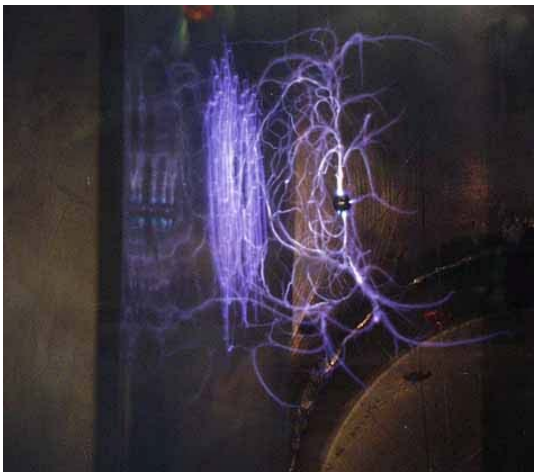

Fig.7.2. Appearance of the streamer discharge initiated by a metallic ball located outside a surface of a quartz plate.

The discharge still keeps its streamer character and “runs about” over the plate surface, as it is shown in Fig. **7.3,** in the case of MW discharge initiator’s location directly on the opposite plate surface with respect elements forming EM beam. The discharge in the figure is initiated by EM vibrator.

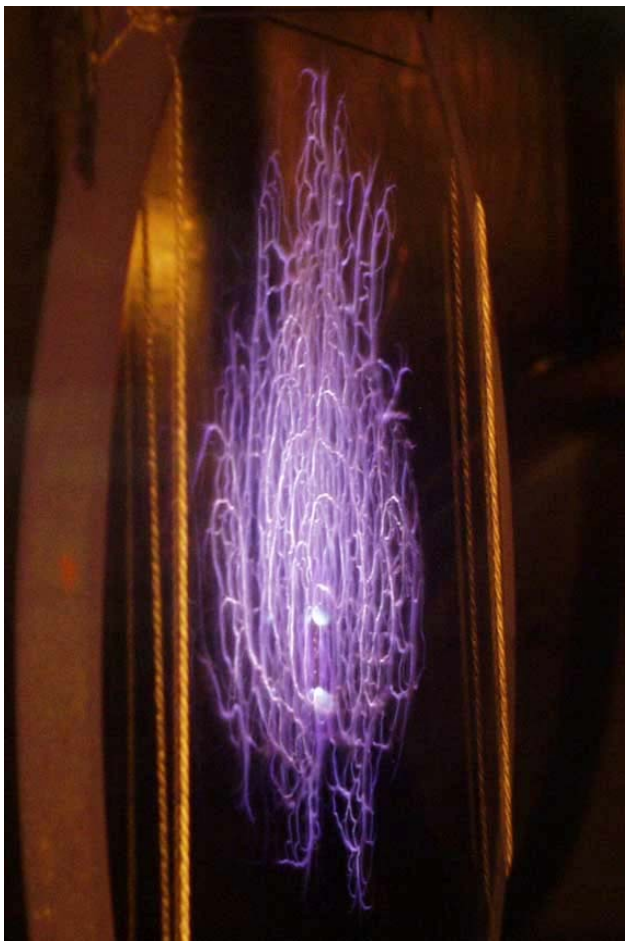

Fig.7.3. Undercritical transversal MW dischargeinitiated by a vibrator located on a surface of a quartz disc.

Surface streamer MW discharges, which photos are represented in Fig.**7.2** and Fig.**7.3,** were obtained with a help of the setup with c λ = 8.9 cm. In the present investigations we additionally have investigated a situation when a surface of a dielectric material lies in a plane of the vector $\boldsymbol{E_0}$ Pointing vector $\boldsymbol{\Pi}$ of EM beam with λ = 8.9 cm. Besides, discharges of considered type have been realized also with a help of the setup with λ = 2.5 cm. Results described below are especially preliminary. Beforehand we did not know, even at a qualitative level, which surface MW discharge types will be realized.

7.1. Longitudinal surface MW discharge in quasi-optical EM beam with λ = 8.9 cm

Let us agree to call a discharge realized on a surface of a dielectric a transversal if it is perpendicular to the vector $\boldsymbol{\Pi}$; and a discharge realized on a surface of a dielectric plate lying in $\boldsymbol{E_0 - \Pi}$ plate – a longitudinal one.

A realization schema of the longitudinal surface discharge in the setup with λ = 8.9 cm is represented in Fig.**7.1.1**. Experiments have been carried out using this scheme in air at atmospheric pressure $\boldsymbol{p}$.

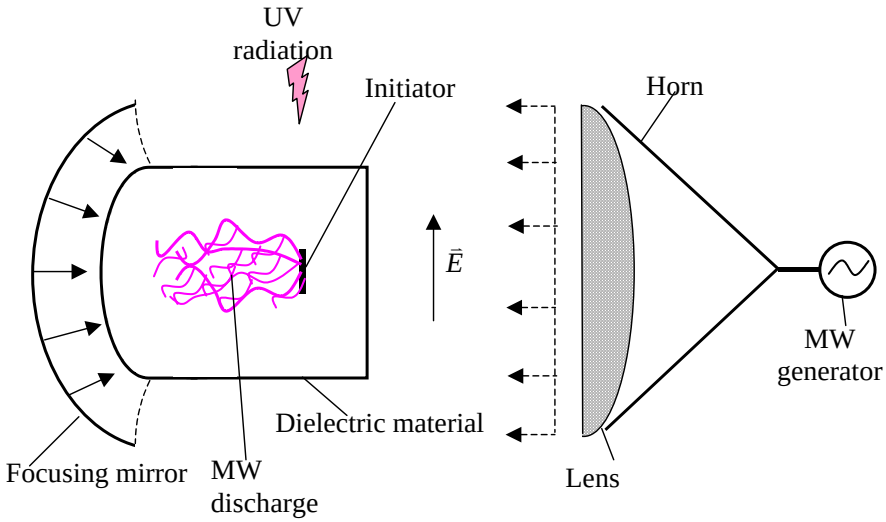

Fig.7.1.1. A scheme of MW discharge realization on a surface of a dielectric plate located in $E_0 - \Pi$ plane

The experiment has shown that the longitudinal undercritical surface MW discharge in quasi-optical EM beam was realized in the streamer form at this wavelength λ . At that the streamer plasma discharge channels are running over the dielectric surface and not running away from it. A typical photo of this discharge on a textolite plate with a width of 1 mm is represented in Fig. **7.1.2**, the discharge was initiated by EM vibrator with 2a = 0.15 mm and 2L = 12 mm placed on the plate's surface.

An equipment of a high-speed frame-by-frame discharge process photo detection has been tested in this experimental series. It can give nine frames with minimum exposure time τ_{exp} = 0.1 μs and minimum time between frames τ_p = 0.1 μs. This equipment allows to investigate a dynamics of the discharge development. For example In Fig.**7.1.3** one can photo frames obtained with a help of this equipment. Here τ_{exp} = 0.1 μs and τ_p = 1 μs. Analysis of these pictures gives $v_{fr} \approx 5 \cdot 10^5$ cm/s. These pictures allow to investigate spatial and temporary discharge parameters and details of its energy interaction with EM field.

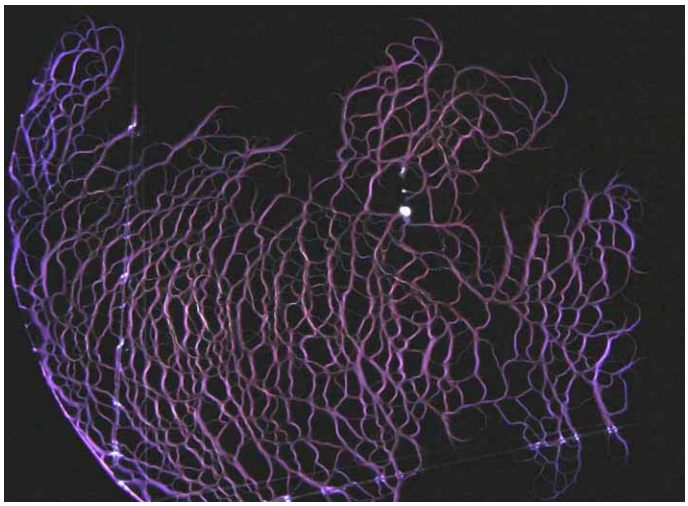

Fig.7.1.2. Appearance of the streamer vibrator initiated discharge on a surface of a dielectric plate placed along E_0 – П plane

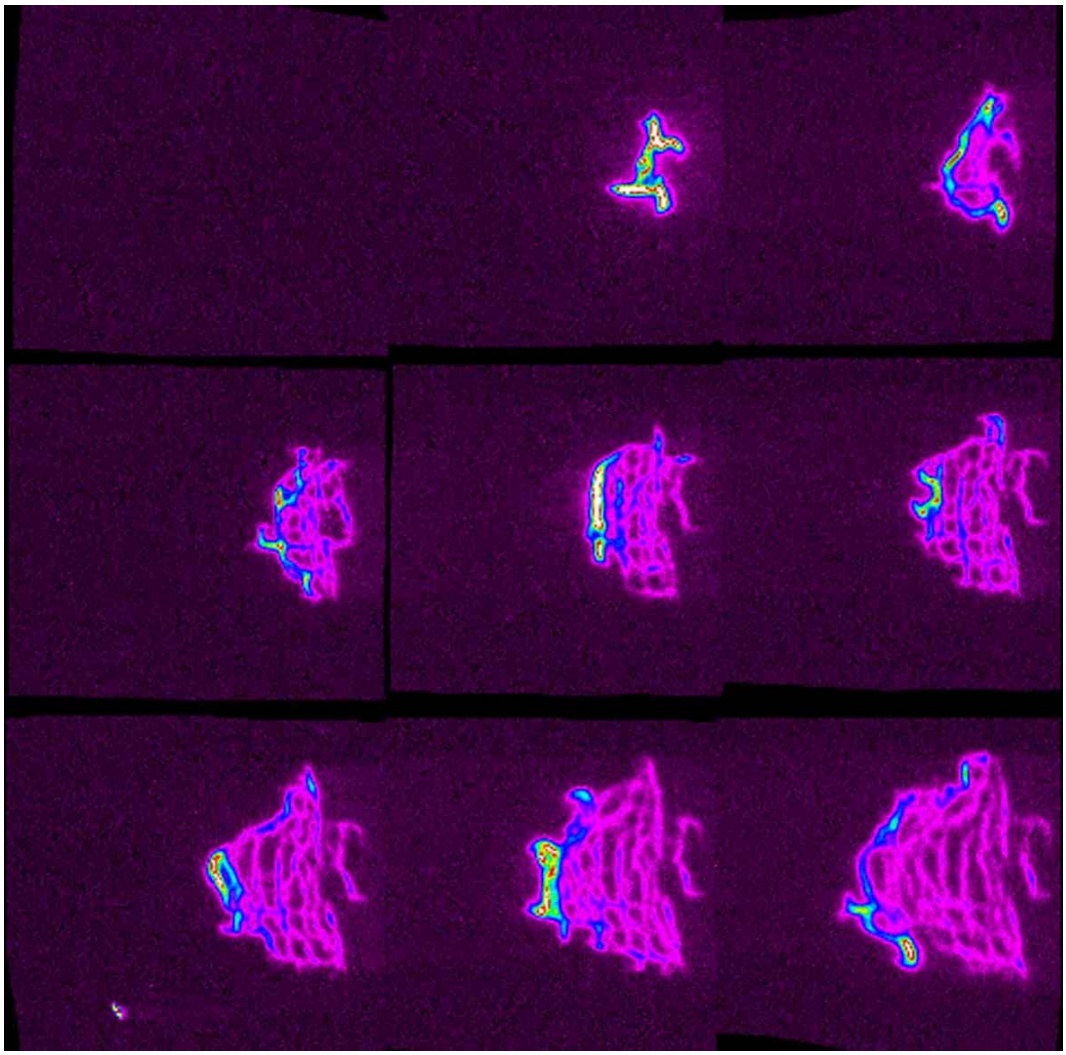

Fig.7.1.3. Frame-by-frame scan of initiated longitudinal surface MW discharge process development with τ_{pul} = 0.1 μs and τ_p = 1 μs

7.2. Streamer surface MW discharge in quasi-optical EM beam with λ = 2.5 cm

Since these investigations have been carried out during the third final stage of the present Project then they will be described in more details in the present report.

7.2.1. Experimental conditions

In this part we will describe an electrodynamical system of MW beam formation, characteristics of the submerged high-speed stream in the working chamber and a scheme of experiments undertaking.

EM wave with $\lambda = 2.5$ cm in experiments comes to spherically concave surface of a metallic mirror and it is focused. Linearly polarized TEM wave has electric component amplitude $E_0 = 3.3$ kV/cm in the focal area. A typical transversal size of the focal area has a scale of 1÷2 cm along the vector $\boldsymbol{E_0}$. The radiation is essentially modulated in the longitudinal direction with a typical period ≈ 1.5 cm. Thus a value of the field in the EM beam focus is $E_0 \approx 3.3$ kV/cm, and it is $E_0 \approx 2.8$ kV/cm in the nearest to it minimum. The field value falls in average at moving away from the focus to both sides along EM beam axis. A controlling scheme allows to generate both the single MW pulses with duration of $\tau_{pul} = 30$ μs, and their sequence with the same $\boldsymbol{\tau_{pul}}$ and with repetition frequency up to $f_{pul} = 100$ Hz.

A submerged high-speed air stream is formed in the setup at initial pressure of $p_c \approx 100$ Torr in the working chamber. It has approximately constant characteristics $\tau_{fl} = 1$ s: a transversal diameter 28 mm; flow Mach number M = 2 at static pressure of $p_{st} \approx 100$ Torr and temperature T = 150°K. Air pressure p ≈ 200 Torr at its normal temperature T = 300°K correspond to these characteristics. Flow vector $\mathbf{v_{fl}}$ direction is collinear to the vector $\boldsymbol{E_0}$.

Experiments, in which MW discharge was investigated at this wavelength in a free space, have shown that the an undercritical discharge with spatially developed volumetric streamer structure can be realized in the focus of EM beam at indicated above values of $\boldsymbol{E_0}$ and air pressure $\boldsymbol{p}$. The discharge in this case is initiated by the linear EM vibrator parallel to the field vector $\boldsymbol{E_0}$. An analogous initiator can be placed on a surface of radiotransparent dielectric plate for realization of the surface discharge.

The plate in these experiments was placed in EM beam so that the initiator on it was in the beam focus. In experiments we investigated three schemes of dielectric plate positional relationship with respect to the EM beam Pointing vector **Π** and its $\boldsymbol{E_0}$ vector. Explanation schemes are represented in Fig.**7.2.1.1**, **Fig.7.2.1.2** and **Fig.7.2.1.3**, corresponding photos are in Fig.**7.2.1.4**, **Fig.7.2.1.5** and Fig.**7.2.1.6**.

One can see in Fig.**7.2.1.1** that the dielectric plate in the first experimental formulation is almost perpendicular to the vector $\boldsymbol{\Pi}$, i.e. it lies approximately in the plane of EM beam $\boldsymbol{E}$ and $\boldsymbol{B}$ vectors. In experiments the plate was made of textolite of 2 mm thickness; its size is 390x100 mm. Upper and lower (with respect to the flow) edges are sharpened and polished. Discharge photo detection is possible only through an illuminator during experiments; the last one is located on a side surface of the working chamber. The illuminator surface is perpendicular to **E-Π** plate of EM beam and goes through its focus. Namely because of it we had to incline the plate with respect to the vector $\boldsymbol{\Pi}$ for an angle $\alpha = 12°$ in experiments, insuring a possibility of discharge photo detection, see Fig.**7.2.1.1**.

The vibrator on a dielectric plate is located on its surface opposite to the focusing mirror. The vibrator is made of a copper wire of a diameter 2a = 0.26 mm and length 2L = 12.5 mm. It is attached to the plate's surface by a glue "Supercement".

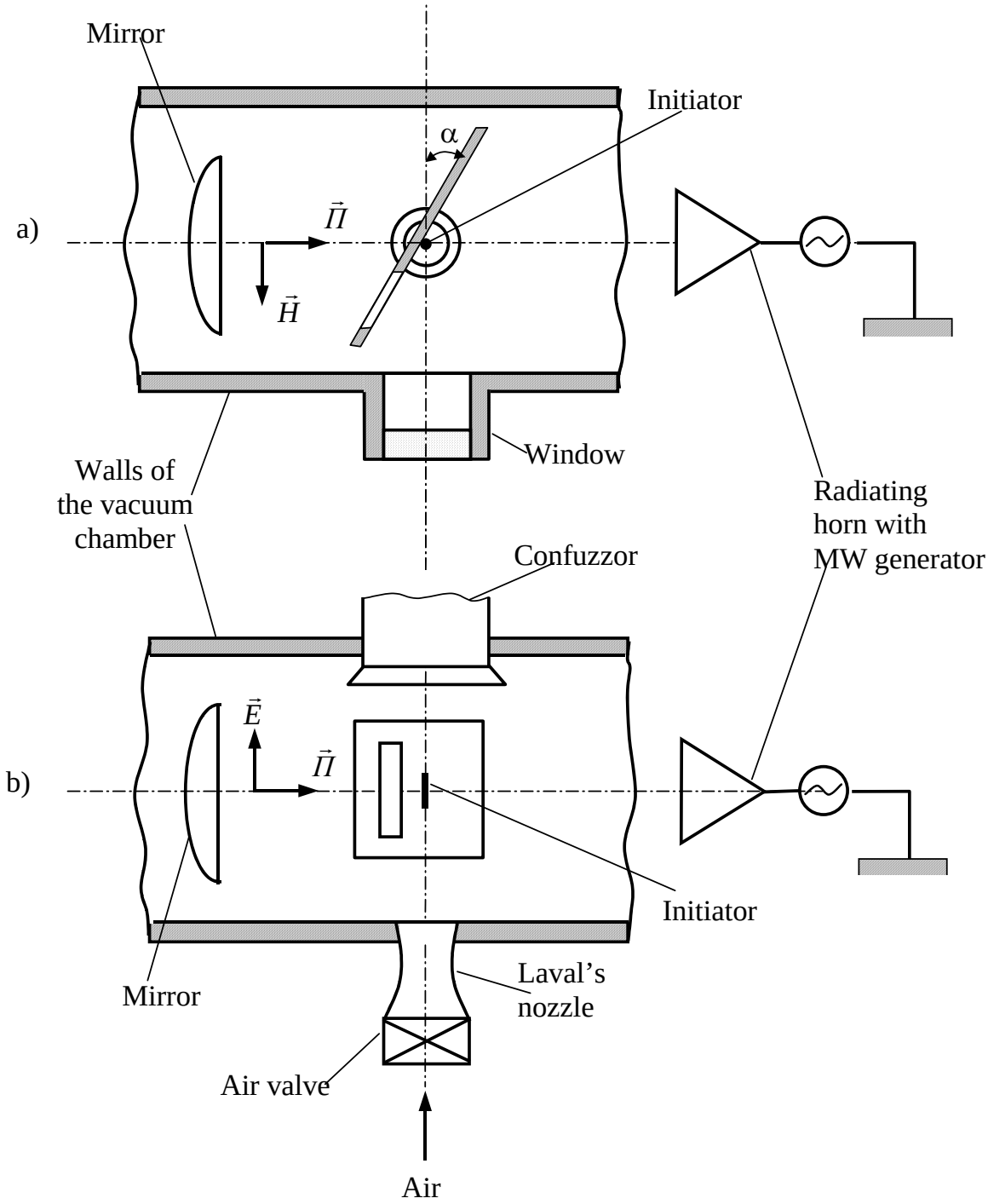

Fig.7.2.1.1. Experimental scheme on investigation of surface transversal MW discharge: a)- above view; b) – side view

The plate in the scheme represented in Fig. **7.2.1.2** still lies almost in the plane of **E – H** vectors. Its only inclined for a small angle $\alpha = 12°$ with respect to EM beam Pointing vector **Π,** but to another side with respect to the scheme shown in Fig.**7.2.1.1**. The vibrator is still fixed to its surface opposite to the mirror focusing EM wave. It also has 2a = 0.26 mm and 2L = 12.5 mm. The plate has a technological aperture. Its sizes are clear from Fig.**7.2.1.7**. Presence of additional flat optical mirror in this scheme allows to undertake the surface discharge photo detection from the perspective more perpendicular to the plate's surface than in the scheme in Fig.**7.2.1.1**. The photo detection scheme is clear from Fig. **7.2.1.2**.

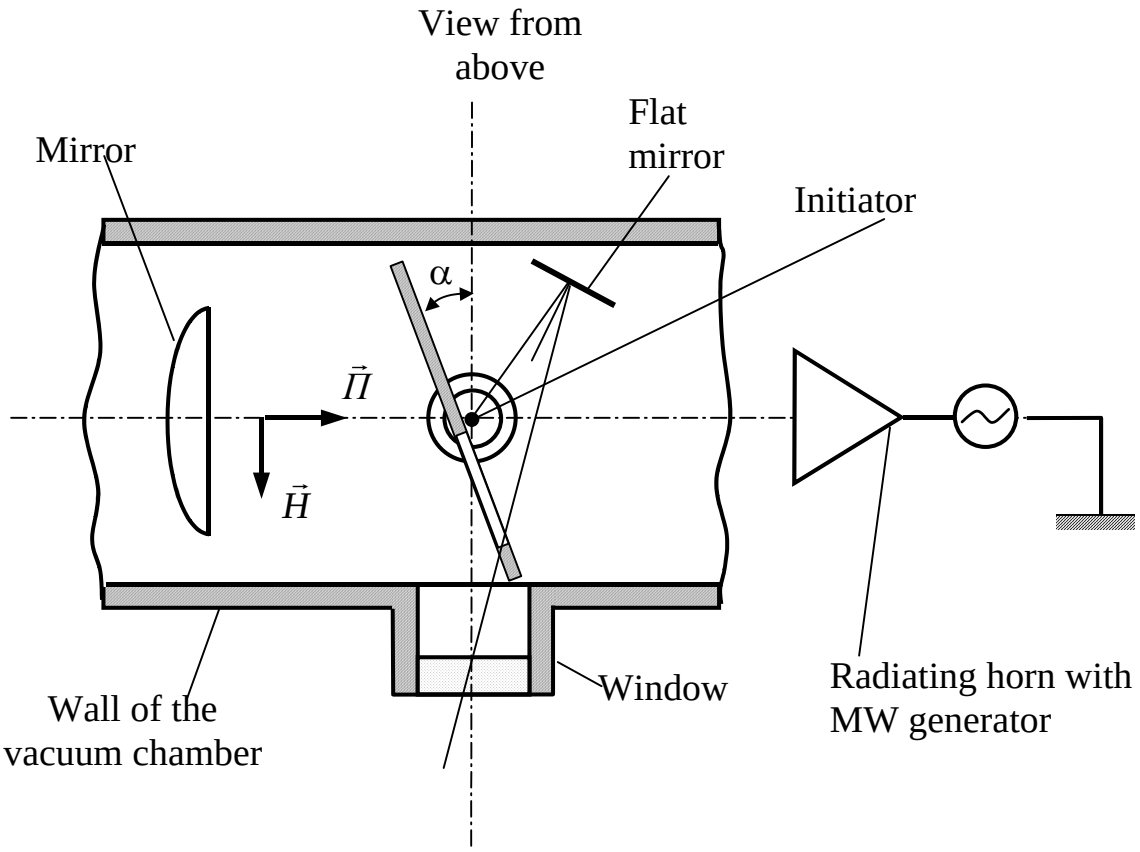

Fig.7.2.1.2. An experimental scheme on investigations of surface transversal MW discharge with application of a flat mirror

One can see In Fig. **7.2.1.3** that the dielectric plate with the fixed vibrator to it in the third experimental formulation lies in the plain of EM beam **E - Π** vectors. It is placed along the axis of this beam. The plate is also made of textolite of 2 mm width and has a working size 0x100 mm. Upper and lower edges of the plate working part are also sharpened and polished for better streamlining. EM vibrator fixed to the plate's surface facing the illuminator also has 2a = 0.26 mm and 2L = 12.5 mm.

Later according with our agreement we call the discharge realized by schemes represented in Fig**.7.2.1.1** and Fig**.7.2.1.2** – the transversal, and realized by the scheme represented in Fig**.7.2.1.3** – the longitudinal.

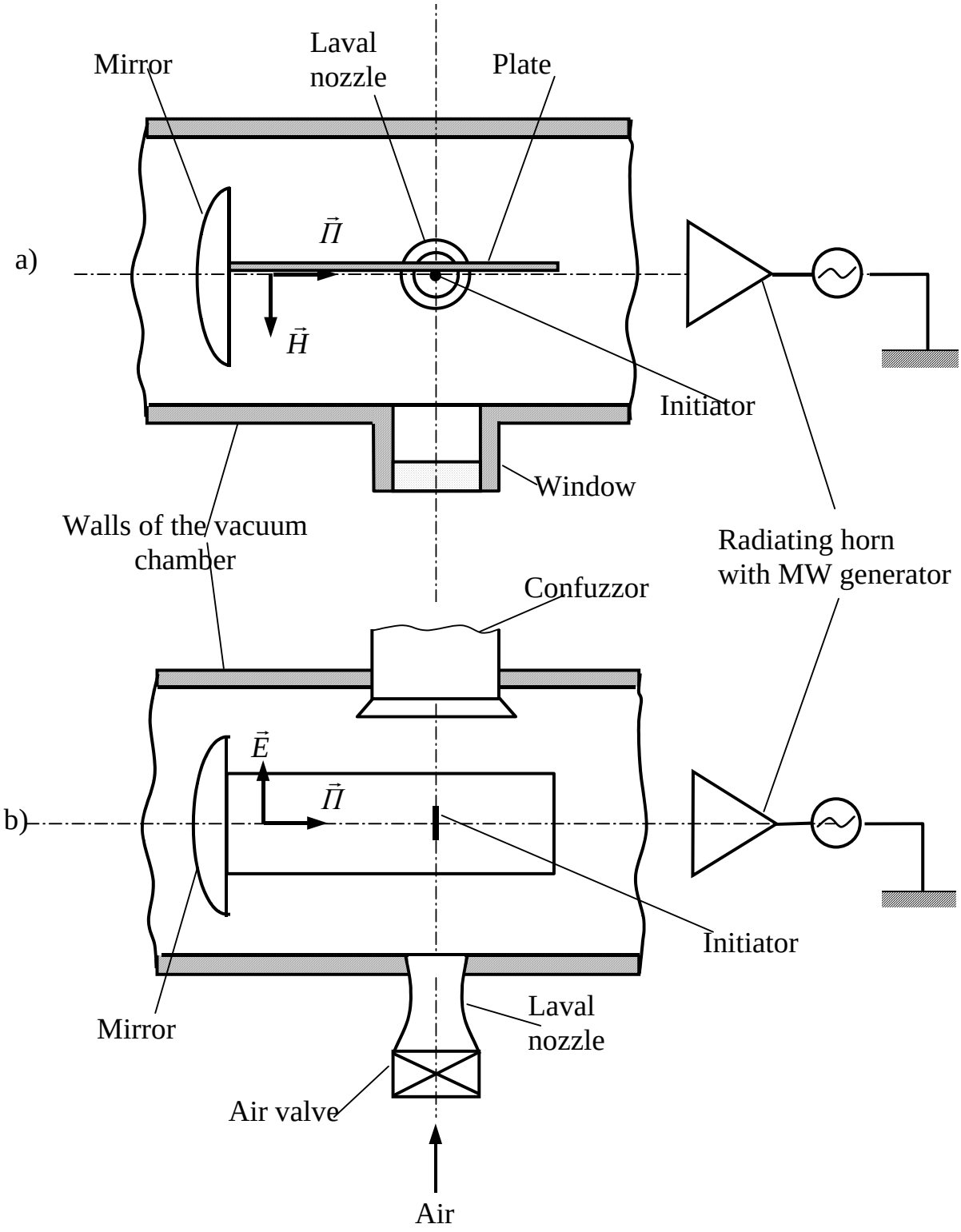

Fig.7.2.1.3. Experimental scheme on investigations of MW surface longitudinal discharge: a)-view from above; b)-side view

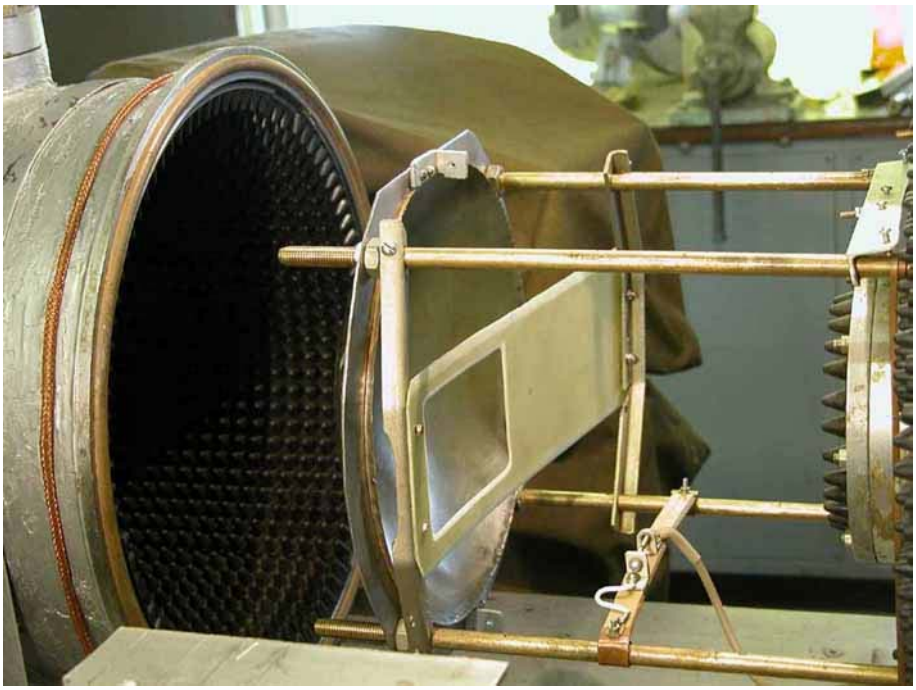

Fig.7.2.1.4. Appearance of the chamber's working area in experimentson investigations of surface transversal MW discharge

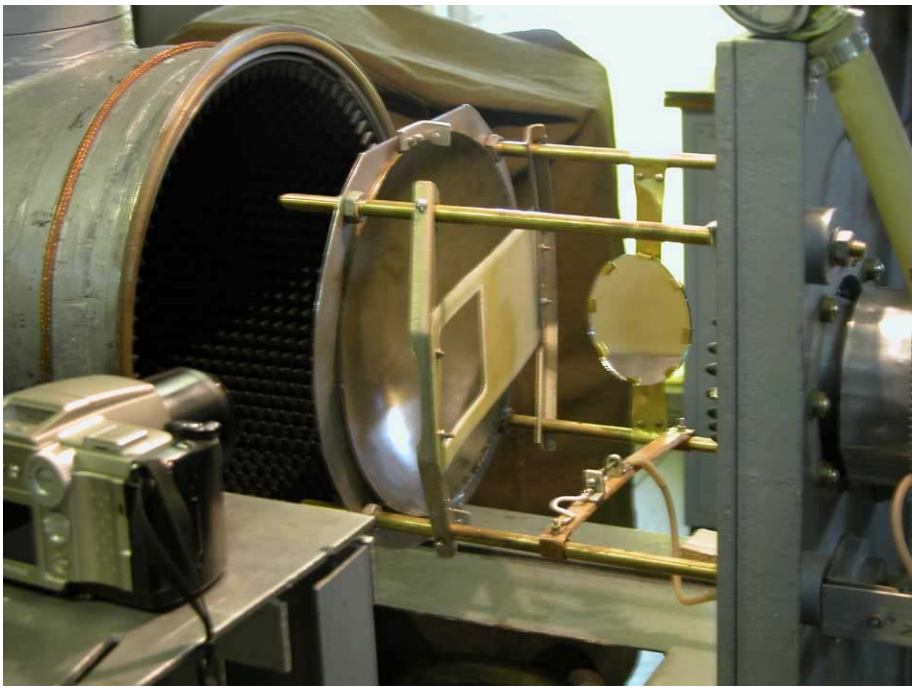

Fig.7.2.1.5 Appearance of the chamber's working area in experimentson investigations of surface transversal MW discharge with application of a flat mirror

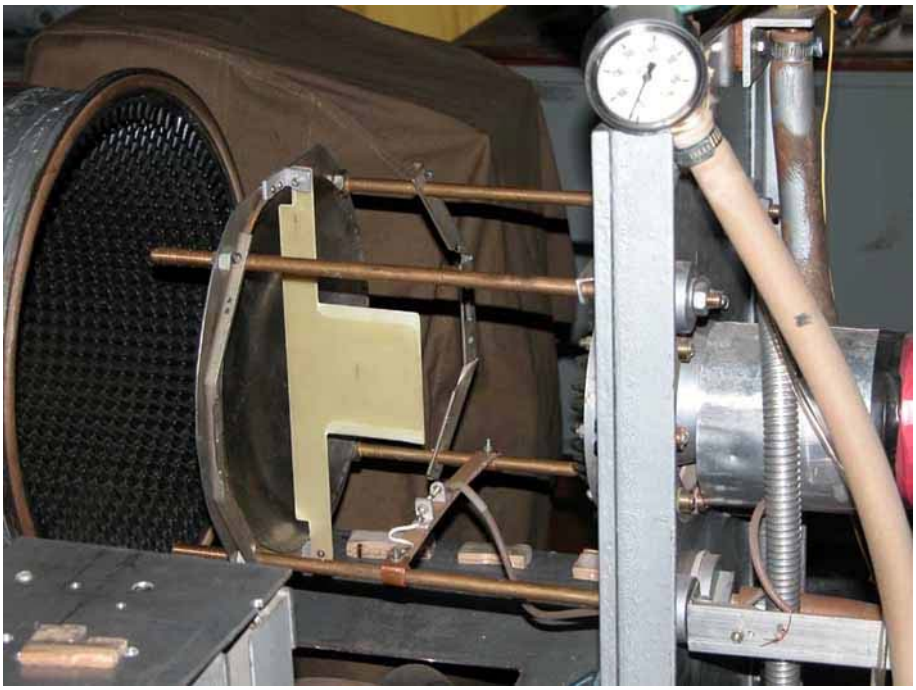

Fig.7.2.1.6. Appearance of the chamber's working area in experimentson investigations of surface longitudinal MW discharge

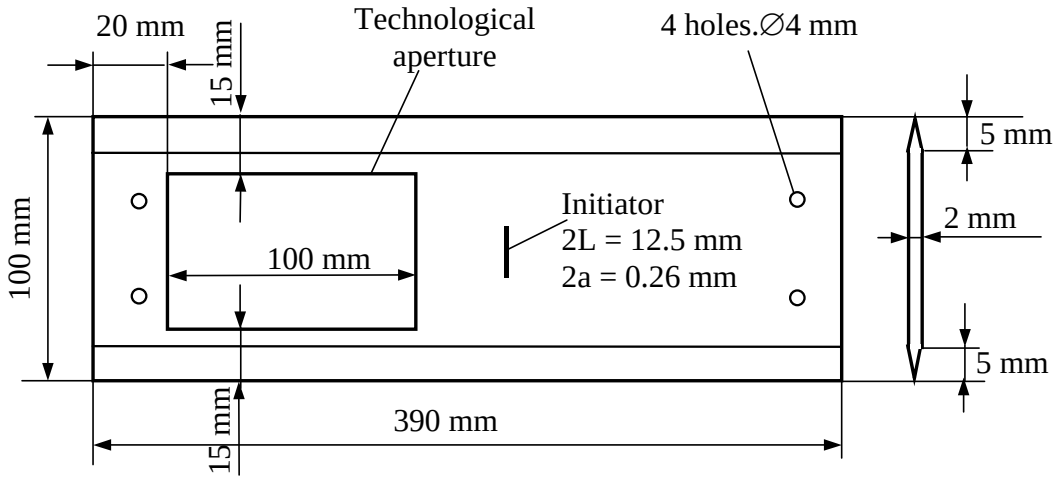

Fig.7.2.1.7. A design of a dielectric plate for experiments on creation of longitudinal MW discharge

7.2.2. Experimental results with a transversal discharge

In Fig.**7.2.2.1** one can see photos illustrating experimental results on investigations of transversal surface MW discharge realized by a scheme from Fig.**7.2.1.1**. The size of the initiator 2L = 12.5 mm is a scale of image.

Photos are placed in rows. Every row corresponds to definite experimental conditions: the upper – to absence of a discharge and a flow; the second and third – to discharges in dead air at different ***p***; the fourth to the discharge at presence of a high-speed stream flowing around the plate. The upper photo was obtained at moved aside chamber (open), i.e. at natural plate illumination. The following photos were obtained at closed chamber.

In the upper photo one can see an initiator attached to the surface of a dielectric plate.

The next row of photos illustrates appearance of surface transversal discharge in dead air at p = 200 Torr. Remember that air molecule concentration in cold air corresponds namely to this pressure.

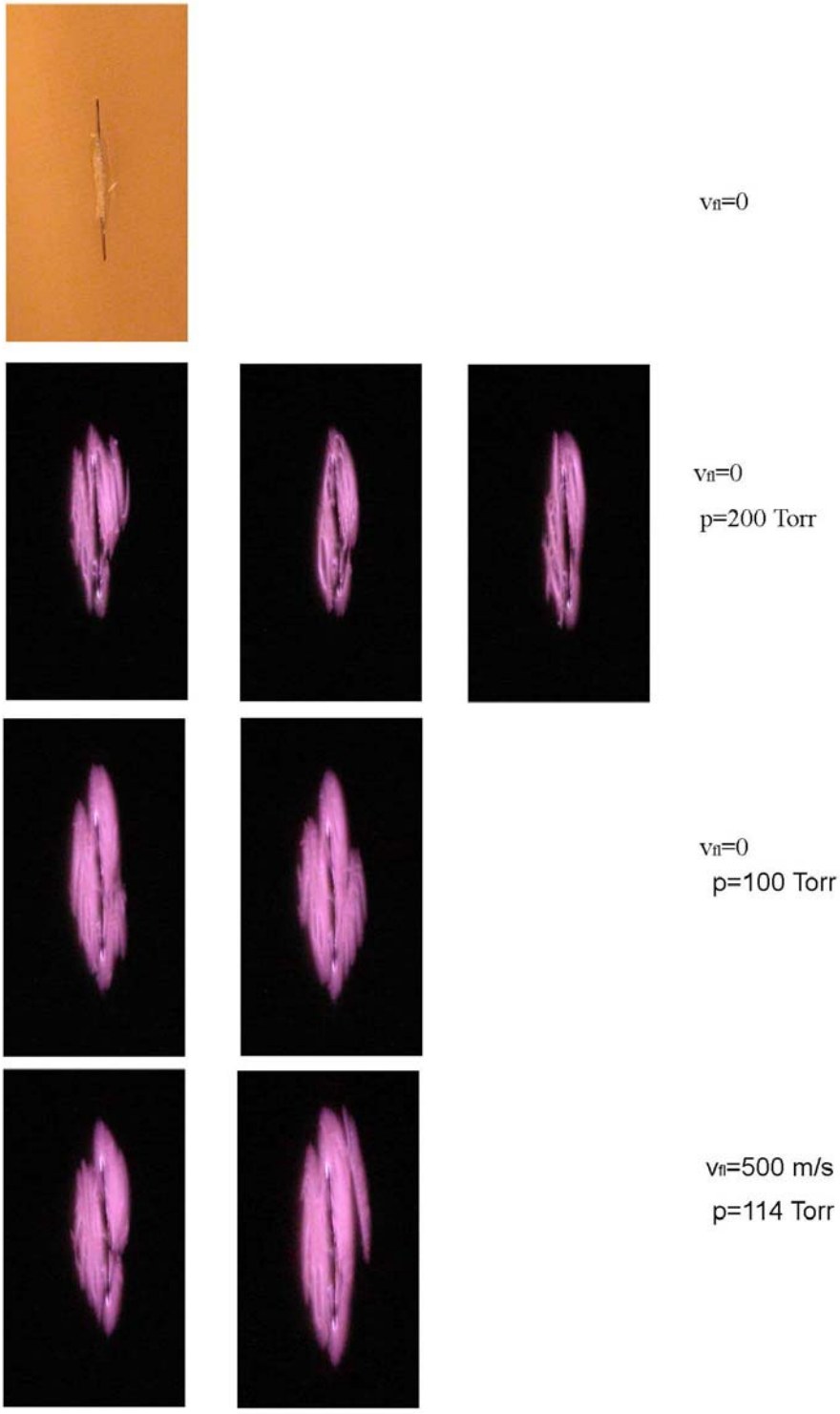

Fig.7.2.2.1. MW transversal discharge appearance photos

One can see in them that the discharge area is localized near the initiator and as if it visualizes a typical size of EM beam focus transversal cross section. We placed in this row three photos corresponding to three consequent MW pulses. A pause duration between them was sufficiently long to insure the following pulse initial discharge condition independence from the previous one. It follows from the photos that the discharge is realized in the streamer form, i.e. it consists of thin

plasma channels. Their typical transversal size does not exceed the initiator's diameter 2a = 0.26 mm. One can see in photos that definite geometry of the streamer plasma channels is not the same in different MW pulses.

For a comparison in the third row of photos we put photos of discharges in two MW pulses in dead air but at lower pressure p ≈ 100 Torr. It can be seen that these discharges still occupy only a size of EM beam focus transversal cross section. They are still the streamer ones, but plasma channels composing them are "more diffuse".

And finally we give photos of three realizations of transversal undercritical EM vibrator initiated MW discharge realized on a surface of a dielectric plate in a flow. One can see in them that the streamer channels forming the discharge are as if "smeared" along the flow. Remember that the flow is directed down-up.

In Fig.**7.2.2.2** we represent photos illustrating experimental results on investigations of transversal surface MW discharge obtained with a help of the scheme from Fig.**7.2.1.2**. In them experimental conditions are still different for each row and are analogous to those from Fig.**7.2.2.1**. Discharge photos in Fig.**7.2.2.2** additionally confirm the transversal surface MW discharge is the streamer one in the experimental conditions. At that at given conditions it is realized with surface developed structure.

These discharges in a flow practically do not differ from those in dead air. One can suppose that it can be explained by the fact that the plasma discharge channels are pressed to the surface of a dielectric plate. It means that they are realized in areas where the flow velocity is practically zero. Indirectly it is confirmed by a fact that the discharges in a high-speed flow are by their appearance closer to the discharges in dead air at lower pressure p = 100 Torr, than at p = 200 Torr. Discharge plasma channels have comparably larger thickness in the flow.

For confirming of this hypothesis we undertook a control experiment with surface discharge realization on a plate, when it is placed in the plane strictly perpendicular to the vector **Π**. A scheme of this experiment is represented in Fig.**7.2.2.3**.

One can see the corresponding photos in Fig.**7.2.2.4**. Left photo corresponds to $v_{fl} = 0$ and p = 200 Torr, the middle – to $v_{fl} = 0$ and p = 114 Torr, and the right one - to $v_{fl} = 500$ m/s and p = 114 Torr. In the photos one can see glowing areas vertically elongated. A scale of images can be estimated with a help of typical maximum transversal size of glowing areas, which is not larger than ≈ 1.7 mm. Naturally, in these photos we do not see the plasma channels that are situated along the plates surface. In this connection a reason responsible for fixing of glowing areas in the photos is unclear. This can be an optical radiation going directly from the plasma channels, or a glow of air adjoining to these channels appearing due the hard radiation from these plasma channels. One can see from the photos represented in Fig.7.2.2.4 that external side appearance of the surface "strictly" transversal MW discharge area practically does not depend on air pressure or on the flow longitudinally streamlining the plate.

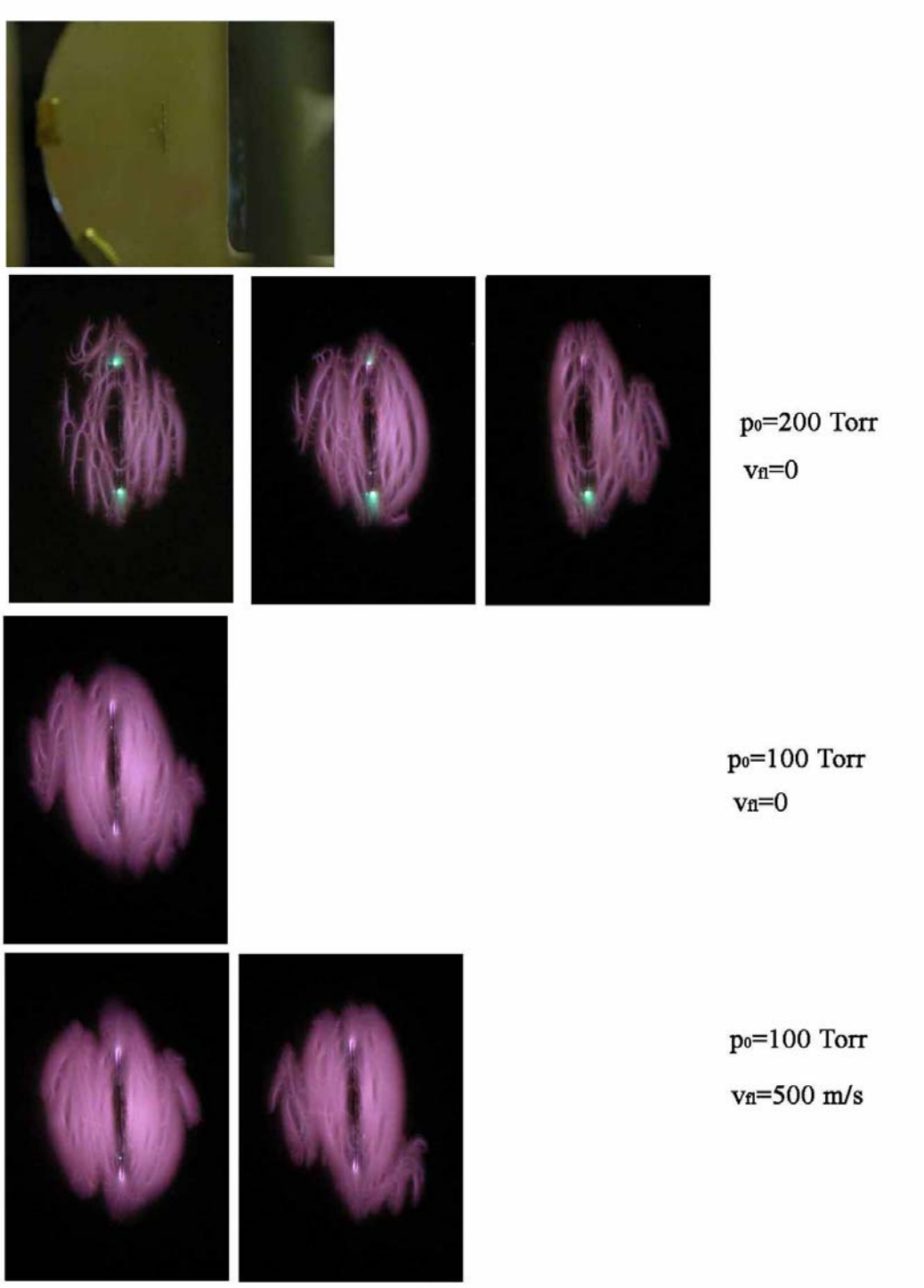

Fig.7.2.2.2. Transversal MW discharge appearance photos at their detection through additional flat mirror

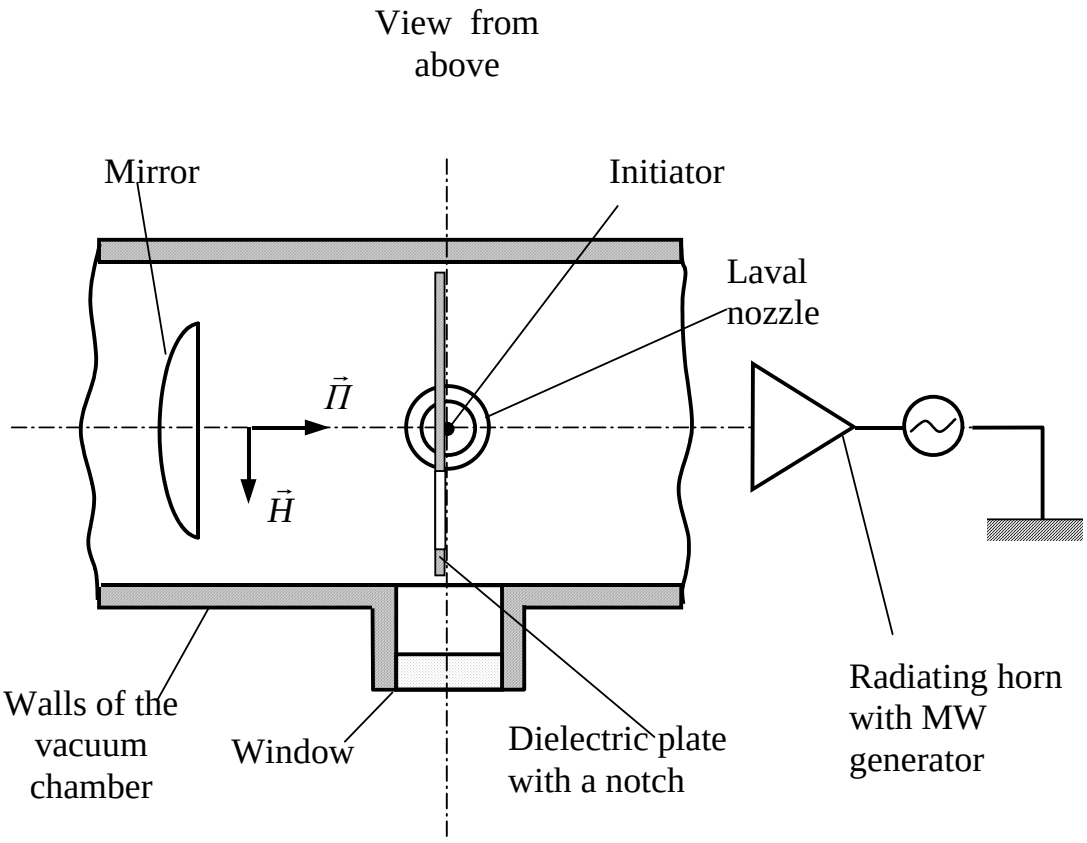

Fig.7.2.2.3. Experimental scheme on investigations of surface transversal MW discharge in the plane strictly perpendicular to the vector $\vec{\Pi}$

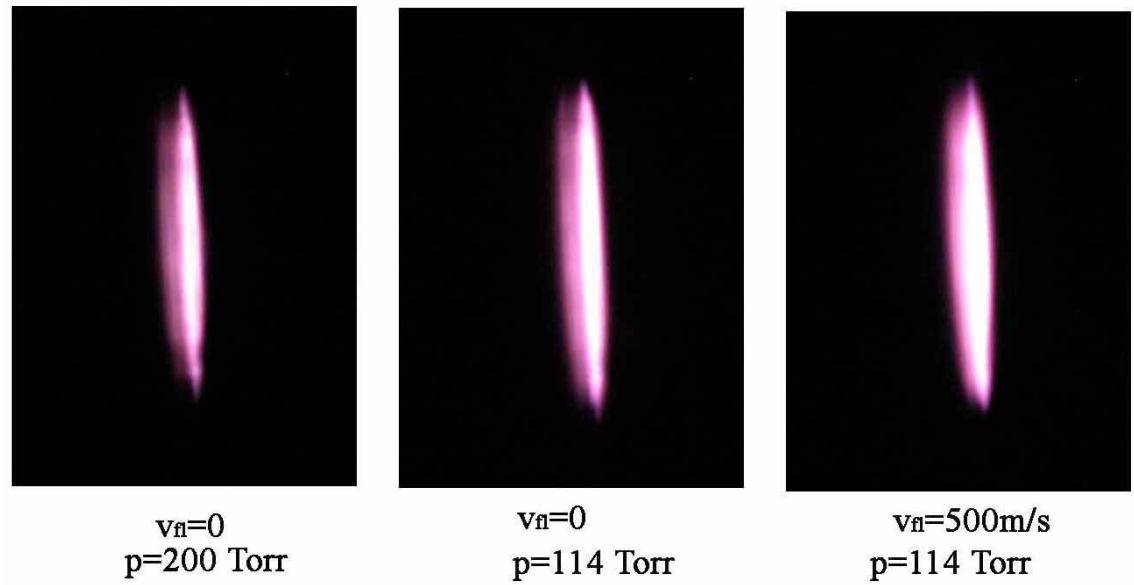

Fig.7.2.2.4. Appearance of MW discharge along a surface of the dielectric plate

7.2.3. Experimental results with a longitudinal discharge

These experiments were carried out at the plate position along EM beam axis in the plane of its **E - Π** vectors, as it was described above. Influence of the plate being in EM beam on the spatial structure of its field can be determined by discharge realization at low air pressure. In Fig.**7.2.3.1**

one can see a corresponding photo of diffuse MW discharge at air pressure of p = 30 Torr. One can see in it that the vibrator located on the plate is in the loop of EM beam field.

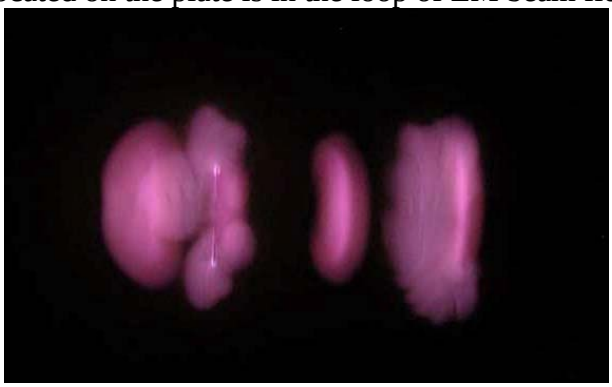

Fig.7.2.3.1. EM field structure visualizing in the working are at application of the diffuse discharge

In Fig.**7.2.3.2** one can see photos illustrating experimental results on investigation of longitudinal surface MW discharge. A size of an initiator 2L = 12.5 mm can be used in them as an image scale.

In the upper photo one can see the initiator fixed to the surface of a dielectric plate. The next row of photos illustrates different realizations of the surface longitudinal discharge in dead air at pressure of p = 200 Torr. It follows from the photos that the discharge is located in the longitudinal focal field loop. At the same time one can notice that the longitudinal discharge is more elongated in the vertical direction along the field vector ***E*** in difference with the transversal discharge. The discharge has a streamer structure. Separate plasma channels forming it are very thin. Their diameter is substantially smaller than the diameter ***2a*** of EM vibrator initiating the discharge. At the same time separate plasma channels of the discharge elongated mainly along the vector **E** have the larger transversal size and are more diffuse. One can suppose that these sections presence is connected with spatial limitation of the discharge area, and it is connected with essential modulation of $\boldsymbol{E_0}$ field value along EM beam. A following fact attracts attention: plasma channels density is small in direct vicinity to the middle area of the initiator. Position of the streamer channels on the dielectric surface is still different in different MW pulses.

For a comparison in the third row we put photos of discharges in dead air at its lower pressure p ≈ 100 Torr. It can be seen that the discharge on a dielectric surface has as if four zones: two side ones with respect to the vibrator and upper and lower with respect to the dielectric. The discharge is practically absent in the central zone adjoining it. The diffuse background is essential in discharge areas and thing plasma channels are also visible. The discharge area in the longitudinal direction with respect to EM beam ***Π*** vector still practically does not go out of the focal area of the beam. The size of the discharge area is substantially enlarged along the vector ***E*** in difference to the discharge at p = 200 Torr.

And finally photos of undercritical vibrator initiated MW discharge on a surface of a dielectric plate realized in a high-speed flow are given in the lower row. This discharge is externally very much alike the discharge at p ≈ 100 Torr. At the same time one can not see thin plasma channels in its diffusely smeared four zones. Upper and lower zones of this discharge are more elongated along the field vector ***E*** and **v** vector of the flow.

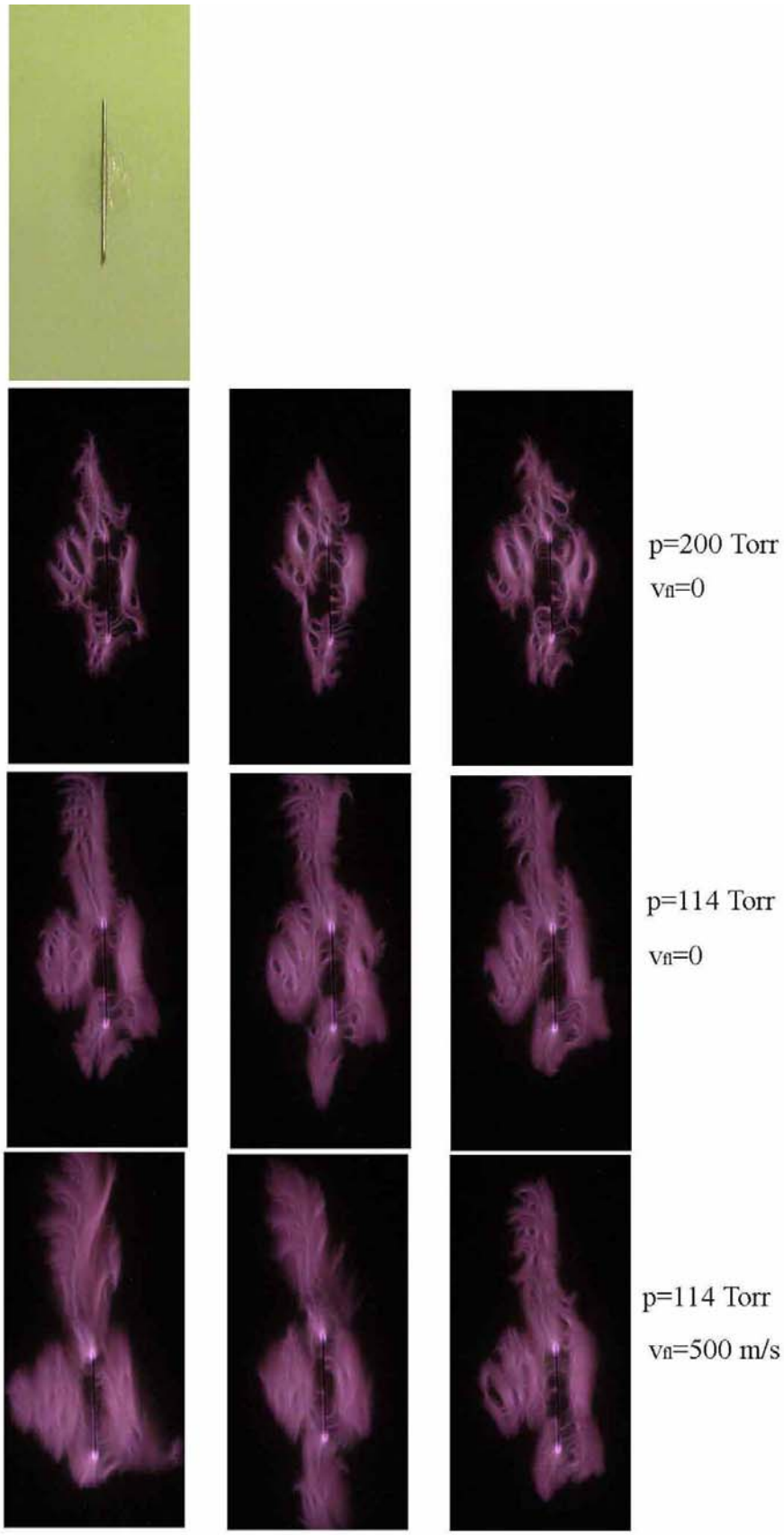

Fig.7.2.3.2. Appearance of longitudinal MW discharge

7.2.4. Surface MW discharge in a bunch of EM pulses

Previous parts describe surface EM discharges in essence in a single EM pulse. Applied experimental setup allows to realize them also in a continuous consequence of EM pulses.

In Fig.**7.2.4.1a** and Fig.**7.2.4.1b** one can see photos of transversal surface vibrator initiated MW discharge in dead air at p = 200 Torr and p = 100 Torr, respectively, at EM pulses repetition frequency f_{pul} = 100 Hz during a time of their giving 0.3 s. These are integral photos. They were obtained with exposure time longer than EM pulse bunch duration. One can see that the discharge

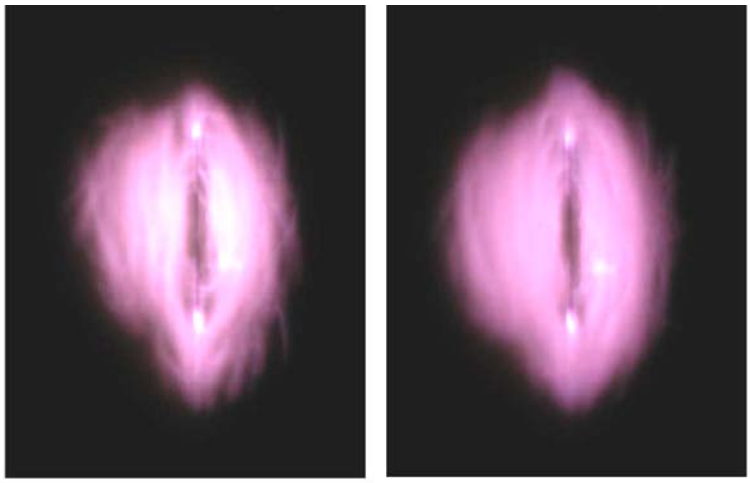

Fig.7.2.4.1. Appearance of longitudinal MW discharge from a bunch of EM pulses

area is essentially "light-struck" in these photos. It also follows from them that a luminescent trace goes up from the discharge area in this experimental formulation. It is connected with air heating in each MW pulse. A density of air molecules decreases in the consequent pulses near the plate surface. So the discharge "physics" can be changed. It can be transformed to a diffuse surface MW discharge from the streamer surface MW discharge. The trace presence carries some definite information also about the surface MW discharge information with EM field. A convective molecule drift in principle allows to estimate EM beam field energy part, which went to air heating in the discharge.

In Fig.**7.2.4.2** one can see an integral photo of this discharge but in a high-speed flow.

Fig.7.2.4.2. Appearance of longitudinal MW discharge from a bunch of EM pulses in a high-speed flow

The discharge occupies only an area of EM beam focus cross section with its typical size. This is connected with a fact that the discharge is realized in a new air portion in each of MW consequent

pulses. The streamer channels are already indistinguishable in the discharge area, because their position is changed in each MW pulse.

In Fig**.7.2.4.3a** and Fig.**7.2.4.3b** one can see integral photos of longitudinal undercritical EM vibrator initiated surface MW discharge in dead air at p = 200 Torr and p = 100 Torr, respectively, at EM pulse repetition frequency f_{pul} = 100 Hz during their giving time 0.3 s.

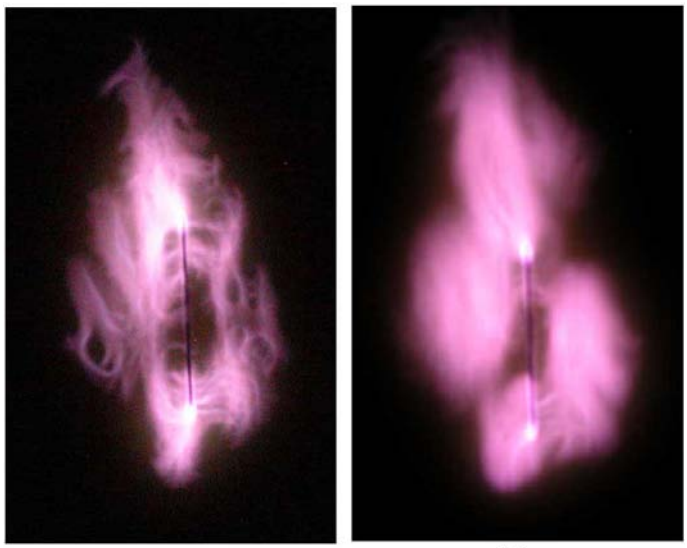

Fig.7.2.4.3. Appearance of MW longitudinal discharge from a bunch of pulses

And finally one can see in Fig**.7.2.4.4** an integral photo of this discharge but already in a high-speed flow. It can be seen that the discharge area in this case is distinctly separated in four fragments. Naturally, thin discharge structure inside these fragments can not be seen.

Fig.7.2.4.4. Appearance of longitudinal MW discharge from a bunch of pulses in a high-speed flow

7.3. Discussion of experimental results

Thus pulsed transversal and longitudinal MW discharges in air in quasi-optical EM beam have been realized in our experiments. The experiments have shown that these discharges are realized in the streamer form at comparably high air pressure ***p***. In this connection one can suppose that they energy effectively interact with EM field exciting them. This gives grounds to consider perspectives of their application and stimulates fundamental investigations of their features. The experiments have shown that typical times of these discharges development allow to realize them also in high-speed air flows with velocity of several m/s.

Accumulated experience on free localized MW discharges investigation allows to create a program of these investigations. First of all one has to determine a level of a critical field $\boldsymbol{E_{cr}}$ for given discharge types. One has to determine a boundary over air pressure ***p*** separating areas of diffuse and streamer types of these discharges. One has to determine a boundary separating surface streamer MW discharges on an undercritical type with surface developed structure from the discharges of deeply undercritical type. Equipment already applied in experiments will allow to undertake these investigations at two wavelengths λ of EM field both in a single pulse and in bunch. These discharge types can be realized also in a high-speed flow of propane-air flammable mixture.

Surface MW discharges in quasi-optical EM beam are in some sense more easily technologically realized in comparison with analogous free localized discharges. This is an additional stimulating circumstance for undertaking of their investigation cycle.

8. Theoretical and computation assistance of experimental investigations

8.1. MW electric field amplitude absolute value local measurements method

Measurements of electric field strength in the given point of a space represent a serious methodical problem because an application of any electro-technical sensors inadmissibly deforms its initial distribution. Use of the mediated methods (such as heating of small bodies with known conductivity, ignition of discharge in sealed small-size bulbs, optical methods and so forth) does not allow to obtain an information about an absolute value of electric fields with a reasonable accuracy.

Development of MW-initiated gas discharges theory has allowed to formulate, to work out and successfully to apply the method of electric field amplitude absolute value measurement in experimental practice. The developed method may be applied in any wavelength band smaller than 1 cm down to a constant field.

It is well-known from classical electrodynamics that if we place a metallic sphere with a radius $\mathbf{a} << \boldsymbol{\lambda}/\mathbf{4}$ in the field of linearly polarized electromagnetic radiation with a wavelength $\boldsymbol{\lambda}$ the electric field in the nearest vicinity of this sphere in quasi-stationary approach is described by a relation:

$$\vec{\mathrm{E}} = -\nabla\varphi, \tag{8.1.1}$$

where

$$\varphi = -\vec{\mathrm{E}}_0 \cdot \vec{\mathrm{r}} \cdot \left(1 - \frac{\mathrm{a}^3}{\mathrm{r}^3}\right). \tag{8.1.2}$$

Thus, the field on an axis of the sphere oriented along the electric field vector is distributed by the law

$$E = E_0 \cdot \left(1 + \frac{2}{(r/a)^3}\right). \qquad (8.1.3)$$

Distribution of the electric field amplitude around the metallic sphere of a small radius is shown in Fig.8.1.1.

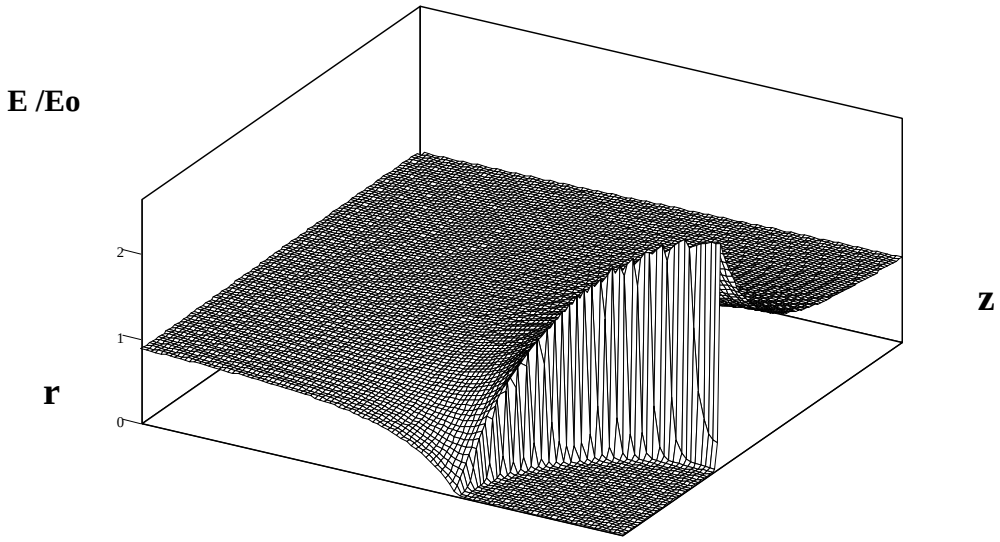

Fig.8.1.1. MW field amplitude spatial distribution in the vicinity of a small-sized metallic sphere.

The maximal value of an electric field on a sphere surface exceeds its undisturbed value by 3 times. The field distortion caused by the presence of sphere has a local character and is relatively small at removal from the sphere on distance bigger than the radius. If the field on a sphere surface exceeds its critical value $\mathbf{E_{cr}}$ (well-known value from numerous investigations in gas-discharge physics) there will be a breakdown. Occurrence of breakdown is easily detected by any suitable instrumentation. Dependence of critical field $\mathbf{E_{cr}}$ on gas pressure is also well-known. Reducing a gas pressure in the experimental volume at the fixed level of an electric field one can determine a boundary pressure $\mathbf{p_{br}}$ when the breakdown occurs. The measured amplitude of an electric field in the point of sphere location is equal

$$\mathbf{E} = \frac{\mathbf{E_{cr}}(\mathbf{p_{br}})}{3}. \qquad (8.1.4)$$

However, at measurement of small values of electric fields, pressure should be lowered down to values, at which the breakdown field differs from the critical one due to the influence of diffusion escape of electrons from the area of maximal field near the sphere. Calculations of the electron diffusion influence are represented in Section 9.

Presence of the sphere reduces the breakdown field by 3 times at high air pressure but practically does not influence it at low pressure because of the diffusion. Theoretical dependence of the breakdown field with a ball [8] and similar known dependence in the case of free space at the radiation wavelength λ = 2.5 cm are shown in Fig. 8.1.2.

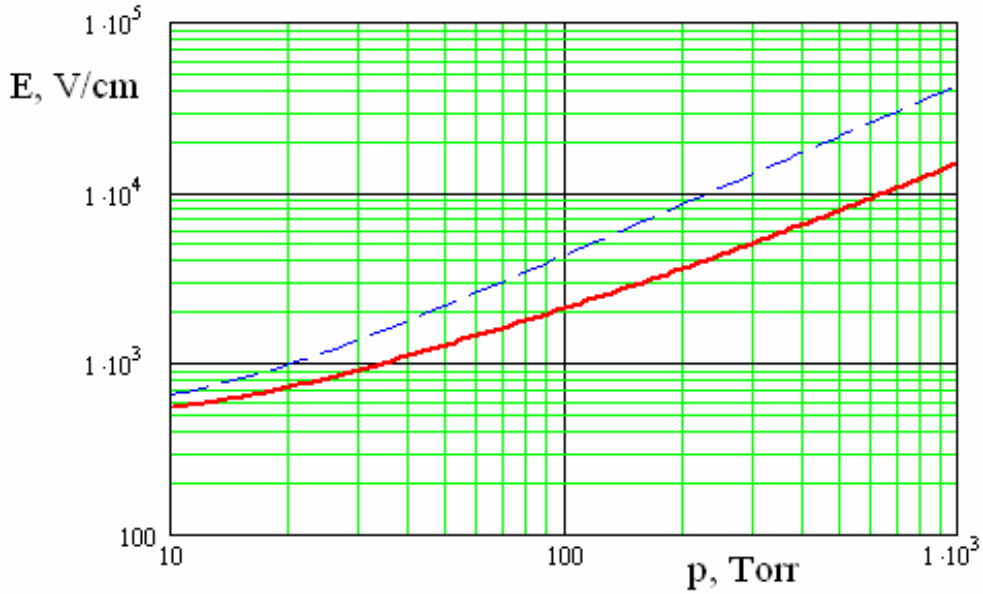

Fig.8.1.2. Breakdown field amplitude as an air pressure function at 2 mm (in diameter) metallic sphere presence (red solid line) and without it (blue dashed line) at the radiation wavelength λ = 2.5 cm.

8.2. Calculation of a field structure in an experimental volume (λ= 2.5 cm)

The computational program was developed for a calculation of electric field spatial distribution in the working volume. In this program output horn aperture, surfaces of a mirror and a lens are broken into separate elementary radiating units. Fields of their radiation are summarized in each point of the space. Certainly, all the necessary boundary conditions and phase shifts brought in by these elements are taken into account.

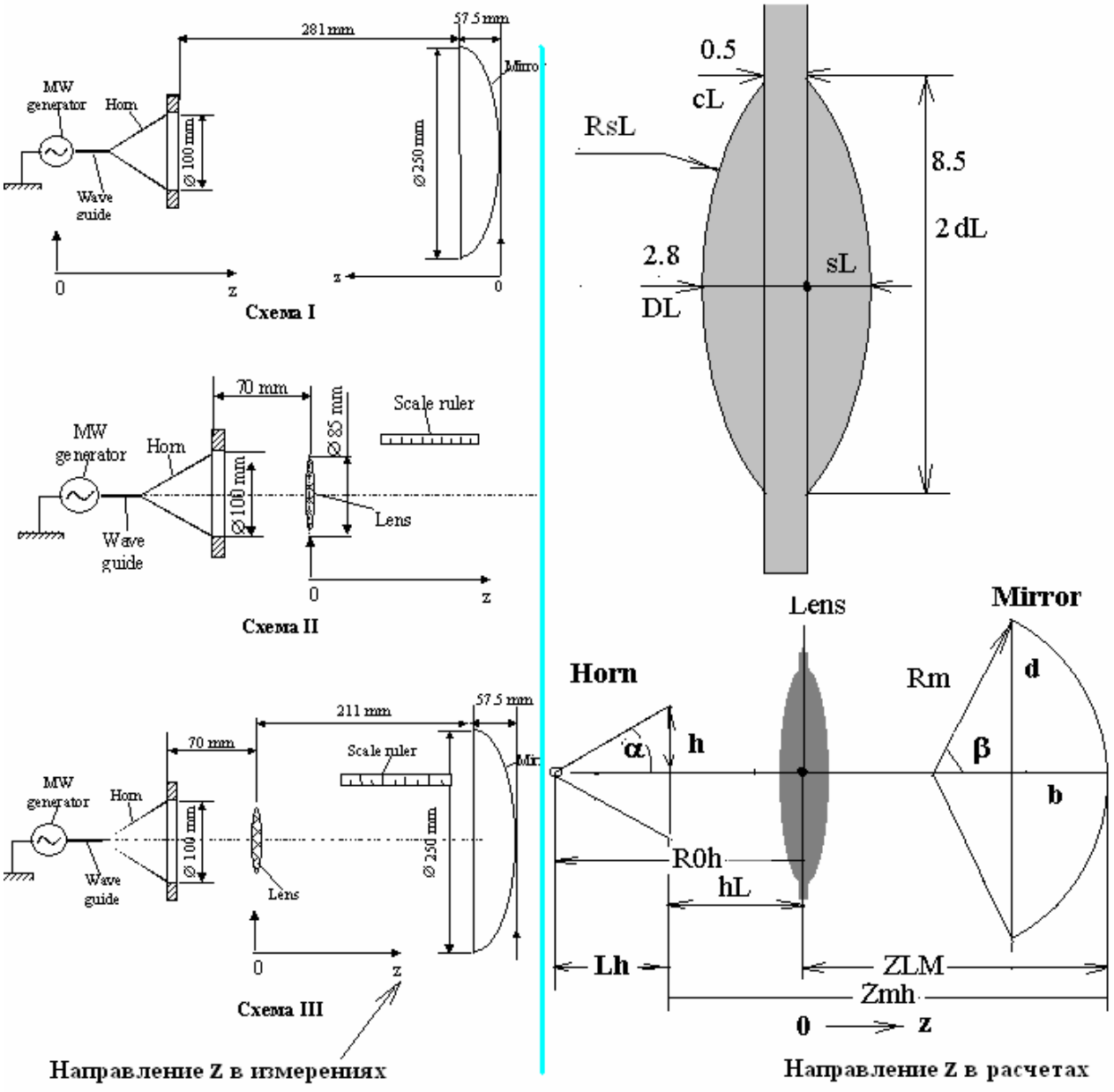

Fig.8.2.1. Variants of antenna system schemes: I – horn + mirror, II – horn + lens, III – horn + lens + mirror, λ = 2.5 cm.

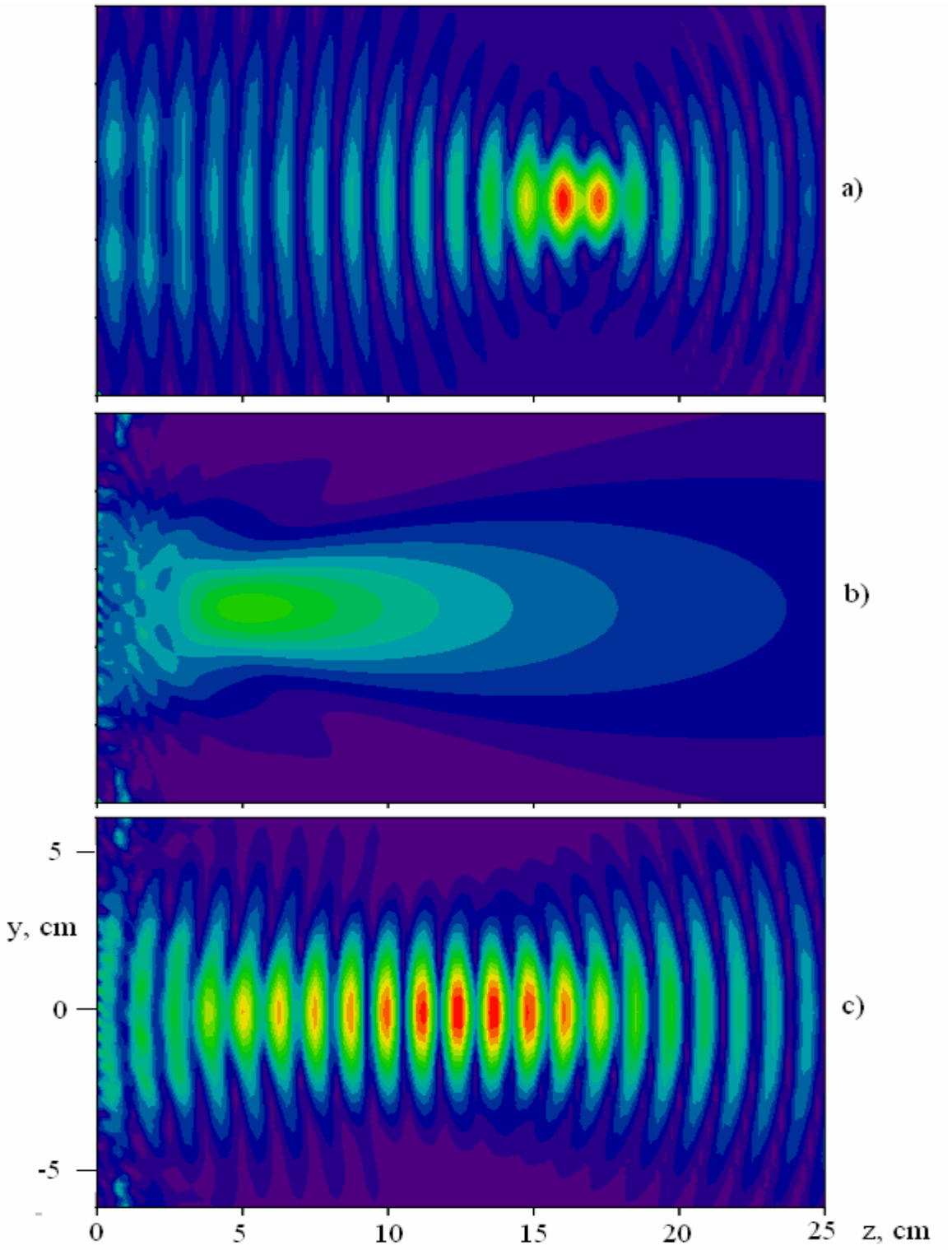

Fig.8.2.2. Calculated distribution of electric field amplitude in experimental space in a coordinate plane (z, y): scheme I (a) – horn + mirror, scheme II (b) – horn + lens, scheme III (c) – horn + lens + mirror, λ = 2.5 cm.

Distributions of field amplitude in the test chamber for three variants of investigated schemes, shown above in Fig.8.2.1, are presented in Fig.8.2.2. Values of coordinates z =0 and z =25 cm in Fig.8.2.2 correspond to positions of the lens (to the left) and the mirror (to the right). Red color indicates areas with the peak field amplitude.

Distributions in Fig.8.2.2 confirm that the Scheme III really allows to obtain more extended segment (along the system axis) with a high value of the amplitude. This significantly expands experimental opportunities.

Quantitative values of the amplitude are resulted in Fig.8.2.3 where are shown the distributions of the amplitude along the system axis, calculated in the case of radiation power of 50 kW in a horn

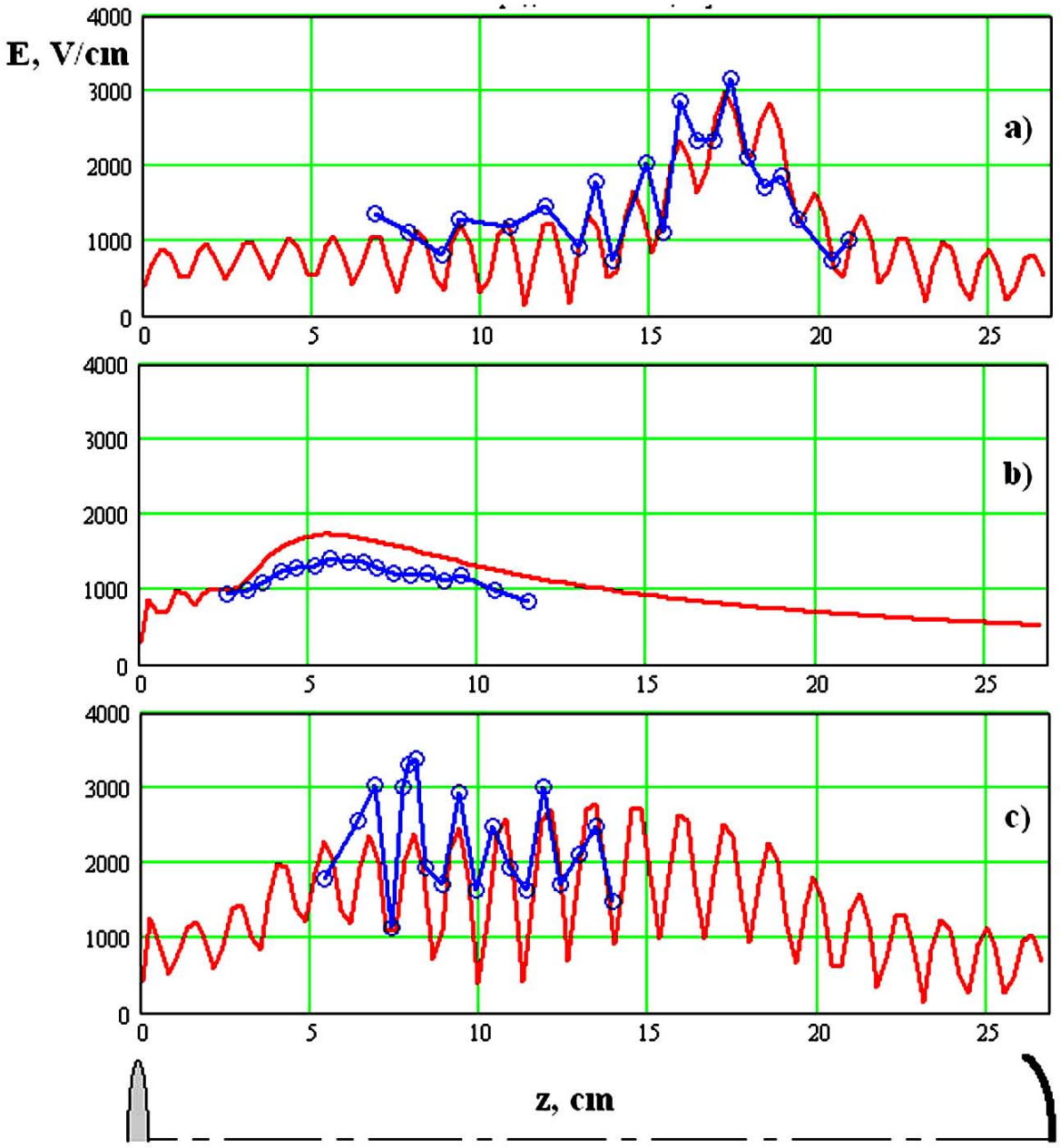

Fig.8.2.3. Comparison of the electric field amplitude calculated distributions along the axis z of experimental chamber: scheme I (a) – horn + mirror, scheme II (b) – horn + lens, and scheme III (c) – horn + lens + mirror. Calculated values of electric fields correspond to radiation power of 50 kW.

The calculated distributions in this figure are compared with results of the amplitude measurement carried out with the air pressure determining breakdown value method at placing of a metallic sphere with a small (in comparison with radiation wavelength) radius in the given point of space. A quite good correspondence of distributions and absolute values is observed as a whole.

In order to form an extended caustic of the microwave radiation we investigated a scheme with a conic lens (axicon). The axicon shape is shown in Fig.8.2.4.

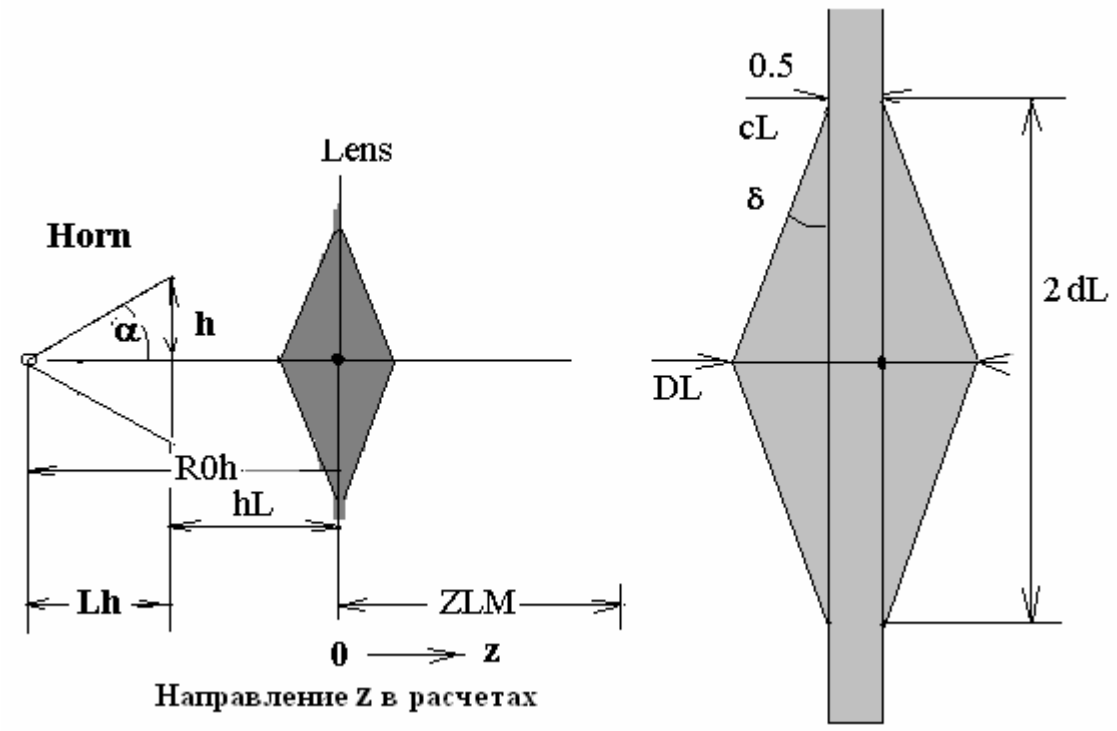

Fig. 8.2.4. Scheme with a conic lens (axicon) and its geometric shape.

The results of calculation for a concrete axicon lens are depicted in Fig.8.2.5. The main feature of the problem is insufficiently small radiation wavelengths in relation to the lens diameter. The reached distribution of the electric field amplitude along the microwave beam axis (at the wavelength of 2.5 cm) is more inform than in the case of a spherical lens.

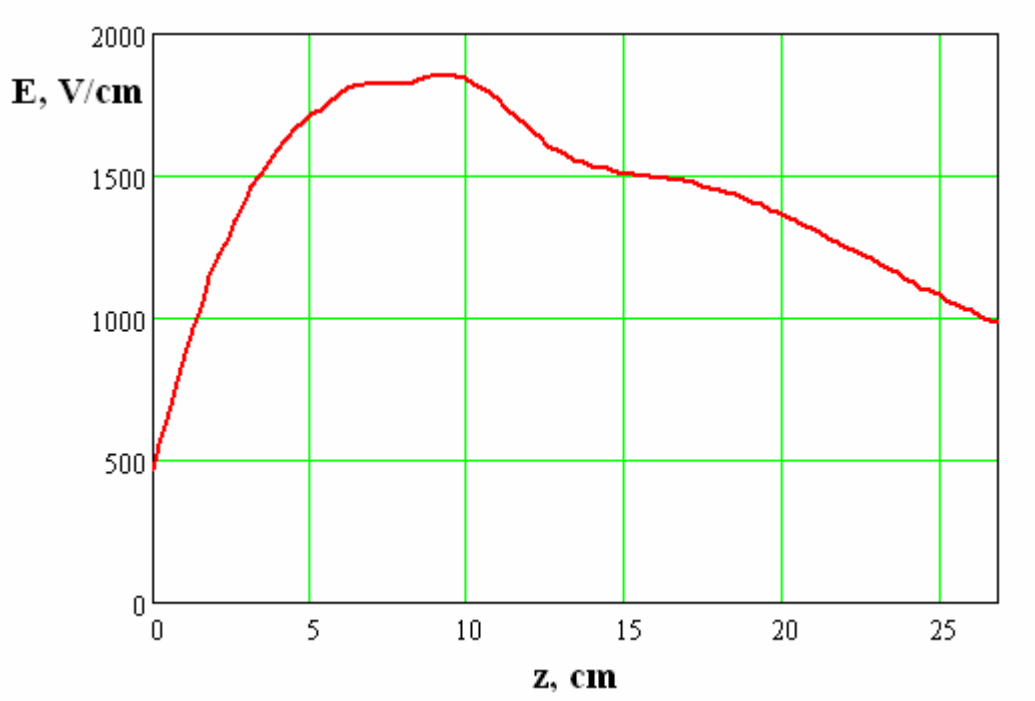

Fig.8.2.5. Results of MW electric field calculation in the scheme with the axicon lens.

9. MW discharge in different conditions theory development

Results given in the section 9 generalize and develop results of works carried out earlier in references [1,**2**,**3**,**4**].

9.1. Electron diffusion influence on a breakdown field value at a presence of an initiator

The continuity equation for an electron component in stationary electronegative gas mixture (in particular, in air) in linear approach has a form

$$\frac{\partial \mathbf{n}}{\partial \mathbf{t}} = \mathbf{D}\Delta\mathbf{n} + (\nu_{\mathbf{i}} - \nu_{\mathbf{a}})\mathbf{n}, \tag{9.1.1}$$

Here $\boldsymbol{n}$ is electron concentration, $\boldsymbol{\nu_i}$ and $\boldsymbol{\nu_a}$ – frequencies of ionization and attachment, $\boldsymbol{D}$ – diffusion coefficient. The threshold of breakdown is defined by a condition

$$\partial n / \partial t = 0. \tag{9.1.2}$$

A dependence of ionization frequency by electron impact via an electric field amplitude can be approximated near a threshold, by an expression [9]

$$\nu_i = \nu_a \cdot \left(\frac{E}{E_{cr}}\right)^{\beta}, \ \beta=5.3, \tag{9.1.3}$$

where **E** is local value of electric field amplitude, $\mathbf{E_{cr}}$ – the critical value of amplitude corresponding equality $\nu_{\mathbf{i}} = \nu_{\mathbf{a}}$, $\omega = 2\pi \cdot \mathbf{c}/\lambda$ – circular frequency (c – speed of light). Frequency of attachment and critical field, depending on air pressure can be estimated by means of following relations

$$\nu_a = 6.4 \cdot 10^4 p; \quad \mathrm{s}^{-1}, \tag{9.1.4}$$

$$E_{cr} = 30 p \sqrt{2\left(1 + \omega^2 / \nu_c^{\,2}\right)}, \ \mathrm{V/cm}, \tag{9.1.5}$$

where

$$\nu_c = 4.10^9 p; \ \mathrm{s}^{-1}, \tag{9.1.6}$$

is a transport frequency of electron collisions. Hereinafter is used a unit of a gas pressure - 1 Torr.

The maximum field on a surface of the small radius metallic sphere exceeds its unperturbed value by 3 times, as it was pointed out in the section 8.1, (see formula (8.1.3)). Near the breakdown threshold, when $3E_0/E_{cr}-1 << 1$, the area where the field exceeds its critical value represents a thin (almost flat) surface layer.

It allows to search an equation (9.1.1) solution in a flat one-dimensional approach. In this approach the equation (9.1.1) can be transformed to the Airy equation

$$\frac{\partial^2 \Psi}{\partial \mathbf{z}^2} + \frac{\mathbf{z}}{\mathbf{b}^2\mathbf{B}^2}\Psi = 0, \tag{9.1.7}$$

where the constants are $b=\nu_a a^2/D$, $\varepsilon_{0=}E_0/E_{cr}$, $A=(3\varepsilon_0)^\beta-1$, $B=2\beta(3\varepsilon_0)^\beta$ and variables are $\rho=r/a$, $\Psi=n\rho$, $z=bA - bB(\rho-1)$.

The solution of equation (9.1.7) is known [10,11]:

$$\Psi = \mathbf{C}\begin{cases} \mathbf{z}^{1/2}\left[\mathbf{J}_{1/3}\left(\dfrac{2\mathbf{z}^{3/2}}{3\mathbf{bB}}\right)+\mathbf{J}_{-1/3}\left(\dfrac{2\mathbf{z}^{3/2}}{3\mathbf{bB}}\right)\right], \mathbf{z}>0 \\ \left(-\mathbf{z}^{1/2}\right)\cdot\left[-\mathbf{I}_{1/3}\left(\dfrac{2(-\mathbf{x})^{3/2}}{3\mathbf{bB}}\right)+\mathbf{I}_{-1/3}\left(\dfrac{2(-\mathbf{z})^{3/2}}{3\mathbf{bB}}\right)\right], \mathbf{z}<0 \end{cases} \qquad (9.1.8)$$

where $J_{\pm1/3}$ (x), $I_{\pm1/3}$ (x) are Bessel functions. This solution will satisfy the smallness condition on the remote boundary $\rho \to \infty$ **(**$\mathbf{z \to -\infty}$**)**. On the sphere surface the condition $\mathbf{\Psi(\rho=1)=0}$ should be also satisfied, that takes place at

$$2\cdot z^{3/2}/(3bB)=2.338\ . \qquad (9.1.9)$$

Higher eigenvalues are not taken into a consideration because Ψ changes a sign. A distribution of electron concentration in this case is shown in Fig.9.1.1.

On a surface we have z=bA and, from (19), obtain the required relation between E_0/E_{cr} and ***p***

$$\frac{1}{\sqrt{b}} \equiv \frac{l_a}{a} = \frac{\left[\left(3\varepsilon_0\right)^\beta - 1\right]^{3/2}}{7{,}2\beta\left(3\varepsilon_0\right)^\beta}\ , \qquad (9.1.10)$$

where

$$l_a = \sqrt{\frac{D}{\nu_a}}\ - \qquad (9.1.11)$$

is a diffusion length of attachment which depends on pressure.

In (9.1.11) we mean the ambipolar diffusion coefficient under a symbol *D* since the sphere in a short time after the beginning of ionization will get a potential of several units of electron temperature order. For estimations one can recommend approximate a formula for the ambipolar diffusion

$$D = D_a = \frac{1.4\cdot10^4}{p},\ \text{cm}^2/\text{s}. \qquad (9.1.12)$$

In view of (9.1.4) and (9.1.12) the relation (9.1.11) can be transformed to

$$\mathbf{l_a} = \frac{0.33}{\mathbf{p}},\ \text{cm}. \qquad (9.1.13)$$

Dependence (9.1.10) is compared with measurements in Fig.9.1.2in coordinates ($3E_0/E_{cr}$, l_a/a). Good concurrence specifies the correctness of the theoretical model.

It follows from (9.1.10) that the breakdown takes place at high values of pressure ***p*** **(** that is if $\mathbf{l_a/a \to 0}$) at $\mathbf{E_0=(1/3)E_{cr}}$, But the sphere presence will not affect at small pressure, and the breakdown takes place at $\mathbf{E_0 = E_{cr}}$.

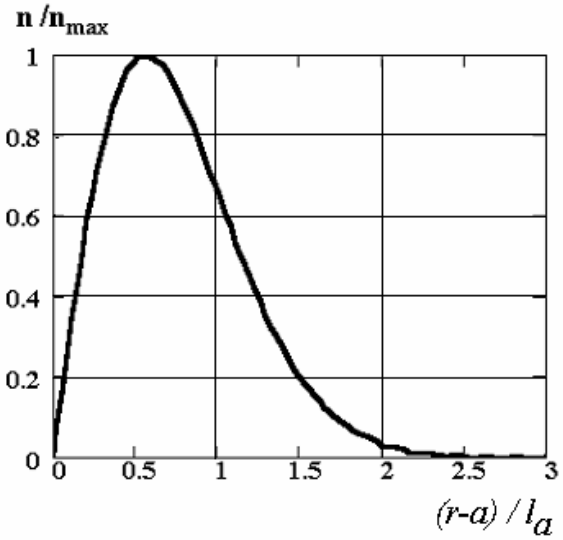

Fig.9.1.1. Distribution of electron concentration near the initiator surface at the breakdown threshold. $l_a/a=0.1$

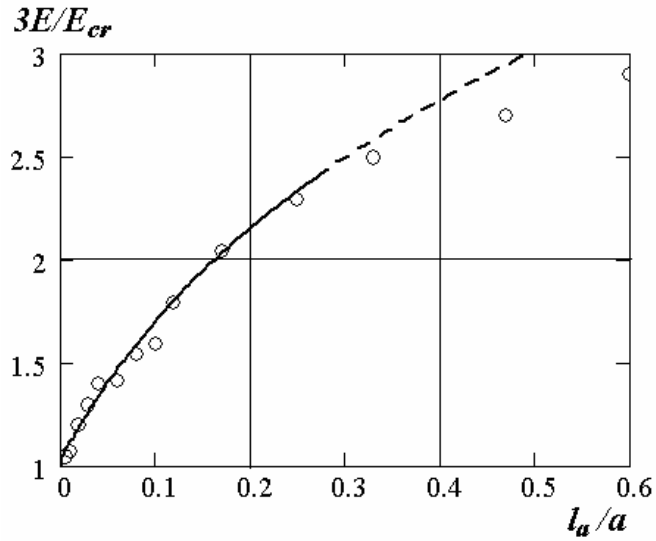

Fig.9.1.2. A ratio of the maximum field on the initiator surface and a critical field value Ebr/Ecr via a ratio of attachment length and a curvature radius a; the line corresponds to equation (9.1.10), points – experimental data

Effect of the diffusion on breakdown field can be similarly calculated for initiators of any shape if a factor ϑ of electric field increasing near the point of its surface with the minimum curvature radius **a** is known.

In the common case the following universal formula takes place instead of (9.1.10)

$$\frac{\mathbf{l_a}}{\mathbf{a}} = \frac{\left[\left(\vartheta\cdot\varepsilon_0\right)^{\beta}-1\right]^{3/2}}{7{,}2\beta\left(\vartheta\cdot\varepsilon_0\right)^{\beta}} \quad . \tag{9.1.14}$$

This equation has been used for the calculation of the dependence represented in Fig.8.1.1.

9.2. Overcritical and undercritical MW discharge streamer channel characteristics

9.2.1. Overcritical streamer MW discharges

An occurrence of a free electron in an area of MW field with the amplitude exceeding a critical value leads to an occurrence of the avalanche ionization with time-space distribution being a solution of the equation (9.1.1)

$$n = \frac{1}{\left(4 \cdot \pi \cdot D_e \cdot t\right)^{3/2}} \cdot e^{\nu_i \cdot t - \frac{r^2}{4 \cdot D_e \cdot t}}, \qquad (9.2.1)$$

where n is electron concentration, D_e –a factor of electron free diffusion, $\nu_{ia} = \nu_i(E) - \nu_a$. The average drift speed of electrons in the MW field is equal to zero unlike the avalanche in a constant electric field. Free diffusion is replaced by the ambipolar one when the radius of developing avalanche becomes equal to Debye radius, and plasmoid growth becomes slower. It occurs at radius value

$$a_s = \sqrt{D_e / \nu_i} \cdot \ln\left(N_e\right), \qquad (9.2.2)$$

where N_e – is a full number of electrons in a plasmoid by this moment. Typical value of a logarithm in this formula is $\ln(N) \approx 10\text{-}15$. The estimation of (9.2.2) coincides quite well with results of measurements [12] presented in Fig. 9.2.1.1.

However, the full number of electrons in a plasmoid continues to grow, and its conductivity also grows. The plasmoid disturbs a distribution of an electromagnetic field as soon as the conductivity will exceed a value $\omega/4\pi$, as it is described in Section 9.1. It is the moment of the streamer birth. The more extended is the streamer, the higher is the field at its end. The growth rate of a streamer can be estimated with a help of a formula

$$\mathbf{V_s} = \Delta_\mathbf{f} \cdot \nu_\mathbf{i}. \qquad (9.2.3)$$

A depth of ionization front on a streamer head Δ_f in common case is defined by a coefficient of free electron diffusion and by a total ionization frequency

$$\Delta_{dif} = 2 \cdot \sqrt{\frac{D_e}{\nu_i}}. \qquad (9.2.4)$$

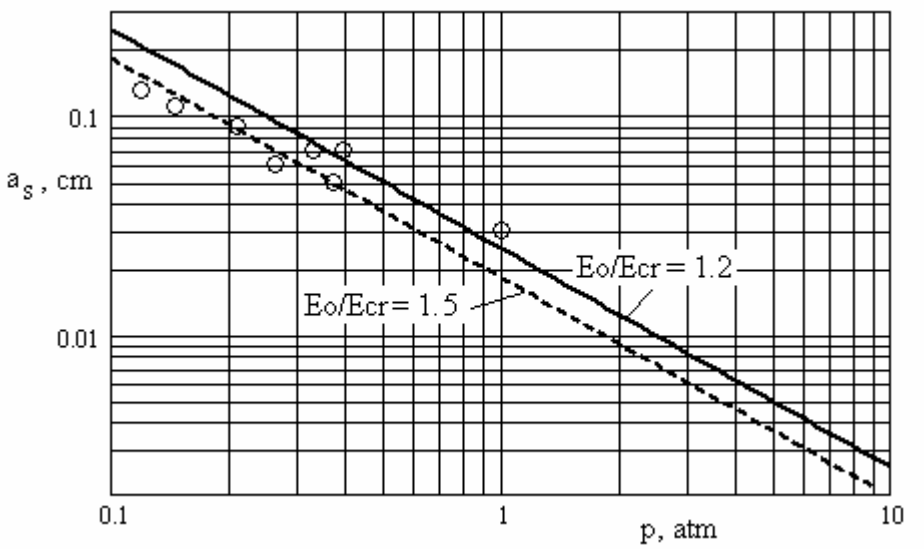

Fig.9.2.1.1. Dependence of a streamer radius via air pressure: circles is a result of photos processing with opened shutter, lines – dependence (9.2.2) at E_0/E_{cr} = 1.2 and 1.5.

A speed of the streamer depends only on a parameter of overcriticality and does not depend on the gas pressure. However, an amplitude of drift fluctuations in a streamer head is

$$\Delta_\omega = \frac{|\mu| \cdot E}{\omega} \tag{9.2.5}$$

(μ is an electron mobility) at pressure above the atmospheric one can exceed the front thickness defined by the diffusion (9.2.4). In this case the core process is the propagation drift mechanism [13] instead of the diffusion one. Drift oscillation speed of electrons exceeds the thermal speed. This mechanism at a high degree of overcriticality E/E_{cr} can provide a streamer growth rate of about 10^8 cm/s and more. Generally, the speed of the streamer propagation is defined by the sum (9.2.3) and (9.2.4)

$$V_s = 2 \cdot \sqrt{D_e \cdot \nu_i} + \frac{|\mu| \cdot E}{\omega + \nu_i} \cdot \nu_i . \tag{9.2.6}$$

The calculated values of the streamer growth rate in hydrogen depending on pressure and oveercriticality parameter are presented in Fig.9.2.1.2.

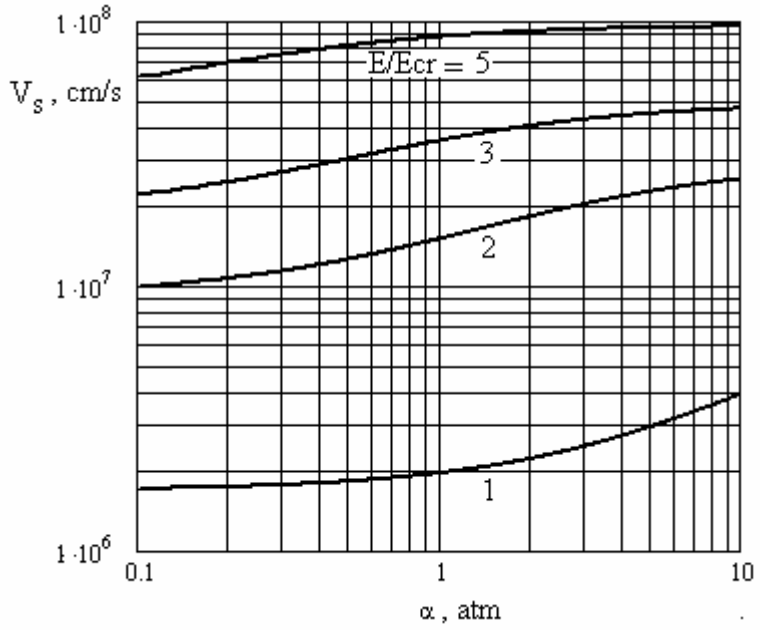

Fig.9.2.1.2. Calculated values ofthe streamer growth rate in hydrogen depending on pressure and overcriticality parameter E/E_{cr}

Notice, that the lateral surface of a streamer practically does not extend in a radial direction, because an electric field on this surface is too small.

9.2.2. Undercritical streamer MW discharges

High speed of the streamer head propagation is possible due to the fact that in the case of the overcritical field it is not necessary to have a drop of density for maintaining of ionization in all the volume of the streamer. However, a propagation of a streamer at a field with the amplitude smaller than the critical one is impossible without decreasing of a gas density in the streamer channel as a result of the ohmic heating by the induced MW currents. This is necessary for satisfying of the ionization condition: $E/N = (E/N)_{cr}$.

As the undercritical electric field is too small, the drift term in formula (9.2.6) can be neglected. Estimations of propagation speed can be made taking the following elementary assumptions into consideration

- a heating and ionization proceed in a streamer head at field values differing little from its critical value for an undisturbed gas E_{cr},
- a conductivity σ in a streamer head is limited by a value $\omega/4\pi$,
- a heating process goes on isobarically.

One can write the following equations basing on these assumptions and the energy-conservation equation on a streamer axis in its head:

$$\frac{1}{T}\cdot\frac{dT}{dt}=\frac{\sigma\cdot E_{cr}{}^{2}}{C_p\cdot p} \quad . \tag{9.2.7}$$

Integration of the equation (9.2.7) results in the following equation

$$\ln\frac{T}{T_0}=\ln\left(\frac{E_{cr}}{E}\right)=\frac{E_{cr}{}^{2}}{C_p\cdot p}\cdot\int_0^t\sigma_0\exp(\nu_i\cdot t)dt=\frac{E_{cr}{}^{2}}{C_p\cdot p}\cdot\frac{\omega}{4\cdot\pi\cdot\nu_i} \tag{9.2.8}$$

Thus the estimation of the ionization frequency in a streamer head is:

$$\nu_i = \frac{E_{cr}^{\ 2}}{C_p \cdot p} \cdot \frac{\omega}{4 \cdot \pi \cdot \ln\left(\frac{E_{cr}}{E}\right)} \qquad (9.2.9)$$

After substituting of (9.2.9) into the formula (9.2.6), in which the second item is eliminated, it is possible to obtain an expression for a propagation speed of the undercritical streamer microwave discharge

$$V_s = 2 \cdot \sqrt{D_e \cdot \frac{E_{cr}^{\ 2}}{C_p \cdot p} \cdot \frac{\omega}{4 \cdot \pi \cdot \ln\left(\frac{E_{cr}}{E}\right)}} \qquad (9.2.10)$$

Using usual estimating formulas for the electron diffusion coefficient

$$D_e = \frac{10^6}{p_{Torr}}, \text{ cm}^2/\text{s}, \qquad (9.2.11)$$

and a critical field

$$E_{cr} = 30 \cdot p_{Torr}, \text{ V/cm}, \qquad (9.2.12)$$

it is easy to result an expression (9.2.10) in a form convenient for estimations

$$V_s = \frac{3.6 \cdot 10^5}{\sqrt{\lambda_{cm} \cdot \ln\left(\frac{30 \cdot p_{Torr}}{E_{V/cm}}\right)}}, \text{ cm/s}. \qquad (9.2.13)$$

The formula (9.2.13) specifies weakness of undercritical discharge propagation speed dependence on an undercriticality degree if the field amplitude is far from its critical value. A speed of a streamer sharply increases in the last case, that corresponds to a transition to a mode of a overcritical discharge with its high values of the propagation speed.

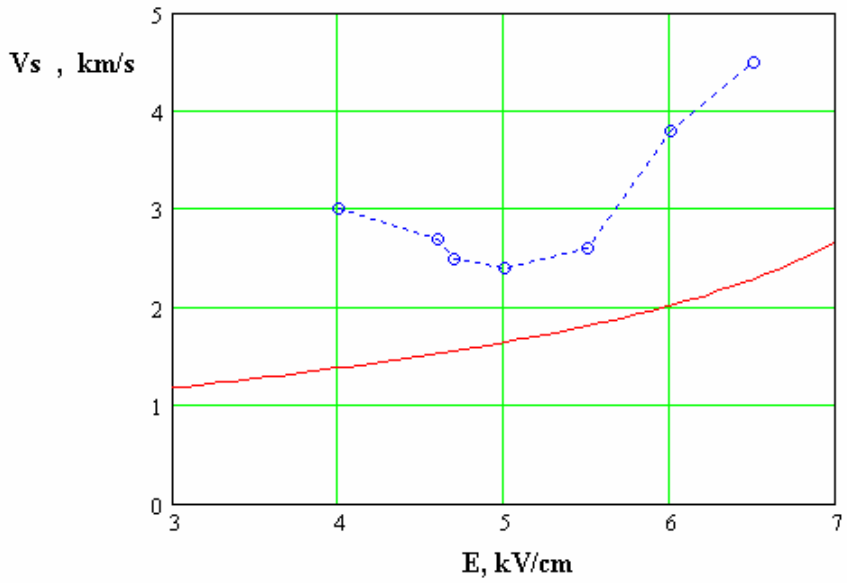

Fig.9.2.2.1. Dependence of the streamer propagation speed on the electric field amplitude at constant pressure, p = 200 Torr, λ = 8.5 cm. Estimation (9.2.13) – solid red line, measurements – dash-dot line

So such a simplified approach can not be applied for a strict description of the phenomenon, however, the formula (9.2.13) gives values of propagation speed very close to the observed ones

[14], that proves our choice of the determining factors during the streamer propagation. In Fig.9.2.2.1 an estimation of undercritical streamer MW discharge propagation speed (9.2.13) (solid red line) is compared with results of measurements [14] for the case of p = 200 Torr and λ = 8.5 cm (dash-dot line). It is obvious that the estimated values slightly exceed the measured ones, but the general view of these curves coincides.

9.2.3. Deeply undercritical (attached) streamer MW discharges

Basing upon the developed concept, it is possible to find a boundary between the undercritical form of MW discharge (freely propagating away from the initiator) and deeply undercritical form (attached to the initiator). The radius of a head part of a streamer is defined by a depth of ionization front.

$$a_s = 2 \cdot \sqrt{\frac{D_e}{\nu_i}} \tag{9.2.14}$$

The main property of a streamer, i.e. increase of the amplitude at its head, appears if a head radius is smaller than its length. If this condition is not met, the propagation of a streamer is impossible. Having taken a value $\lambda/2\pi$ as typical, it is possible to write a condition for the boundary dividing freely extending and attached streamer discharges:

$$a_s = \frac{\lambda}{2 \cdot \pi} \tag{9.2.15}$$

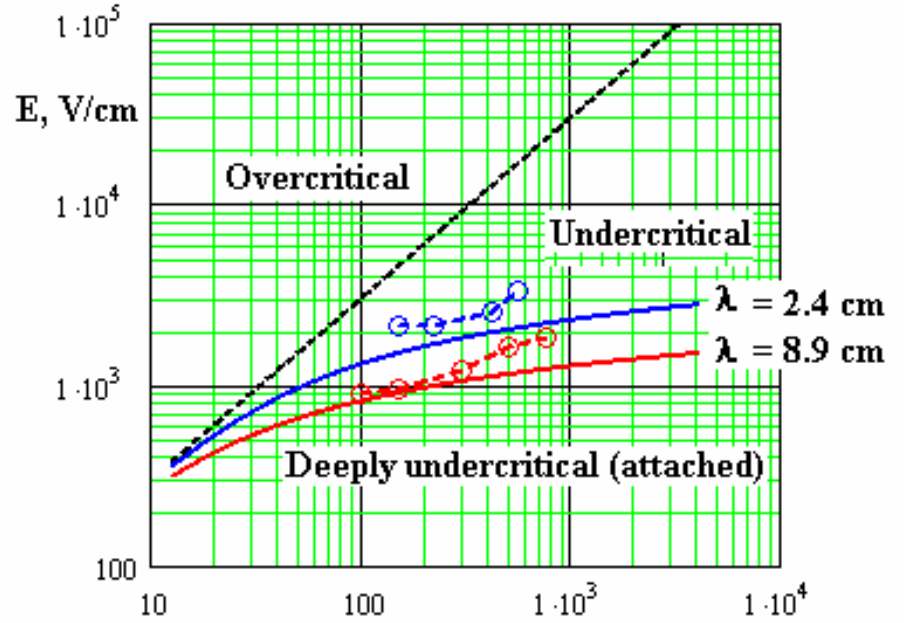

Fig.9.2.3. A boundary dividing existence areas of undercritical (freely propagating) and deeply undercritical (attached) discharges. Continuous lines – numerical estimations, dash-dot lines – measurements

A condition (9.2.15) together with (9.2.9), (9.2.11), (9.2.12), and (9.2.14) give the transcendental equation

$$\frac{E_{V/cm} \cdot \sqrt{\lambda}}{\sqrt{\ln\left(\frac{30 \cdot p_{Torr}}{E_{V/cm}}\right)}} = 2 \cdot 10^3 \tag{9.2.16}$$

In Fig.9.2.3 the numerical solution of the equation (9.2.16), for wavelengths used in experiments, is compared to results of observation (see Fig.5.4.2).

9.2.4. MW discharge plain front instability

Observations show that a radius of a streamer starting from the initiator surface is significantly smaller than a curvature radius of the initiator surface. The photo of the streamer microwave discharge initiated by a small-sized (as compared with wavelength) metallic ball is shown in Fig.9.2.4. The initiator surface illuminated by UV radiation is covered on both poles by a thin plasma layer, which properties are described in Section 9.1. Streamers have started from the sphere poles. Their radiuses are of the thickness of a plasma layer Δ order and are smaller than the sphere radius **a**. One can explain the process of formation of such a thin streamer by the front instability of propagating discharge. Instability is caused by an action of two factors: 1) a magnification of MW field at the surface of the conducting layer increases with decreasing of the surface curvature radius; 2) the greater is the electric field (under a condition of its local overcriticality), the greater is the discharge front speed. Joint action of these two factors results in accelerated growth of any protuberances on a plasma surface. Elementary calculation gives an expression for the maximum increment:

$$\gamma = \frac{V_s}{\Delta} \qquad (9.2.16)$$

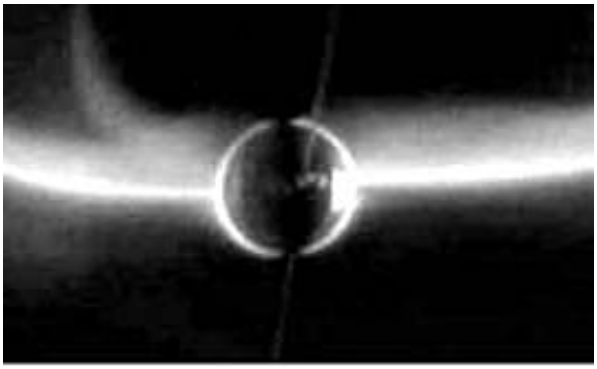

Fig.9.2.4. Plasma layer near the spherical initiator and streamers started from it. p = 60 Torr, 2a = 0.5 cm, $E_0/E_{0\,br}$ = 1, τ_{dis} = 35 μs.

9.2.5. Efficiency of MW power transformation to air heating in a supersonic flow

The attached undercritical discharges represent a significant applied interest as their generation is possible at rather small levels of electromagnetic field source energy. Results of experimental investigations of their properties in various conditions, are described in works [15,16,17,18], including their burning in high-speed streams of various gas mixes. Naturally there is a question about of radiation source energy transformation efficiency to energy realized in the discharge. The present section is devoted to this problem.

Efficiency of MW power transformation to the heating power of a gas in a discharge can be defined as:

$$\eta_{\mathbf{MW}} = \frac{\mathbf{P_{MW}}}{\mathbf{P_{gen}}} \qquad (9.2.17)$$

The method of this coefficient calculation is similar to the method stated in the work [19]. A formulation of the problem is explained in Fig.9.2.5.1. The initiator (a metallic vibrator having a

diameter 2a = 0.4 cm and length 2L) is placed in the MW field with an amplitude E_0 and a wave vector $\kappa=2\pi/\lambda$ (λ = 12.5 cm) parallel to the electric field. The MW discharge extended along the vibrator (as it occurs in a high-speed stream) is attached to the point end of this vibrator. A conductivity distribution in the discharge is approximated by Gaussian law with a given dispersion d = 0.8 cm. Variable parameters of the problem are L and σ_{max}.

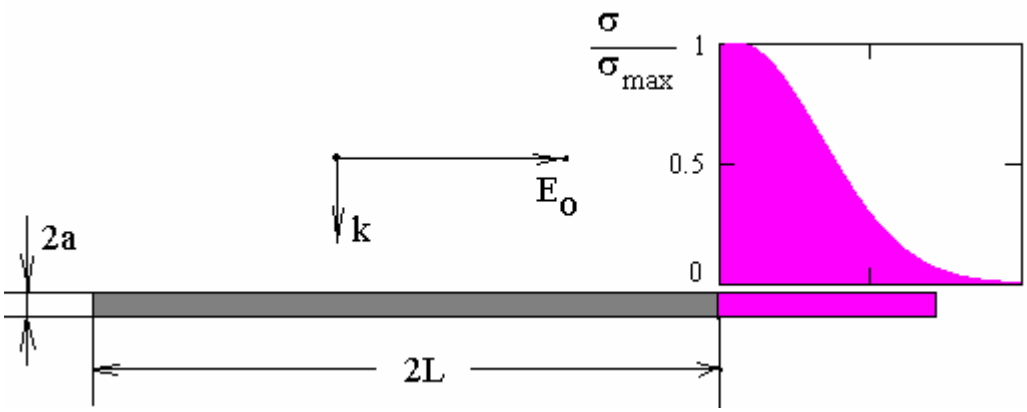

Fig.9.2.5.1. Statement of the task about absorbing ability of a metallic vibrator with attached discharge

MW power absorbed in the discharge and a power reradiated by the vibrator depends on these parameters L and σ_{max}. Results of calculation are shown in Fig.9.2.5.2.

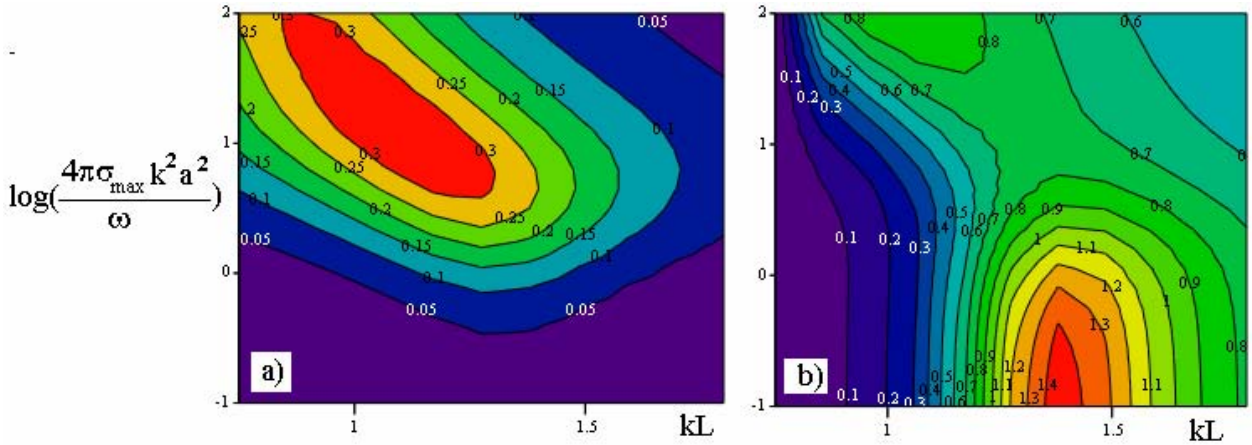

Fig.9.2.5.2. Power absorbed in the discharge (a) and power reradiated by the vibrator (b), [cE_0^2/k^2], depending on maximum discharge conductivity and vibrator length, ka=0.1

The MW power absorbed in the discharge has a maximum at optimum values of the vibrator length and maximal conductivity. A dependence of power characteristics on maximum discharge conductivity at optimum value of the vibrator length (kL_{opt}=1.1) is shown in Fig.9.2.5.3. In this case

$2L_{opt}$=4.3 cm

(c – speed of light, ω – circular frequency of MW field)

The discharge length measured for the case on photos, is compared to the calculated dependence of a power absorbed by the discharge depending on the vibrator length, see Fig. 9.2.5.4.

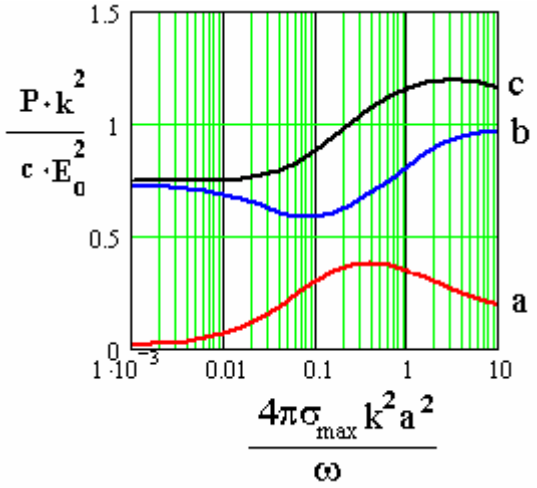

Fig.9.2.5.3. Power of absorption by the attached discharge (a), reradiated by the vibrator (b) and a total power (c), [cE_0^2/k^2], depending on maximum discharge conductivity at optimum vibrator length, ka=0.1

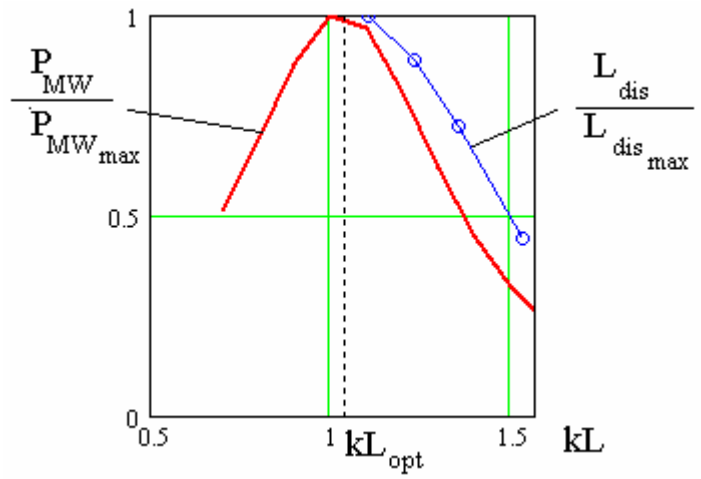

Fig.9.2.5.4. Dependence of calculated power, absorbed in the discharge at optimum value of its maximum conductivity and measured discharge length on the vibrator length (see Fig.4.5.1).

One can see that the discharge length is similar to a curve of the power calculated for a value of maximal discharge conductivity, which is optimum for MW energy consumption. This fact confirms our view on the MW discharge as a system, which is self-adjusted to the maximum consumption.

A power of absorption and a power of reradiation are characterized by so-called absorption cross-sections S_a

$$S_a = \frac{\int_0^a \int_{-\infty}^{\infty} \sigma |E(r)|^2 2\pi r dr dz}{c\frac{E_o^{\ 2}}{4\pi}} \qquad (9.2.18)$$

and reradiation section S_r

$$S_r = \cdot \frac{4\pi}{cE_0^{\,2}} \cdot \int_{-\infty}^{\infty} \mathrm{Re}\left(J \cdot \left(\overline{E_0 - E(a)}\right)\right) dz \,. \qquad (9.2.19)$$

The developed theory of a passive vibrator loaded by the attached discharge allows to define the maximally possible effective section of MW radiation absorption by the discharge:

$$S_{MW} = 0.12 \cdot \lambda^2 \,. \qquad (9.2.20)$$

By a definition the absorbed power is equal

$$P_{MW} = \Pi_{MW} \cdot S_{MW} \,, \qquad (9.2.21)$$

where Π_{MW} – is energy flux density of MW radiation. This value can be estimated by the following relationship

$$\Pi_{MW} \approx \frac{P_{gen}}{S_{beam}} \,, \qquad (9.2.22)$$

where S_{beam} is an effective area of MW radiation beam's cross-section in the place of the vibrator and discharge location.

9.3. Undercritical discharge electrodynamics

9.3.1. Formulation of a problem

It is known that MW discharge can propagate in a field with the amplitude smaller than its critical value at high gas pressure. This fact is usually explained by the streamer mechanism analogous to the spark discharge propagation in a constant electric field explanation. But there is also one essential difference: in a constant electric field its amplitude grows at top of a streamer with increase of the streamer length, and the amplitude of MW electric field at the top of the streamer increases with length of streamer channel while its length is smaller than the half-wave length of radiation and it decreases to small values at higher lengths. Thus there is a question: whether the head part provides such a configuration of the channel, which holds a high value of a field at the top of conducting channel continuously during an increase of its length, creating conditions for the streamer effect appearance.

The situation is the same as in the spark DC discharge in an initial stage of the MW streamer channel development, when the discharge length is smaller than the than half-wave length of the radiation. The greater is the length of the channel, the greater is electric field at the top of the channel, and the greater is ionization speed because the growth rate of the channel increases continuously. However if the discharge length is greater than the half-wave length (than electrodynamical resonant length) the amplitude of an electric field at the top of the channel falls down to a small value (down to the amplitude of undisturbed field and less). It doesn't matter when the initial field is above-critical, that is the propagation proceeds. But in the case of the undercritical field amplitude, the experimentally observable propagation of a discharge from the initiator for a distance greater than the half-wave length requires an explanation.

Earlier it has been determined, that MW discharge in a dense gas represents a complex network of thin hot channels filling some area, which boundary moves towards the radiation with a speed of several km/s. The spatial density of channels in the discharge area is high if the field's undercriticality is small. But if the undercriticality parameter is close to the bottom boundary of the existence range of the undercritical discharge, then the discharge is presented by only several channels or even by only one channel. In the latter case the discharge has a certain configuration: the sine wave basic channel with branches in its each extremum. For the first time it was clearly

observed by V. Brovkin and Yu. Kolesnichenko [20]. They paid attention to the discharge ability to self-organizing, an ability to form the structure similar to a simple broadband antenna system. This is well visible in the photo of such a discharge (center photo in Fig. 9.3.1.1, λ=4.3 cm). Later the same structures were observed at other radiation wavelengths (the left and right photo in Fig. 9.3.1.1, λ = 8.9 cm and 2.5 cm). Supervision of undercritical discharge development in time (Fig. 9.3.1.2) has shown the same picture: the discharge channel forms the sine-wave main channel with additional branches. Brightness of channels is maximal at the front areas of unloading.

We decided to check up with a help of a numerical model whether such a form of the discharge channel (the sine wave main channel with branches) allows to maintain a continuous development of its head.

Fig. 9.3.1.1. Typical view of the undercritical MW discharge initiated by the metal vibrator , which is directed along the electric field of linearly polarized electromagnetic wave. The radiation propagates from left to right, p = 200 Torr

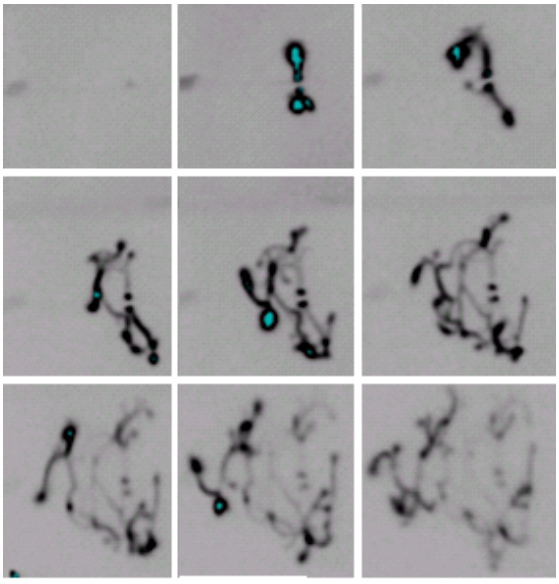

Fig. 9.3.1.2. Negative photography of the undercritical MW discharge initiated by a metallic sphere in one impulse during serial time moments. Exposure time – 1 μs, pause – 1 μs.

9.3.2. Numerical model

Fully adequate model suitable for description of MW discharge development in undercritical fields requires using of the equation system consisting of the Helmholtz equation for electromagnetic field amplitude, gas dynamic equations for the multicomponent plasma considering

necessary physical and chemical processes in three-dimensional treatment. Experience of such model development has shown that technological difficulties of calculations with such model do not allow to study process defining its main properties [21,22]. Therefore for solution of the formulated task the simplified model of the plasma thin channel dynamics was used. Earlier this model has been described in [23] and in more detail in [24].

The equation (1) describes processes of ionization by electron impact, electron diffusion, attachment and recombination for air.

$$\frac{\partial f}{\partial t} = N \cdot \left(K_i\left(\frac{E}{E_{cr}}\right) - K_a \right) \cdot f + \frac{\partial}{\partial l}\left(D(N) \cdot \frac{\partial f}{\partial l} \right) - \beta \cdot (f \cdot N)^2 \qquad (9.3.2.1)$$

$$C_v\left(T_g, N\right)\frac{dT_g}{dt} = \frac{\sigma(f)\cdot|E|^2 \cdot \Phi(\sigma, a)}{N} - T_g \cdot \frac{2V}{a} \qquad (9.3.2.2)$$

$$\frac{\partial N}{\partial t} = -2\frac{V}{a} \qquad (9.3.2.3)$$

$$\frac{dV}{dt} = 2 \cdot \frac{P_0 - P}{\rho_0 \cdot a} \qquad (9.3.2.4)$$

$$\frac{da}{dt} = V \qquad (9.3.2.\ 5)$$

where

t – time,
f – ionization rate,
D – coefficient of free electron diffusion,
β – recombination coefficient,
K_i, K_a – rates of reaction of ionization and electron attachment,
N – gas concentration,
T_g – gas temperature,
σ – plasma electric conductivity in discharge channel,
C_v – gas heat capacity at constant volume
a – radius of discharge channel,
V – radial speed of expansion of discharge channel,
E – MW field amplitude,
E_{cr} – critical amplitude of electric field,
p – gas pressure.

The equation (2.7.2) considers ohmic gas heating in the discharge channel. The equations (2.7.3)-(2.7.5) correspond to so-called “envelop” model often used for simplified simulation.

The system (2.7.2)-(2.7.5) is completed by the first-order integral equation for an electric field inside arbitrary oriented elements of thin channels with a given distribution of conductivity [25] calculated on each time step. As compared with [24] the used integral equation is generalized for the case of complicated special pattern of thin channels. The integral equation defines current distribution of an electric field in channels with known distribution of conductivity. The calculated current in channels defines distribution of an electromagnetic field in all volume by means of known operators. Thus, the model considers all the main physical factors controlling development of the discharge in undercritical fields: ionization and electronic diffusion, increase in a field at heads of plasma channels, and also gas heating.

The trajectory form of discharge development is chosen similar to observable configuration, Fig. 9.3.2.1.

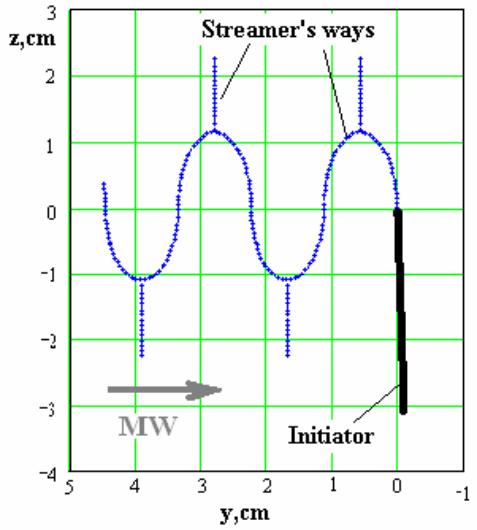

Fig.9.3.2.1. Configuration of streamer channel trajectory development.

Calculations have been executed for air with initial pressure of 200 Torr and temperature of 300 K at amplitude of MW field $E_o = 0.3E_{cr}$ and $\lambda = 8.9$ cm. The spatial period and amplitude of a sine-wave part of a trace and length of branches are equal to $\lambda/8$ (as in Fig. 9.3.1.1). The length of the initiator is equal to $\lambda/4$. Its radius (0.15 cm) is quite sufficient for discharge initiation at a given field.

9.3.3. Results of modelling

Numerical modelling confirms ability of the discharge to propagate beyond all bounds in undercritical fields towards to radiation through its branching.

It is possible to see in Fig. 9.3.3.1 the calculated distribution of current amplitude in the discharge trace at various time moments (0, 13.4, 27.2, 41.0, and 54.9 μs). Fig. 9.3.3.2 shows spatial distribution of amplitude of an electric field at the final moment of time (t = 54.9 μs). At t = 0 current exists only in the initiator. But later the current (light parts of a trajectory) propagates far from the initiator along a trajectory of the discharge forming branches. The current increases in the next branch at the moment when the electric field in a head part of a sinusoid decreases to an undercritical level. Occurrence of a current in a branch holds discharge system in a status of an electrodynamical resonance.

As it is well-known from the theory of wire antennas, wire system with many transversal branches (which length is equal to $\lambda/8 \div \lambda/4$) directed against radiation possesses resonant properties in a wide band of wavelengths. In such system, only a few first elements located within the limits of one radiation wavelength are active. Other elements are in a shadow of the first part and do not work. This process can be seen in Fig. 9.3.3.1. The current maximum moves forward shading a part located more close to the initiator. The same is observed in experiments: the discharge front (about $\lambda/2$ in depth) shields other part of hot channels from radiation. The rear part of the discharge saves channels with high gas temperature at rather small additional charging from radiation.

Average speed of discharge front is equal to 0.82 km/s and speed of the discharge in a trace – 2.04 km/s. It well coincides both with observations and estimations [26] based on taking into account of primary factors: frequency of ionization, free diffusion of electrons, ohmic heating and increase in a field in a head of streamer channels.

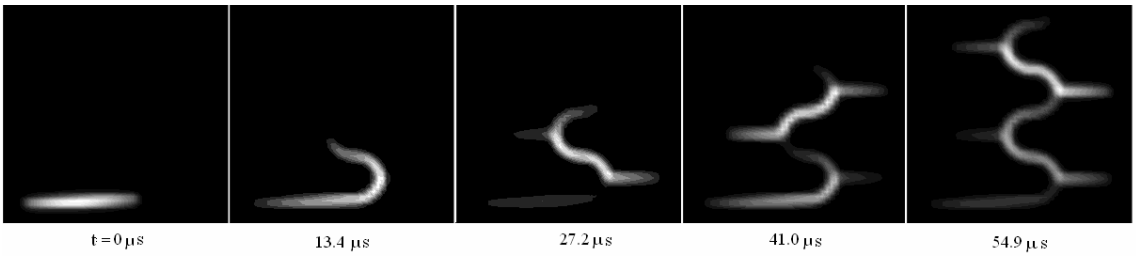

Fig.9.3.3.1. Calculated time development of currents idistribution in discharge channels.

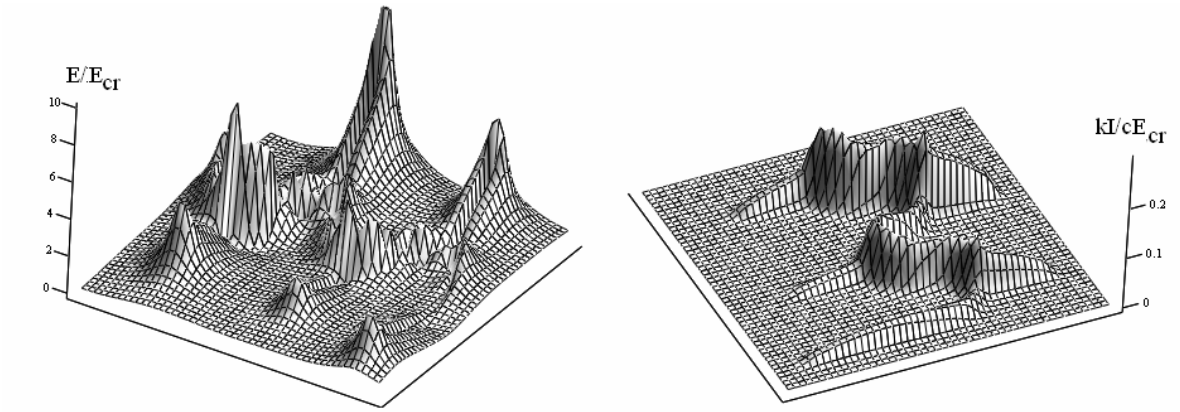

Fig.9.3.3.2. Spatial distribution of an electric field amplitude (to the left) and a current (to the right) of the discharge at t = 54.9 μs

9.3.4. Conclusions on modeling

Resonant character of freely extending undercritical discharge is confirmed by direct modeling which considers ionization by electronic impact, free electronic diffusion, ohmic gas heating, and increase in an electric field in a head part of streamer channels. The discharge can show the last property if a streamer makes periodically branches during growth. The main channel with branches forms analogue of antenna system which has resonant character irrespective of its length. The developed discharge consists of many such elementary subsystems arising simultaneously and consistently. Carried out numerical modeling shows this opportunity removing all doubts about the streamer nature of the undercritical microwave discharge.

There is also a question: why the main discharge channel forms a curved trajectory? Preliminary researches showed that it is caused by instability of the channel concerning a deviation of its direction at strong excess of the induced electric field at top of a streamer in comparison with its undisturbed value. But this question is beyond the present work and will be investigated later.

9.4. Aerosol influence of MW breakdown field values

Experiments on air breakdown at various humidity and presence of a water aerosol have indicated insignificant influence of these factors on breakdown characteristics and properties of the microwave discharge. The maximal diameter of aerosols in experiments reached 50 microns. However there is a question about influence of water drop components with diameter about 1-3 mm on a threshold of MW breakdown.

It is known that dielectric permittivity ε of the distilled water reaches value of 100. In MW band its value decreases and becomes complex with $|\varepsilon| >> 1$. Spherical object with permittivity ε and radius, which is small in comparison with radiation wavelength, disturbs the uniform MW

electric field. Due to polarization the amplitude of MW field on poles of dielectric sphere increases up to value:

$$\mathbf{E}_{\max} = \mathbf{E}_0 \cdot \frac{\varepsilon}{1+(\varepsilon-1)/3}.$$

At $|\varepsilon|>>1$ amplitude of a field increases by 3 times. This increase at poles of the sphere does not depend on its diameter and gas pressure. Thus, presence of drops generally should lead to decrease of breakdown values of MW field. However, presence of a drop results in not only increase in amplitude of a field and corresponding local increase of ionization frequency by electron impact. Its presence leads also to loss of electrons from ionization zone due to their diffusion and recombination on a drop surface. Diffusion losses from a region of increased field are inversely proportional to square of characteristic size (radius of sphere) and gas pressure. So, the smaller is a drop radius and gas pressure, the smaller is effect of a drop on breakdown field. Calculated values of breakdown fields depending on a drop diameter and gas pressure are resulted at λ = 2.5 cm in Fig.9.4.1.

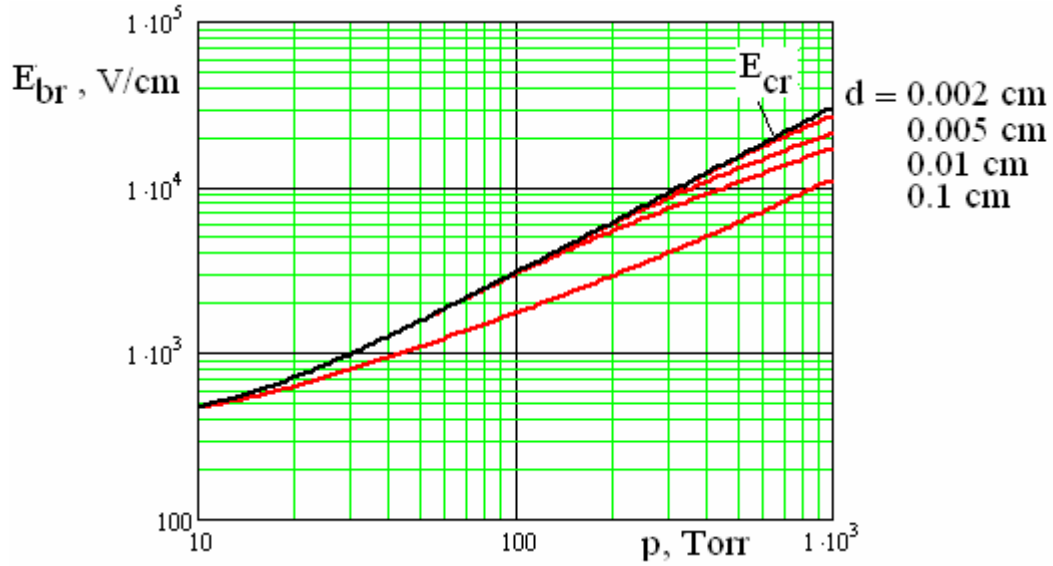

Fig.9.4.1. Theoretical dependence of breakdown field decreasing factor on a drop with diameter d and gas pressure p. λ = 2.5 cm.

Certainly, these dependences assume presence of free electrons in an active zone but in usual real conditions this assumption is not always valid.

9.5. Factors determining a development of surface streamer discharges

There are two modifications of the surface discharge which we shall name “transversal” and “longitudinal” surface discharges. The transversal surface discharge develops near a dielectric surface located between the initiator and MW radiation source across the direction of electromagnetic wave propagation. The dielectric radiotransparent plate blocks all section of MW radiation beam not allowing the discharge to extend in a direction towards the MW radiation source. Streamer channels develop exclusively along a surface, so the discharge has the surface character. If we place a dielectric plate along the direction of MW propagation and along the electric field vector with linear polarization, the discharge will propagate from the initiator in the form of thin streamer channels along a dielectric surface not filling a space above a plate. It is the

longitudinal surface MW discharge.

In the case of the transversal surface MW discharge it is possible to explain its surface character by a common property of volumetric discharges to be developed aside a source because of electromagnetic screening of MW fields by the foremost channels. Presence of a radiotransparent barrier does not give an opportunity for propagation of ionizing processes over a barrier, and the channels developing on a barrier, shielding a field, exclude an opportunity of discharge propagation in the opposite direction.

The screening factor is practically absent in case of the longitudinal surface discharge. In this case propagation of channels exclusively along a dielectric surface is dictated by another controlling factor. First of all the process of ionization occurring in a streamer head near a surface should be considered as such factor.

Development of a streamer in its head part is determined by increase in a field at an edge and ionization by electronic impact in this field, and also by losses of electrons because of attachment and diffusion leaving from an area of above-critical field near a streamer head.

Influence of a dielectric plate having thickness greater than distances between a streamer and a surface can be estimated making the following assumptions. During each half-cycle some electric charge is accumulated in a streamer head. With some reservations, one can consider this charge as a physical point. On distances of the order of radius of a streamer head, which is smaller than wavelengths, an electric field of a charge $\boldsymbol{q}$ above a dielectric plate with permeability $\boldsymbol{\varepsilon}$ in arbitrary point (x=0, z=a) can be estimate in electrostatic approach:

$$E = -\nabla\phi,$$

where

$$\phi = \frac{q}{\varepsilon}\left(\frac{1}{\sqrt{x^2+(a-z)^2}} + \frac{1-\varepsilon}{1+\varepsilon}\cdot\frac{1}{\sqrt{x^2+(a+z)^2}}\right).$$

Distribution of the electric field module above a plane at a distance z = a/2 and in cases of ε = 1 and ε = 2 is depicted in Fig. 4.5.1. One can see that even at ε = 2 the field on a dielectric surface exceeds the streamer field without a dielectric by 1.33 times. This results in increase of ionization frequency near a streamer head, lying on a surface, by several times and thereby facilitates conditions of discharge propagation. At higher values of permittivity $\boldsymbol{\varepsilon}$ the field can be increased on a dielectric surface almost twice.

The resulted estimation confirms the assumption about a significant influence of a dielectric plate on electric field amplitude in a vicinity of a streamer head part.

Another factor accelerating process of ionization near a surface is strong ultra-violet radiation of a streamer head. UV radiation interacting with a solid surface can result in additional photoemission of electrons.

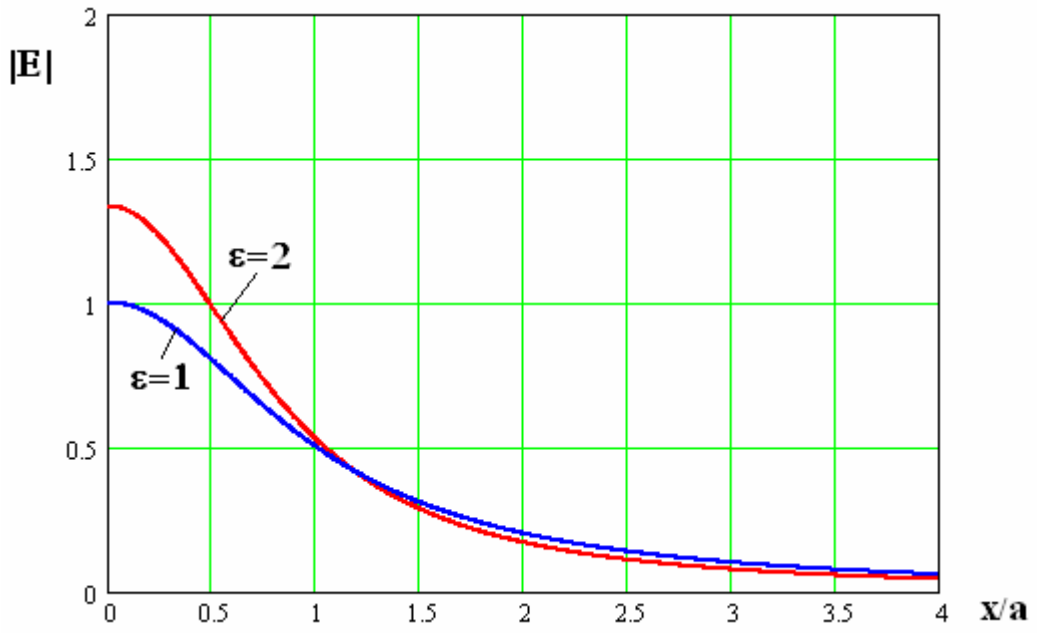

Fig.9.5.1. Distribution of the electric field module of the charge located above a flat dielectric surface with permittivity $\varepsilon = 1$ (dark blue line) and $\varepsilon = 2$ (red line) at $q = 1$, $a = 1$, $z = 0$.

Otherwise situation with diffusion losses is. As it is known, growth rate of a streamer is determined by ionization frequency and by coefficient of free electron diffusion in that part of space before a streamer head where plasma density is small and polarization fields are weak. Unlike propagation in free space, presence of a dielectric surface leads to accumulation of electrons diffusing in radial (relative to a streamer axis) direction and precipitating on this surface. Accumulation of negative charge results to termination of electron diffusion flux onto a surface and, hence, to reduction of total electron losses in the discharge.

The factors considered with reference to the longitudinal surface discharge in equal measure concern to the transversal-type discharge. The critical value of a field in both cases when the discharge can propagate is less than the corresponding value in the case of propagation in free space. This can explain the absence of MW streamer channels far from a dielectric surface.

10. Conclusion

So, the extensive cycle of the electric gas discharge in quasi-optic electromagnetic beam of radiation in MW region of wavelengths λ scientific investigations has been carried out within the frames of three-year ISTC Project #2820. This discharge typical feature is that it can be realized in the EM beam area being far from antenna elements forming this beam and from construction parts of experimental setup surrounding the discharge area.

Investigations were fulfilled in air under "normal" conditions in moist air, in its mixture with water aerosol, i.e. in a two-phase medium, and also in model gas propane-air mixture. Investigations were carried out in a pressure range $\boldsymbol{p}$ from some tens Torr up to atmospheric the pressure. Experiments were carried out both in a motionless gas medium and in a high-speed gas flow. We realized discharges in EM beam with λ = 12.5 cm, 8.9 cm and 2.5cm. We used the pulse mode of EM radiation at λ = 8.9 cm and 2.5cm with characteristic pulse duration τ_{pul} ranging from units up to several tens microseconds. We studied discharges produced both by a single MW pulse and in their sequence with a repetition frequency f_{rep} up to 100 Hz. The quasi-continuous mode of EM field generation was used at λ = 12.5 cm.

The maximum level of linearly polarized EM field electric component $\boldsymbol{E_0}$in the discharge area allowed to realize a self-maintained gas breakdown only at pressures $p \leq 100$ Torr in available pulsed MW set ups. At the same time, the way of MW breakdown initiating with an application of the linear EM vibrator developed by participants of the Project has allowed to carry out research works at essentially higher pressure values $\boldsymbol{p}$. Experiments have shown, that the MW discharge has a diffuse character at comparatively low pressures; and at high pressures it is realized in a streamer form. We have made the main accent on studying of streamer discharges in the present Project.

Streamer MW discharges in air under normal conditions in above-critical fields at $E_0 > E_{cr}$ (where $\boldsymbol{E_{cr}}$ is the minimal amplitude of the electric component of EM field at which the self-sustained gas breakdown is realized) represent the space-developed systems of thin plasma channels. Experience has shown that the MW discharge in the undercritical fields is originated on the ends (poles) of EM initiator in the form of thin plasma channels also. Herewith these channels growing and branching in certain range of electric field undercriticality $E_0 < E_{cr}$ in some E_0–p interval form the space-developed structure. Just a capability of these channels to grow in the fields $E_0 < E_{cr}$ has caused a presence of the word "streamer" in the name of this kind of MW discharges. The discharge streamer channels lose their ability to form the space-developed structure at deeper undercriticality of MW fields, that is at $E_0 << E_{cr}$. They remain attached to the ends of the EM vibrator initiating the discharge during all the time of EM field generation. Such streamer MW discharges were called "deeply undercritical".

The experiments executed within the frames of the present Project have shown that the area of undercritical MW discharges E_0–p existence coordinates with the spatially-developed streamer structure is displaced towards higher values E_0 and p with decrease of EM wavelength $\boldsymbol{\lambda}$. Herewith, the boundaries separating diffuse types of MW discharges from the streamer ones and also undercritical streamer discharges from deeply undercritical type have been quantitatively determined at used $\boldsymbol{\lambda}$. Experiments in a humid air and in air at presence of a water aerosol indicated that in this case there also remain listed kinds of MW discharges, and $\boldsymbol{E_0}$–$\boldsymbol{p}$ boundaries of their existence, in fact, do not change.

Investigations of spatial and temporary characteristics of the streamer MW discharges have shown that the growth rate of their plasma channels $\mathbf{v_{str}}$ in dead air depends little on the field wavelength $\boldsymbol{\lambda}$ and its order of magnitude is 10^6 cm/s. Streamer channels of the undercritical discharge grow mainly towards the EM radiation source. Herewith, the propagation speed of the discharge area front $\mathbf{v_{fr}}$ towards a field is about some units times 10^5 cm/s. Experiments indicated that the value of $\mathbf{v_{fr}}$ in air with water aerosol impurity decreases by several tens percents. Additionally the scale of speed $\mathbf{v_{str}}$ was experimentally checked by a realization of such discharges in high-speed flows of air and of air - water aerosol mixture. Experimental tests with such flows at their speed $\mathbf{v_{fl}} = 5 \cdot 10^4$ cm/s showed that initial structure of such MW discharges realized in dead gas practically does not vary. These experiments confirmed that value $\mathbf{v_{str}}$ is much higher than the used values of flow speed $\mathbf{v_{fl}}$.

Streamer MW discharges energetically interact with the EM field excited them, and efficiency of this interaction is very high. This property of undercritical streamer discharges speaks that separate parts of their plasma channels possess resonant properties. In case of deeply undercritical streamer MW discharges the resonant system is formed by the EM vibrator and attached plasma channels. As a result the gas temperature $\boldsymbol{T}$ in some plasma channels of the streamer discharges reaches several thousand degrees. So the high temperature $\boldsymbol{T}$ was additionally estimated in experiments on ignition of such discharges in a model propane-air gas mixture. Its ignition temperature is $T \approx 1300$ °C. Experiments showed that the streamer MW discharges can ignite this mixture, and moreover they are capable to ignite not only a dead gas mixture but also its high-speed flow.

Experiments on ignition of propane-air gas mixture high-speed flow by undercritical streamer MW discharge in EM field with $\lambda = 2.5$ cm have shown that a propagation speed of a flame over

the gas mixture $\mathbf{v_{fl}}$ essentially increases in the area of the streamer channels. In our experiments its value was about 150 m/s in contrast to those of ignition "traditional" methods when $v_{fl} \approx 0.5$ m/s. This important result demands additional special research.

Executed experiments on realization of the streamer MW discharge under very different initial conditions listed above have allowed to develop the model of a MW streamer in air in the undercritical EM fields. This model defines the geometric form of a single characteristic element of the undercritical streamer discharge; it explains a scale of a velocity $\mathbf{v_{str}}$ detected in the experiment, and resonant properties of the discharge.

The possibility of the streamer MW discharge realization in the undercritical and deeply undercritical fields in humid air, in the two-phase environment, in a high-speed air flow, in high-speed flows of two-phase medium and in a flammable gas mixture allows to analyze various practical application variants of this electric discharge type.

In frames of the present Project the surface MW discharge in air has been also studied. It was realized in quasi-optic EM beam at undercritical levels of MW fields. The discharge was realized both on a surface of a radiotransparent dielectric plate being perpendicular to the Pointing vector $\boldsymbol{\Pi}$, and on its surface lying in the plane of vectors $\boldsymbol{\Pi}$–$\boldsymbol{E_0}$. Experiments showed that such transversal and longitudinal surface MW discharges can be also realized in the streamer form. Besides, a characteristic time of streamer channels development allows to ignite these discharges in the high-speed air flows.

The physical processes defining development of such discharges allow to approve that they also energetically interact with an EM field exciting them. This circumstance stimulates the future detailed research of their physical properties. Besides, from a viewpoint of practical application it can appear that a realization of the surface MW discharge in a quasi-optic EM beam is technically simpler than a realization of a freely localized MW discharge.

Basing on accumulated experience and using of already available experimental equipment during further physical research of the surface MW discharge properties the following primary goals can be formulated and have to be determined: boundaries of diffuse and streamer discharge-types realization; areas of undercritical and deeply undercritical discharges realization; character of the MW discharge power interaction with EM fields; spatial and temporary characteristics of the MW discharge; influence of moist air at various humidity levels and at presence of a water aerosol on the discharge properties; characteristics of this type discharges realized in the high-speed flows of air and air-aerosol mixtures; a possibility of model gas mixture and its high-speed flow with a help of such discharges, etc.

List of published reports

1. *"The study of properties of the microwave streamer discharge in a high-speed flow of gas and of two-phase medium"*. Annual Technical Report on Project ISTC #2820p (027007). 2004.
2. *"The study of properties of the microwave streamer discharge in a high-speed flow of gas and of two-phase medium"*. Annual Technical Report on Project ISTC #2820p (027007). 2005.
3. *"The study of properties of the microwave streamer discharge in a high-speed flow of gas and of two-phase medium"*. Final Technical Report on Project ISTC #2820p (027007). 2006.

List of published papers

1. Kirill V.Khodataev. *The physical basis of the high ability of the streamer MW discharge to a resonant absorption of MW radiation.* //42nd AIAA Aerospace Sciences Meeting. Reno, NV, USA. 2004. Paper AIAA-2004-0180.
2. V.L.Bychkov, I.I.Esakov, L.P.Grachev Experimental determination of the microwave field threshold parameters insuring realization of a streamer discharge of the high temperature form. 42rd AIAA Aerospace Sciences Meeting and Exhibit (5-8 January 2004, Reno, Nevada), AIAA 2004-181.
3. I.I.Esakov, V.L.Bychkov, L.P. Grachev, K.V. Khodataev *Plasma-Aerodynamic Forces Created by Microwave Discharge*. The International Symposium "Thermochemical a and plasma processes in aerodynamics. Saint-Petersburg. 12-14 July 2004. Paper, p.24
4. Kirill V. Khodataev *The power efficiency of a microwave undercritical attached discharge, initiated by resonant vibrator*. Proc. of the 43rd AIAA Aerospace Sciences Meeting and Exhibit. Plasmadynamics and Lasers Conference 7th Weakly Ionized Gases (WIG) Workshop. (10-13 Jan 2005, Reno, Nevada, USA). Paper AIAA-2005-0596.
5. Kirill V. Khodataev *Numerical modeling of the combustion, assisted by the microwave undercritical attached discharge in supersonic flow* Proc. of the 43rd AIAA Aerospace Sciences Meeting and Exhibit. Plasmadynamics and Lasers Conference 7th Weakly Ionized Gases (WIG) Workshop (10-13 Jan 2005, Reno, Nevada, USA). Paper AIAA-2005-0985.
6. Kirill V. Khodataev *Initial phase of initiated undercritical microwave discharge*. Proc. of the 43rd AIAA Aerospace Sciences Meeting and Exhibit. Plasmadynamics and Lasers Conference 7th Weakly Ionized Gases (WIG) Workshop (10-13 Jan 2005, Reno, Nevada, USA). Paper AIAA-2005-0598.
7. K.Khodataev. *Development scenario and main parameters of different types of the microwave streamer discharges*. Proc. of 6th Workshop on Magnetoplasma Aerodynamics for Aerospace Applications. May 24-27, 2005. Institute of High Temperatures RAS, Moscow, Russia
8. Kirill V. Khodataev. *Investigation of undercritical microwave discharge ability to propagate limitlessly by continuous branching of the streamer*. 44th AIAA Aerospace Sciences Meeting 9-12 January 2006, Reno, NV. Paper AIAA-2006-0785
9. I.I.Esakov, L.P.Grachev, V.L.Bychkov, D.VanWie *Investigation of undercritical MW discharge with volumetrically developed streamer structure in propane-air supersonic stream*, 44th AIAA Aerospace Sciences Meeting and Exhibit (9-12 January 2006, Reno, Nevada), AIAA 2006-0790.
10. Kirill V. Khodataev. *Investigation of undercritical microwave discharge ability to propagate limitlessly by continuous branching of the streamer.* 44th AIAA Aerospace Sciences Meeting 9-12 January 2006, Reno, NV. Paper AIAA-2006-0785
11. V.L. Bychkov, I.I. Esakov, L.P. Grachev, K.V. Khodataev *"Air microwave streamer discharge features at its different humidity and at presence of water aerosol"* 5th Workshop Thermochemical and Plasma Processes in Aerodynamics Saint-Petersburg 19 – 21 JUNE, 2006.

Figure captions

References

1. *The study of properties of the microwave streamer discharge in a high-speed flow of gas and of two-phase medium.* Annual Technical Report on Project ISTC #2820p (027007). 2004.

2. *The study of properties of the microwave streamer discharge in a high-speed flow of gas and of two-phase medium.* Annual Technical Report on Project ISTC #2820p (027007). 2005.

3. *Investigation of the possibility of the application of the under-critical microwave streamer gas discharge for the ignition of a fuel in the jet engine.* Annual Technical Report on Project ISTC #1840p. 2001.

4. *The study of possibility of ignition of a combustible gas mix by the undercritical microwave streamer discharge.* Final Technical Report on Project ISTC #2429. 2005.

5. V.L.Bychkov, I.I.Esakov, L.P.Grachev, K.V.Khodataev. "*Properties of microwave streamer discharge in air at various humidity and presence of water aerosol*". Proc. Of Intern. Simposium "Thermo-Chemical and plasma processes in aerodynamics". Sankt-Petersburg, June 2006.

6 I.I.Esakov, L.P.Grachev, V.L.Bychkov, D.VanWie "*Investigation of undercritical MW discharge with volumetrically developed streamer structure in propane-air supersonic stream*", 44rd AIAA Aerospace Sciences Meeting and Exhibit (9-12 January 2006, Reno, Nevada), AIAA 2006-0790

7 I.I.Esakov, L.P.Grachev, K.V.Khodataev, V.A.Vinogradov "*Combustion efficiency in deeply undercritical MW discharge area in cold high-speed airflow"*, 44rd AIAA Aerospace Sciences Meeting and Exhibit (9-12 January 2006, Reno, Nevada), AIAA 2006-1212.

8 . L.P.Grachev, I.I.Esakov, K.V.Khodataev, V.V.Tsyplenkov. Microwave air breakdown at metal ball presence. Fizika plasmy, 1992, V.

9. W.Sharfman, T.Morita. IEEE Trans., AP-12, 6, 709,1964; W.Sharfman, T.Morita. Appl. Phys. 33, 2016, 1964.

10. R.O.Kuzmin. Bessel functions. 1935.

11. V.L.Ginzburg. Propagation of electromagnetic waves in plasma. Moscow. "Nauka". 1967.

12. I.I.Esakov, L.P.Grachev, K.V.Khodataev. The pinch effect in microwave resonant streamer discharge and its possible applications. // Proc. of the international workshop " Strong microwaves in plasmas (2-9 August 1999 ", Nizhny Novgorod), 2000, v.1 pp. 291-305.

13. K.V.Khodataev, B.P. Gorelik. Diffusion and drift modes of plane ionization wave in MW field propagation. // Fizika Plazmy. 1997, V.23, №3, P. 236-245.

14. L.P.Grachev, I.I.Esakov, G.I.Mishin, K.V.Khodataev. Stimulated MW discharge in the wave beam front velocity.// Zhurnal Technicheskoi Fiziki, 1995, V.65, N.5, P.21-30.

15 Igor Esakov, Lev Grachev, Kirill Khodataev and David Van Wie. *Experiments on propane ignition in a high-speed airflow with a help of deeply undercritical microwave discharge.* 42nd AIAA Aerospace Sciences Meeting 5-8 January 2004, Reno, NV. Paper AIAA-2004 – 0840.

16 . I.Esakov, L. Grachev, K. Khodataev and D. Van Wie. *Investigation of the Undercritical Microwave Streamer Gas Discharge for Jet Engine Fuel Ignition.* AIAA Plasmadynamics and

Laser Conference, 32nd, and Weakly Ionized Gases Workshop, 4th, Anaheim, CA. Jun 11-14, 2001. AIAA Paper 2001-2939.

17. K. Khodataev. *The Ignition of the Combustion and Detonation by the Undercritical Microwave Discharge.* AIAA Plasmadynamics and Laser Conference, 32nd, and Weakly Ionized Gases Workshop, 4th, Anaheim, CA. Jun 11-14, 2001. AIAA Paper 2001-2941

18 . Igor I.Esakov, Lev P. Grachev, Kirill V.Khodataev and D.M.Van Wie. *Efficiency of Microwave Discharges for Propane Ignition in Cold High-Speed Airflows.* 43rd AIAA Aerospace Sciences Meeting 10-13 January 2004, Reno, NV. Paper AIAA--2005-0989.

19. Kirill V. Khodataev. *The physical basis of the high ability of the streamer MW discharge to a resonant absorption of MW radiation.* 42-nd AIAA Aerospace Sciences Meeting 5-8 January 2004, Reno, NV. Paper AIAA--2004-0180.

20. V.G.Brovkin, Yu. F.Kolesnichenko. *Structure formation in initiated MW discharge.* Proc. "Radiophysika" MRTI, Moscow, 1991, pp. 71-79.

21. O.I.Voskoboynikova, S.L.Ginzburg, V.F.D'achenko, K.V.Khodataev. *Numerical investigation of subcritical microwave discharge in high-pressure gas.* Tech. Phys. Vol.47, No. 8, pp. 955-960.

22. S.L.Ginzburg, V.F.D'achenko, V.V.Paleychik, K.V.Khodataev.. *3-D model of microwave gas discharge*. Preprint M.V.Keldysh Applied Math. Inst. RAS. 2005.

23. K.V.Khodataev. *Physics of super undercritical streamer discharge in UHF electromagnetic wave.* Proc. XXIII ICPIG, 17-22 July 1997, Toulouse-France, Contributed papers, IV-24.

24. K.V.Khodataev. *Theory of the microwave high-pressure discharge.* Proc. of IV International workshop " Microwave discharges: fundamentals and applications ", September 18-22, 2000. Zvenigorod, Russia, pp. 35-44. (Yanus-K, Moscow 2001)

25 Kirill V. Khodataev. *Investigation of undercritical microwave discharge ability to propagate limitlessly by continuous branching of the streamer.* 44-rd AIAA Aerospace Sciences Meeting and Exhibit, 9-12 January 2006, Reno, NV, USA. Paper AIAA--2006-0785

26. Kirill V. Khodataev. *Development scenario and main parameters of different types of the microwave streamer discharges.* Proc. of Fifteenth International Conference on MHD Energy Conversion and Sixth International Workshop on Magnetoplasma Aerodynamics (May 24-27, 2005, Moscow, Russia), pp.556-564